Dynamic 3-Dimensional kinematics of the wrist joint and radiocarpal articular contact

Foumani, M.

[Link to publication](#)

Dynamic 3-Dimensional kinematics of the wrist joint and radiocarpal articular contact

Mahyar Foumani

Uitnodiging

Voor het bijwonen van de
openbare verdediging
van het proefschrift

**Dynamic 3-Dimensional
kinematics of the wrist
joint and radiocarpal
articular contact**

Door Mahyar Foumani

Op woensdag
9 december 2015
om 14.00 uur

Agnietenkapel
Oudezijds Voorburgwal 231
1012 EZ Amsterdam

Receptie na afloop ter plaatse

Mahyar Foumani
mahyarfoumani@gmail.com

Paranimfen
Duy Tan Nguyen
Martijn van de Giessen
paranimfen_foumani@outlook.com

Dynamic 3-Dimensional kinematics of the wrist joint and radiocarpal articular contact

Mahyar Foumani

Dynamic 3-Dimensional kinematics of the wrist
joint and radiocarpal articular contact

ACADEMISCH PROEFSCHRIFT

ter verkrijging van de graad van doctor

aan de Universiteit van Amsterdam

op gezag van de Rector Magnificus

prof. dr. D.C. van den Boom

ten overstaan van een door het College voor Promoties ingestelde commissie,

in het openbaar te verdedigen in de Agnietenkapel

op woensdag 9 december 2015, te 14:00 uur

door Mahyar Foumani

geboren te Teheran, Iran

"Let your vision be world-embracing"

Bahá'í Writings

Voor Maaike, David en mijn ouders voor hun onvoorwaardelijke steun

Faculteit der Geneeskunde

PHILIPS

Content

chapter 1

Introduction

Prevalence, social and economic impact of wrist disorders

Pain and malfunctioning of the wrist often lead to reduced quality of life and have profound consequences. It is also a great social-economic problem as wrist complaints are responsible for the longest absence period from work of employees, with substantial financial consequences due to workers' compensation, medical expenses, and productivity losses with an annually cost of approximately €600 million in the Netherlands[1].

The complexity of the wrist biomechanics makes the joint prone to degenerative conditions caused by traumatic events or anatomic abnormalities. Injuries such as fractures of carpal bones, disruption of the carpal ligaments and defects of cartilage layers often gradually develop towards degenerative conditions such as carpal instability and osteoarthritis[2]. Therefore it is of great importance for the patient and the medical doctor to recognize and properly diagnose problems in the wrist at an early stage to prevent irreversible degenerative pathologies of the carpus.

Functional anatomy of the wrist

For a proper diagnosis of carpal pathologies it is crucial to understand the anatomy and function of the wrist joint. The wrist, also named carpus, consists of multiple bones, ligaments and articular surfaces. The bones comprising the wrist include the distal radius, the distal ulna, the eight carpal bones and the bases of the metacarpal bones (figure 1). Functionally, the carpal bones can be divided into two anatomical rows. The proximal carpal row comprises the scaphoid, lunate and triquetrum, while the distal row is formed by the trapezium, trapezoid, capitate and the hamate. The eighth carpal bone is the pisiform, which is a sesamoid bone within the flexor carpi ulnaris tendon. The cartilaginous coverage of the articular surfaces is essential for the functioning of the articulations of the wrist. It provides a nearly frictionless sliding between two articulating surfaces.

Wrist stability can be defined as the ability of the carpus to maintain the balance between the articulating bones under physiologic loads and movements without overloading or loss of motion control. This balance relies on both active and passive factors that contribute to functionally stabilize the wrist. The multi-planar geometry of the articulation surfaces and the arrangement of carpal ligaments stabilize the wrist passively. Numerous ligaments interconnect the wrist bones and other surrounding structures allowing the carpal bones to function cohesively. These ligaments can be subdivided in two groups. As intrinsic ligaments interconnect the wrist bones to each other, the extrinsic carpal ligaments connect the carpal bones to the surrounding bony structures i.e. radius, ulnar and metacarpal bones. On the other hand, axial loads applied by forearm muscles are active mechanisms to functionally stabilize the wrist. Although no muscles originate from- or insert to the carpal bones, axial load applied by tendons of flexor and extensor forearm muscles crossing the wrist joint are important stabilizers of the wrist[3].

Carpal instability and developing osteoarthritis

Carpal instabilities can be defined as a loss of normal alignment or functional relationship between the carpal bones if they are placed under physiologic loads. This can be caused by disruption, attenuation of the carpal ligaments or fractures of carpal bones[4]. Patients with carpal instability develop carpal collapse and cartilage degeneration if the instability is not diagnosed at an early stage and addressed properly. Carpal instabilities, in general, have been classified into dissociative (CID) and non-dissociative (CIND) types. CID occurs if there is major dysfunction between bones of the same carpal row, by fracture or disruption of intrinsic ligaments. The scapholunate and lunotriquetral ligaments are often affected in CID[4]. By contrast, if instability occurs between the proximal and distal carpal row, then it is classified as CIND. In CIND, the lack of function of one or more extrinsic ligaments due to rupture, laxity or attenuation is often the main cause of the instability[5].

Carpal instability and often gradually develop towards more degenerative conditions such as osteoarthritis (OA)[2,6]. Osteoarthritis is characterized by progressive deterioration of the articular cartilage. Pathophysiologically, the initiating event in cartilage degradation that leads to secondary OA has been theorized to be mechanical stress dictated by local biomechanical factors, which initiate and perpetuate the process that leads to cartilage microfracture and fibrillation that ends in complete degeneration of the cartilage layer and bone eburnation[7].

Therefore it is of great importance for the patient and the medical doctor to recognize and properly diagnose problems in the wrist at an early stage to prevent irreversible degenerative pathologies of the carpus. As minor cartilage defects of the carpus often could be treated with more motion preserving operations, more severe osteoarthritis of the wrist requires more motion limiting interventions such as wrist arthrodesis[8].
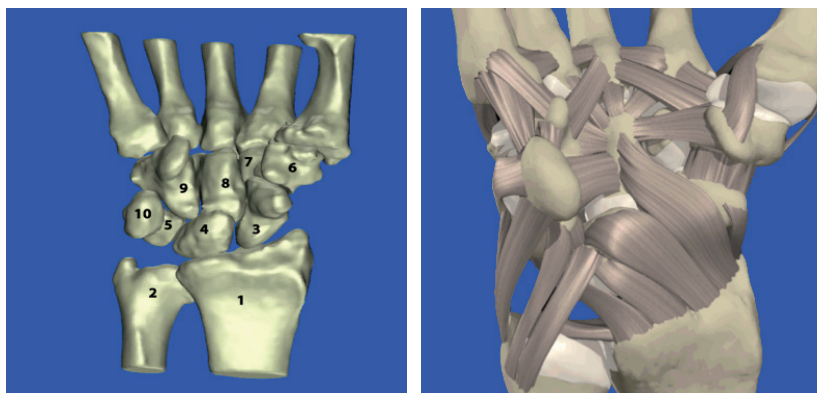
Figure 1: Left: The wrist consists of multiple bones: radius (1), Ulna (2), the scaphoid (3), lunate (4) and triquetrum (5), trapezium (6), trapezoid (7), capitate (8) and the hamate (9) and pisiform (10). **Right:** In order to functionally stabilize the wrist, numerous ligaments interconnect the wrist bones and other surrounding structures allowing the carpal bones to function cohesively.

Current diagnostic imaging tools

Early diagnosis of carpal instabilities and cartilage degeneration is a prerequisite for a fast and adequate treatment that may prevent further irreversible damage of the carpus.

After physical examination, the first step in diagnosing wrist pathologies is usually the evaluation of plain radiographs, which provide qualitative visual information regarding the condition of the wrist. Although for skeletal pathology plain radiographs are in most cases sufficient to diagnose fractures and dislocations of bony structures, for diagnosing carpal instabilities and cartilage damage, static radiographic images are often insufficient. Unless there is an obvious gap between wrist bones, ligamentous injury and its related abnormal wrist movements are often missed[9]. For the purpose of evaluating cartilage degeneration, plain radiographs may be misleading as the projection can only show joint space narrowing for a small part of the articulation. Moreover, the diagnosis of cartilage degeneration is hampered by the anatomical complexity of the wrist in combination with overlapping of anatomical structures on the radiographic images. Plain radiographs have therefore a limited value for the evaluation of degenerative joint disease in the wrist[9,10].

Currently it is possible to diagnose isolated injuries of ligaments and cartilage layers with invasive methods such as arthroscopy, which is now considered as the "gold standard". Besides being an invasive surgical procedure, it has also the disadvantage that it is laborious, time consuming, and too expensive to use as a standard diagnostic tool[11].

Fluoroscopy is the only clinically applicable non-invasive method available for the assessment dynamic wrist pathologies in a qualitative fashion. Fluoroscopy, also mentioned as "cineradiography" is a 2 Dimensional X-ray imaging technique that allows the motions of carpal bones to be recorded. Overlapping of anatomical structures on the fluoroscopic images still exists

similar to what is observed on plain radiographs. Assessment of fluoroscopy images is mainly based on dynamical imaging of provoked specific motion patterns. Therefore, the need for a trained radiologist is required. Because of its qualitative nature, the assessment of dynamic fluoroscopy has the disadvantage of being sensitive to inter- and intraobserver variations[12].

Current 3D diagnostic imaging modalities have shown to be of limited value in detection of ligament injuries and cartilage damage in the wrist[13,14]. In contrast to CT methods, where ligaments and cartilage layers are not visible in the acquired images, MRI methods to visualize cartilage and ligaments have provided valuable clinical advantages in larger joints[15]. In case of the wrist joint, previous studies have suggested that MRI was not sufficiently sensitive for diagnosing cartilage defects or cartilage loss in the wrist where the cartilage is thinner then 1 mm[13,14]. At the present, measurement of ligaments and cartilage layers still remains a challenging task if MRI methods are applied.

At this moment, quantification of wrist instabilities is not possible by commonly available clinical diagnostic modalities and ligament injuries frequently go undiagnosed and untreated, often being passed off as a simple sprain. As a result, such injuries often leads to damage of the cartilage layers that cannot be treated without residual problems in joint function. In these cases, the problem has progressed to such extent that the chances for success after surgical reconstruction are strongly reduced. Unfortunately this is a frequently observed situation for many patients seen in the clinic[16].

State of the art *in-vivo* carpal kinematic measurements
To solve this diagnostic problem we propose to use quantitative analysis of wrist joint motion patterns as tool to detect carpal pathologies. This seems feasible since carpal instabilities can

cause a pathological motion of carpal bones that can occur during a dynamic motion of the wrist[17]. Therefore, we hypothesize that an approach to acquire *in-vivo* carpal kinematics in combination with geometry of carpal structures may have future diagnostic applications.

To acquire *in-vivo* carpal kinematics, quasi-dynamic CT- and MR-based methods were introduced to image and detect 3D carpal movements during a step-wise motion of the wrist[18–23]. Although *in-vivo* carpal kinematics can be measured by the use of quasi-dynamic methods, the resulting kinematics may only provide an approximation of the true continuous kinematics of the carpal bones during a dynamic activity. In the case of ligament dissociations, abrupt dynamic changes such as clicks and clunks cannot be detected with static measurement methods. Therefore, a method to investigate the dynamic carpal kinematics in patients with dynamic wrist problems is highly desirable. Carelsen et al.[24] introduced such a method to acquire the dynamic *in-vivo* carpal kinematics by using the four-dimensional rotational X-ray imaging system (4D-RX). With the 4D-RX system it is possible to make quantitative measurements of *in-vivo* joint kinematics during wrist motion. This creates an opportunity to study *in-vivo* wrist joint kinematics both in healthy and affected wrists.

Research questions
Prior to using the method as a diagnostic tool some experimental conditions for measuring carpal kinematics need further assessment. A point of discussion is that experimental conditions for studying carpal kinematics have not been standardized or investigated properly[25,26]. First, the effect of axial loading on carpal kinematics during the measurements is unclear. Axial loading is often applied during experiments to simulate the natural stabilizing joint compression in the wrist joint caused by muscle tension. The question is whether applying axial loading has an effect on the kinematics of the wrists in passive motion experiments, whereby

the movement of the hand is externally controlled and not by muscle coordination.

Additionally, the dynamically measured carpal kinematics needs to be evaluated and compared to other currently available methods to measure carpal kinematics. Currently, the *in-vivo* carpal kinematics can be measured in a step-wise fashion. It has been suggested that the kinematics of the wrist that are acquired statically in a step-wise fashion may differ from those during a continuous dynamic motion. Tendon contractions and time-dependent soft tissue properties may alter the kinematic outcomes during motion. Therefore, the question is whether the step-wised acquired carpal kinematics differs from dynamically acquired carpal kinematics.

Next, measurement of *in-vivo* joint kinematics is not only suitable as a diagnostic tool, but it is also expected to be a powerful prognostic tool. Since the extent of cartilage deterioration is a determining factor for therapy planning it is crucial to analyse and quantity cartilage deterioration prior to surgery. In the case of osteoarthritis of the wrist, cartilage degradation is reflected on radiographs as a reduction of the distance between the adjacent subchondral bone surfaces, the so called Joint Space Thickness (JST). Although the JST can be measured from static radiographs or 3D CT scans of the wrist, the hypothesis is that analysis of the joint space thickness during wrist motion enables a better reflection of the actual JST since it would allow analysis of a larger extent of the functional articulation surface. To address this hypothesis, a method is required to calculate the JST during wrist motion by using geometrical and kinematical data acquired from the 4D-RX method.

As most surgical procedures have evolved by trial and error, principally, many current wrist surgeries lack a sound biomechanical foundation[25,26]. *In-vivo* acquired carpal motion analyses makes it possible to study the alterations of joint kinematics after an

operation and understand the long-term effects of an intervention on the wrist joint. Assessment of dynamic carpal kinematics can therefore be used as a tool to describe and study articular changes after wrist surgery. Therefore, a method is needed to describe kinematics changes after wrist surgery, which can be based on the dynamic distance maps methodology acquired from geometrical and kinematical data obtained from the 4D-RX measurements.

Outline of this thesis

The main objective of this thesis is to introduce novel methods for assessment and quantification of *in-vivo* carpal kinematics and joint space thickness measurements during wrist motion for diagnostic and prognostic purposes.

In the chapters two and three of this thesis some experimental conditions for measuring carpal kinematics are studied. A point of discussion is that experimental conditions for studying carpal kinematics have not been standardized or investigated properly[26]. In **chapter 2**, the effect of axial loading is investigated during a passive motion of the wrist in an *in-vitro* model. The question is whether applying axial loading has an effect on the kinematics of the wrists in passive motion experiments, whereby the movement of the hand is externally controlled and not by muscle coordination. The effect of axial loading is investigated by measuring carpal kinematics with and without applying 50N force on the extensor- and flexor tendons in cadaveric specimens.

It has been suggested that the kinematics of the wrist that are acquired in a step-wise fashion may differ from those during a continuous dynamic motion[21,25]. Tendon contractions and time-dependent soft tissue properties may alter the kinematic outcomes during motion. In **chapter 3**, the differences between the dynamically and statically acquired *in-vivo* carpal kinematics are compared in a group of healthy volunteers during wrist flexion-extension and radio-ulnar deviation.

In **chapter 4**, the feasibility to quantify cartilage degeneration by using dynamically acquired distance maps are demonstrated. The purpose is to adapt a newly developed CT-based imaging method for measuring the three-dimensional kinematics of the carpal bones to acquire *in-vivo* joint space information of articulating surfaces during motion. The essence of the method is to calculate the joint space thickness using dynamic distance maps. A dynamic distance map gives for every point on a subchondral bone surface the shortest distance to the opposing subchondral bone surface within a set of different joint poses. We hypothesize that the measure of joint space thickness during wrist motion is smaller than the joint space thickness measured in one single 3D CT scan acquired in a neutral position, giving less overestimation of the joint space thickness. The diagnostic potential of the distance maps are illustrated by comparing distance maps from wrists with osteoarthritis of the radiocarpal joint with those from normal joints.

Finally, in **chapter 5**, a method is presented to describe articular changes after wrist surgery by using *in-vivo* acquired kinematical data. As an example, the four-corner arthrodesis (FCA) operated wrists are analysed as a model to study the radiocarpal articulation changes after a FCA procedure. The FCA has been advocated for the treatment of various pathological conditions of the wrist, that involves the arthrodesis of joints between the lunate, capitate, hamate, and triquetrum combined with scaphoid excision 6. The question is how the radiolunate articulation changes after a FCA procedure and to understand why, despite changes in kinematic and morphology of the joint, only minor radiological and functional long-term abnormalities are observed. In a cross-sectional experimental study, the radiocarpal articulation of 10 healthy participants and both operated and non-operated wrists of 8 individuals who have undergone FCA on one side are assessed from dynamic three-dimensional distance maps acquired during wrist joint motion.

References

1. De Putter, C. E. et al. Economic impact of hand and wrist injuries: health-care costs and productivity costs in a population-based study. J. Bone Joint Surg. Am. 94, e56 (2012).

2. Watson, H. K. & Ryu, J. Evolution of arthritis of the wrist. Clin. Orthop. Relat. Res. 57–67 (1986).

3. Kauer, J. M. The mechanism of the carpal joint. Clin. Orthop. Relat. Res. 16–26 (1986).

4. Cooney, W. P., Dobyns, J. H. & Linscheid, R. L. Arthroscopy of the wrist: anatomy and classification of carpal instability. Arthroscopy 6, 133–40 (1990).

5. Wolfe, S. W., Garcia-Elias, M. & Kitay, A. Carpal instability nondissociative. J. Am. Acad. Orthop. Surg. 20, 575–85 (2012).

6. Watson, H. K. & Ballet, F. L. The SLAC wrist: scapholunate advanced collapse pattern of degenerative arthritis. J. Hand Surg. Am. 9, 358–65 (1984).

7. Linscheid, R. L., Dobyns, J. H., Beabout, J. W. & Bryan, R. S. Traumatic instability of the wrist: diagnosis, classification, and pathomechanics. J. Bone Joint Surg. Am. 84-A, 142 (2002).

8. Watson, H. K., Weinzweig, J., Guidera, P. M., Zeppieri, J. & Ashmead, D. One thousand intercarpal arthrodeses. J. Hand Surg. Br. 24, 307–15 (1999).

9. Pliefke, J. et al. Diagnostic accuracy of plain radiographs and cineradiography in diagnosing traumatic scapholunate dissociation. Skeletal Radiol. 37, 139–45 (2008).

10. Peh, W. C., Patterson, R. M., Viegas, S. F., Hokanson, J. A. & Gilula, L. A. Radiographic-anatomic correlation at different wrist articulations. J. Hand Surg. Am. 24, 777–80 (1999).

11. Ahsan, Z. S. & Yao, J. Complications of wrist arthroscopy. Arthroscopy 28, 855–9 (2012).

12. Sulkers, G. S. I., Schep, N. W. L., Maas, M. & Strackee, S. D. Intraobserver and interobserver variability in diagnosing scapholunate dissociation by cineradiography. J. Hand Surg. Am. 39, 1050–4.e3 (2014).

13. Haims, A. H. et al. MRI in the diagnosis of cartilage injury in the wrist. AJR. Am. J. Roentgenol. 182, 1267–70 (2004).

14. Mutimer, J., Green, J. & Field, J. Comparison of MRI and wrist arthroscopy for assessment of wrist cartilage. J. Hand Surg. Eur. Vol. 33, 380–2 (2008).

15. Bredella, M. A. et al. Accuracy of T2-weighted fast spin-echo MR imaging with fat saturation in detecting cartilage defects in the knee: comparison with arthroscopy in 130 patients. AJR. Am. J. Roentgenol. 172, 1073–80 (1999).

16. Jones, W. A. Beware the sprained wrist. The incidence and diagnosis of scapholunate instability. J. Bone Joint Surg. Br. 70, 293–7 (1988).

17. Nielsen, P. T. & Hedeboe, J. Posttraumatic scapholunate dissociation detected by wrist cineradiography. J. Hand Surg. Am. 9A, 135–8 (1984).

18. Crisco, J. J., McGovern, R. D. & Wolfe, S. W. Noninvasive technique for measuring in vivo three-dimensional carpal bone kinematics. J. Orthop. Res. 17, 96–100 (1999).

19. Feipel, V. & Rooze, M. Three-dimensional motion patterns of the carpal bones: an in vivo study using three-dimensional computed tomography and clinical applications. Surg. Radiol. Anat. 21, 125–31 (1999).

20. Snel, J. G. et al. Quantitative in vivo analysis of the kinematics of carpal bones from three-dimensional CT images using a deformable surface model and a three-dimensional matching technique. Med. Phys. 27, 2037–47 (2000).

21. Wolfe, S. W., Neu, C. & Crisco, J. J. In vivo scaphoid, lunate, and capitate kinematics in flexion and in extension. J. Hand Surg. Am. 25, 860–9 (2000).

22. Sun, J. S. et al. In vivo kinematic study of normal wrist motion: an ultrafast computed tomographic study. Clin. Biomech. (Bristol, Avon) 15, 212–6 (2000).

23. Moritomo, H. et al. Capitate-based kinematics of the midcarpal joint during wrist radioulnar deviation: an in vivo three-dimensional motion analysis. J. Hand Surg. Am. 29, 668–75 (2004).

24. Carelsen, B. et al. Detection of in vivo dynamic 3-D motion patterns in the wrist joint. IEEE Trans. Biomed. Eng. 56, 1236–44 (2009).

25. Moojen, T. M. et al. In vivo analysis of carpal kinematics and comparative review of the literature. J. Hand Surg. Am. 28, 81–7 (2003).

26. T.M. Moojen. Carpal kinematics. (2003).

To live for a time close to great minds is the best kind of education.

John Buchan

The effect of tendon loading on *in-vitro* carpal kinematics of the wrist joint

Foumani M, Blankevoort L, Stekelenburg C, Strackee SD, Carelsen B, Jonges R, Streekstra GJ. Journal of Biomechanics.2010 Jun 18;43(9):1799-805.

Abstract

Measurements of *in-vitro* carpal kinematics of the wrist provide valuable biomechanical data. Tendon loading is often applied during cadaver experiments to simulate natural stabilizing joint compression in the wrist joint. The purpose of this study was to investigate the effect of tendon loading on carpal kinematics *in-vitro*.

A cyclic movement was imposed on 7 cadaveric forearms while the carpal kinematics were acquired by a 4-dimensional rotational X-ray imaging system. The extensor- and flexor tendons were loaded with constant force springs of 50N respectively. The measurements were repeated without a load on the tendons. The effect of loading on the kinematics was tested statistically by using a linear mixed model.

During flexion and extension, the proximal carpal bones were more extended with tendon loading. The lunate was on the average 2.0 degrees (p=0.012) more extended. With tendon loading the distal carpal bones were more ulnary deviated at each angle of wrist motion. The capitate was on the average 2.4 degrees (p=0.004) more ulnary deviated.

During radio-ulnar deviation, the proximal carpal bones were more radially deviated with the lunate 0.7 degrees more into radial deviation with tendon loading (p<0.001). Conversely, the bones of distal row were more flexed and supinated with the capitate 1.5 degrees more into flexion (p=0.025) and 1.0 degree more into supination (p=0.011).

In conclusion, the application of a constant load onto the flexor and extensor tendons in cadaver experiments has a small but statistically significant effect on the carpal kinematics during flexion-extension and radio-ulnar deviation.

Introduction

Studies of *in-vitro* carpal kinematics of the wrist provide valuable biomechanical data which are useful to understand the relationship between joint anatomy and its function[1]. Tendon loading is often applied during cadaveric experiments to simulate the natural stabilizing joint compression in the wrist joint. Kobayashi et al.[2] and Gupta[3] reported changes in orientation of the carpal bones after applying or removing an axial load in a static situation. However, it is not clear what effect tendon loading may have on the kinematics of carpal bones during dynamic *in-vitro* experiments.

For conducting dynamic *in-vitro* experiments of the wrist, three basic strategies can be recognized to simulate a wrist motion. In the first situation, carpal kinematics can be acquired during a passive motion of the wrist without applying any load onto the tendons[4,5]. In a second condition, passive motion can be imposed to the wrist in a stepwise fashion, while small amounts of force are applied to the tendons[6–8]. In the third condition, wrist motion can be achieved actively by pulling on the flexor and extensor tendons of the wrist[9]. Patterson et al. showed that kinematics acquired during a simulated active motion were, in general, more difficult to control and less smooth then passively acquired motion parameters[10].

The question is whether applying a load onto the tendons has an effect on the kinematics of the cadaver wrists in passive motion experiments. Therefore the purpose of this study was to investigate whether the *in-vitro* kinematics differ if tendon loading is applied during a passive motion of the wrist.

Carpal kinematics were acquired by using a motion device and a 4 dimensional X-ray imaging system (4D-RX)[4,11]. This method allows precise measurements of carpal kinematics during a cyclic dynamic wrist motion. In this study, a comparison is made between the carpal kinematics acquired with and without applying load to the tendons.

Materials and Methods

The methods employed in this study for acquiring the kinematics of the carpal bones include a so-called handshaker, that is a motion device to impose the motion on the hand, a CT-scan (Philips MX8000) to acquire 3D images for segmentation of the carpal bones, a modified 3D-RX system (BV Pulsera, Philips Medical systems, Best, The Netherlands) to acquire 3D-reconstructions of the bones from dynamically acquired X-ray-images and software tools to calculate the kinematics of the carpal bones[4,11,12].

Specimen preparation

Seven fresh frozen cadaver arms (male, average age of 74 years, range: 69-79 years) were imaged with CT to exclude osteoarthritis, carpal malalignment, or other bony abnormalities that may affect the wrist joint kinematics. The medical history of the donors revealed no history of pathologies affecting the wrist joint integrity. The tendons of the flexor carpi radialis and –ulnaris on the palmar side and of the extensor carpi radialis longus , -brevis and extensor carpi ulnaris on the dorsal side were explored and dissected. The tendons were connected with wires to four constant-force springs, two on the extensor and other two on the flexor side during loaded motion. Constant force springs were detached during unloaded motion. The wires were linked to each other by using a pulley mechanism to assure an equal distribution of the spring forces over the individual tendons. The constant force springs were specially developed to load the extensors and flexors pulleys equally with a total constant force of 50 Newton at each side[6] (figure 1).

Motion device

To induce a cyclic, standardized motion of the wrist, the arm was placed in the specially developed handshaker[11]. The handshaker consists of a detachable drive unit and framework in which the drive unit is placed to impose flexion-extension and radioulnar
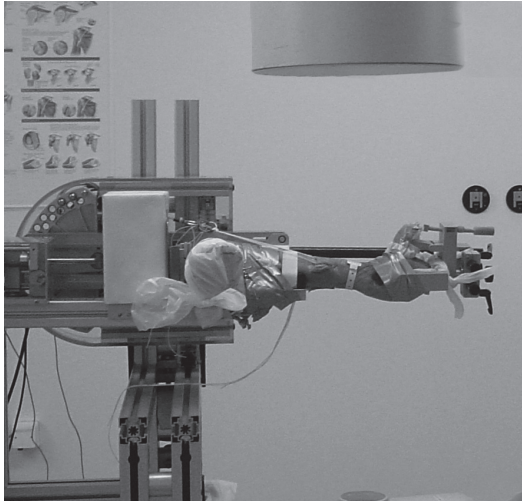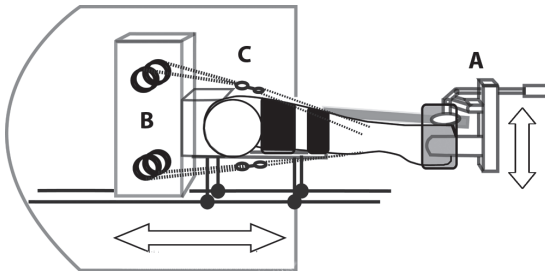
Figure 1: (a): To induce a cyclic, standardised motion of the joint, the upper limbs were placed in a specially developed handshaker. (b): Schematic drawing of the experimental set up. A: handpiece: Clamp screws and adhesive tapes were used to fixate the hand externally. B: to apply motion onto the wrist, the forearm was placed in an axially slidable table allowing it to move freely. The upper limbs including the spring mechanism were placed on a slidable table allowing the forearms to move freely in the axial direction. C: The flexor and extensor tendons were connected with wires to four constant-force springs.

deviation of the wrist. The period of each sinusoidal cycle of the handshaker was 1.6 seconds. The lower arm was neutrally positioned with respect to pro- and supination, with the elbow flexed 90 degrees (figure 1a). To allow the hand to follow the movements of the handshaker, the hand was placed in a hand piece. Clamp screws and adhesive tapes were used to fixate the hand externally to the handpiece. To apply motion onto the wrist without motion restraints and to prevent a locked wrist, the forearm including the spring mechanism was placed in an axially slidable table allowing it to move freely. By using constant force springs the tendon loading remained constant throughout the cyclic motion.

Image acquisition and processing

For the reconstruction of the bony geometry of the carpal bones CT images of the wrists were acquired. Segmentation of carpal bones, radius and the ulna was performed from the CT image using a region growing algorithm. Next, a static 3D-RX scan of the wrist was acquired in a neutral position without applying any load which was used for defining the neutral position of the wrist for both the loaded and unloaded scans. Hereafter, two dynamic scans were acquired during loaded and unloaded flexion extension motion from approximately 50 degrees extension to 50 degrees flexion and back. For radial-ulnar deviation two other dynamic scans were obtained during loaded and unloaded radioulnar deviation motion from approximately 20 degrees radial deviation to 30 degrees ulnar deviation and back.

During the cyclic motion of the wrist the 3D-RX scanner acquired 975 projection images. These images were sorted in 20 sets where each set belongs to a certain motion phase. Each set of projection images was separately reconstructed, where each volume reconstruction belongs to a certain pose of the hand during dynamic motion. To obtain the kinematic parameters of the individual bones in the dynamic scan, the segmented boundary voxels of each carpal bone from the static CT scans

were registered to the corresponding bones in the volumes of the dynamic scan[4,11]. For this purpose we used a stack of double contours as bone boundary characterization. The outer contour is situated just outside the bone (low gray value) and the inner contour at a short distance within the bone on the hard rim (high gray value). The method to register the segmented bone contour with their dynamic counterparts searches for the translations and rotations that maximize the cross correlation between the gray values of the double contours and those in the 4D RX volume. Motion pattern measurement with 4D-RX imaging and processing has a reproducibility of 0.22±0.08 mm for positional displacements and 0.5±0.1 degrees for rotations[4,11].

Kinematic parameters

The motion parameters of the individual carpal bones were expressed relative to an anatomy- based radial coordinate system similar to Kobayashi et al.[13] and Crisco et al.[1]. The longitudinal axis of the radius was defined as the Z-axis by the center line of a cylinder fitted through the segmented radius. The length of the radius included in the image data for the definition of the Z-axis was between 10 and 14 centimeters. The direction of the X-axis orientation was defined by a line perpendicular to the Z-axis and passing through the tip of the radial styloid. The Y-axis was determined as the line perpendicular to the X- and the Z-axis. The point where the Z-axis intersects with the subchondral bone surface was defined as the origin of the global coordinate system.

In this study, the translation of carpal bones was defined as the translation along the finite helical axes between the reference position and the position during motion. For the rotation convention, the attitude vector was used[14]. The attitude vector is defined as the multiplication of the rotation about the finite helical axis and the unit vector in the direction of the helical axis. The components of the attitude vector relative to the global coordinate system describe the anatomic rotation components. Flexion (+) and extension (-)

were defined as rotations around the X-axis, Radial (+) and ulnar (-) deviation as rotations around the Y- axis and pronation (-) and supination (+) as rotations around the Z- Axis. The global wrist motion was defined as the rotation of the capitate with respect to the radius[13]. This is justified since negligible differences are reported between the Capitate and third metacarpal motion[15]. For the flexion-extension motion, the radio-capitate X-component of the attitude vector was defined as the global wrist motion. For radioulnar deviation the radio-capitate Y-component was defined as the global motion of the wrist.

Motion direction effect

Usually referred to as hysteresis, carpal bones are reported to show motion direction effects in the sense that the kinematics are dependent on the direction of the imposed wrist motion[16–19]. The motion direction effect was calculated for both loaded and unloaded acquired datasets, by computing the rotational differences between the two parts of the motion trajectory representing the two opposite motion directions.

Statistical analysis

Each 4D-RX scan provides kinematic outcomes for 20 different positions within one complete cycle of the wrist's motion. Both for the loaded and unloaded conditions, the kinematic data were linearly interpolated to obtain data at every step of 5 degrees of global wrist motion. To investigate the differences between the loaded and unloaded condition the differences of the helical translations, helical rotations and the flexion-extension (X), radioulnar deviation (Y) and pro- supination (Z) components of the attitude vector at every 5 degrees of global wrist motion were defined as the primary outcome values.

For analyzing the dynamic datasets, linear mixed model analyses were used to compare the differences between the loaded and unloaded measurements correcting for first lag autocorrelation
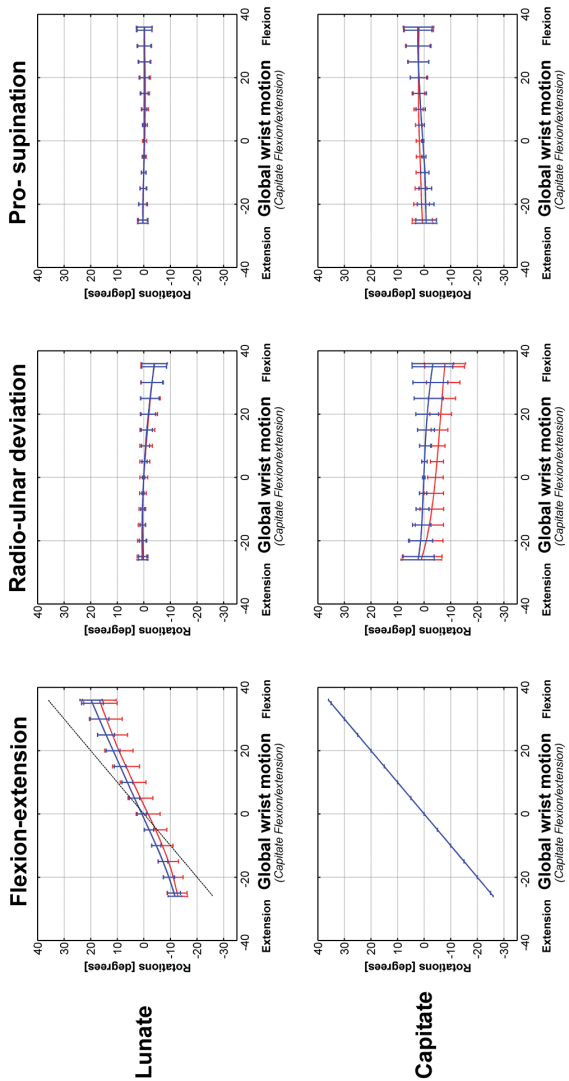
Figure 2: As typical illustrations of bones of the proximal and distal row the lunate's and capitate's average flexion-extension, radioulnar and pro-supination components are plotted for the overlapping motion range during flexion and extension of 7 wrist specimens. Standard deviations of the mean are provided for begin and end values and at every 5 degrees of global wrist motion. Loaded measurements are plotted as red lines, while the blue lines represent the unloaded measurements. Capitate flexion-extension is plotted in black dotted line as a line of identity.

between serial measurements. Analyses were performed for each carpal bone. P-values less than 0.05 were considered statistically significant. Linear mixed model statistics were also used to analyze the motion direction effect for the loaded and unloaded measured differences between the 2 paths that represents opposite directions of wrist motion.

Results

In this study of the carpal kinematics i.e. the magnitude of helical rotations, the flexion-extension (X), radioulnar deviation (Y) and pro- supination (Z) components of the attitude vector and the translations along the helical axes were evaluated with a particular focus on the differences between tendon loading and unloading during the experiments. Additional analyses were performed for the motion direction effects of the loaded and unloaded wrists.

Flexion-Extension

During flexion and extension, the bones of the proximal row follow the motion of capitate both during the loaded and unloaded experiments. During wrist flexion, the bones of the proximal row flex and deviate ulnary, while during wrist extension, they mainly extend (figure 2, average rotations of the lunate and capitate as typical illustrations of bones of the proximal and distal row respectively).

The kinematic changes after tendon loading occur in all cadaver specimens in a similar pattern. During flexion and extension the magnitude of helical rotations were not significantly different between the loaded and unloaded wrists at each step of global wrist motion except for the capitate (table 1). However, the rotation components showed significant differences between loaded and unloaded condition, indicating a change in the orientation of the helical axes.

	Total rotation around the helical axis				Flexion and extension				Radial and ulnar deviation				Pro- and supination			
	Mean difference [°]	Std. Error [°]	95% Confidence Interval [°]	P-value	Mean difference [°]	Std. Error [°]	95% Confidence Interval [°]	P-value	Mean difference [°]	Std. Error [°]	95% Confidence Interval [°]	P-value	Mean difference [°]	Std. Error [°]	95% Confidence Interval [°]	P-value
Lunate	-1,1	0,8	-2,8 : 0,6	0,172	-2,0	0,7	-3,5 : -0,5	**0,012**	0,4	0,3	-0,1 : 0,9	0,142	-0,2	0,2	-0,6 : 0,2	0,338
Scaphoid	-0,4	0,8	-2,2 : 1,3	0,616	-1,8	0,6	-3,1 : -0,6	**0,007**	0,9	0,4	0,0 : 1,8	**0,045**	0,7	0,3	-0,0 : 1,4	0,052
Triquetrum	-0,6	0,6	-1,9 : 0,7	0,329	-1,3	0,5	-2,4 : -0,1	**0,032**	-0,6	0,4	-1,4 : 0,3	0,157	0,2	0,2	-0,2 : 0,6	0,240
Capitate	0,7	0,3	0,1 : 1,2	**0,025**	NA	NA	NA	NA	-2,4	0,7	-3,9 : -0,9	**0,004**	0,3	0,4	-0,6 : 1,3	0,430
Hamate	0,4	0,5	-0,6 : 1,4	0,389	1,0	0,2	0,5 : 1,4	**<0,001**	-2,6	0,6	-3,9 : -1,2	**<0,001**	0,4	0,5	-0,7 : 1,4	0,452
Trapezoid	0,5	0,3	-0,1 : 1,1	0,108	0,1	0,1	-0,2 : 0,3	0,421	-2,2	0,7	-3,7 : -0,6	**0,011**	0,3	0,4	-0,7 : 1,2	0,567
Trapezium	0,0	0,4	-0,7 : 0,8	0,958	0,5	0,2	-0,0 : 1,0	0,057	-2,1	0,7	-3,6 : -0,6	**0,009**	0,5	0,5	-0,5 : 1,5	0,268

Table 1: The mean rotation differences between the tendon loaded and unloaded acquired kinematics during flexion-extension. Analyses are provided for the total rotation differences and separate flexion (+)-extension (-), radio (+) and ulnar (-) and pro(-)- supination(+) rotation components.

At each angle of global wrist motion, the bones of the proximal row were less flexed during the loaded protocol in contrast to the bones in the unloaded wrists. The scaphoid was more radially deviated when tendon loading was applied. The pro-supination rotations of bones within the proximal row were statistically not different between the loaded and unloaded wrists. Concerning the bones of the distal row, the hamate was more flexed when tendon loading was applied. In comparison with the unloaded wrists, the radioulnar rotation component revealed a more ulnary deviated distal row during the loaded protocol. On the other hand, the pro-supination rotations of the bones within the distal row were statistically not different between the loaded and unloaded bones.

The total amount of carpal translations along the helical axes was not statistically significantly different between the loaded and unloaded wrists; mean of all carpal bones was 0.07 mm (95% CI: -0.02: 0.16. p=0.143).

The motion direction effect on the kinematics of the bones was not statistically significant for flexion and extension. The mean rotation difference between opposite direction motions of all carpal bones during the loaded measurements was -0.1 degrees (95% CI: -0.8: 0.6. p=0.713). Also during unloaded measurements the motion direction effect was not statistically significant (0.1 degrees, 95% CI: 0.0: 0.3. p=0.134).

Radioulnar deviation

The bones of the distal row generally followed the global wrist motion while the proximal row's main rotations were primarily flexion and extension (figure 3, average rotations of the lunate and capitate as typical illustrations of bones of the proximal and distal row respectively).

During the radioulnar deviation motion the magnitude of helical rotations between the loaded and unloaded wrists at each step of global wrist motion were significantly different for the capitate, trapezoid, trapezium (table 2). Again, flexion-extension, radioulnar
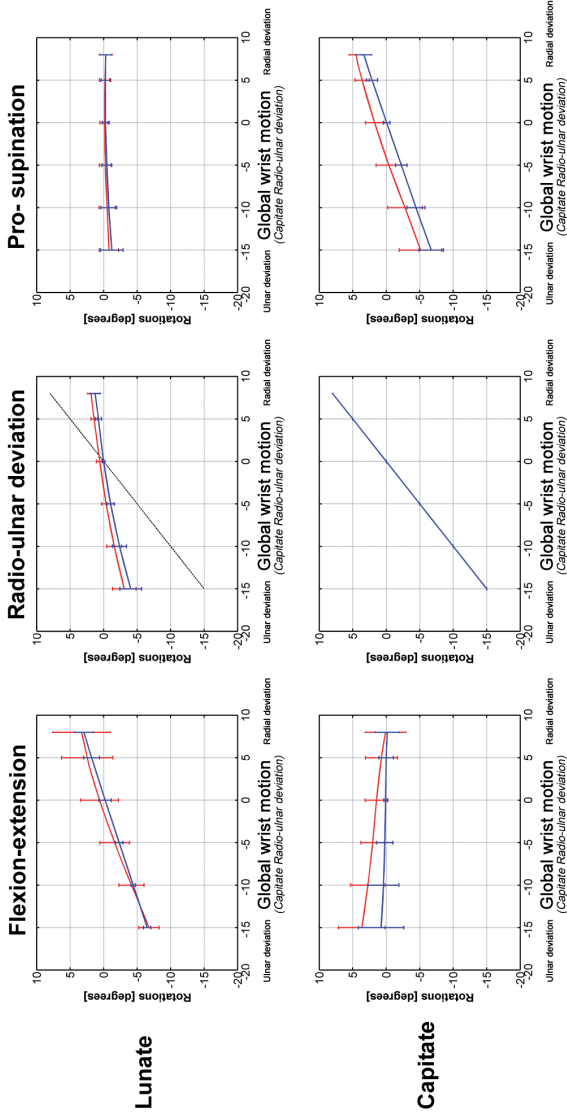
Figure 3: As typical illustrations of bones of the proximal and distal row the lunate's and capitate's average flexion-extension, radioulnar and pro-supination component are plotted in for the overlapping motion range during radioulnar deviation of 7 wrist specimens. Standard deviations of the mean are provided for begin and end values and at every 5 degrees of global wrist motion. Loaded measurements are plotted as red lines, while the blue line represents the unloaded measurements. Capitate radio-ulnar deviation is plotted in black dotted line as a line of identity.

2

	Total rotation around the helical axis				Flexion and extension				Radial and ulnar deviation				Pro- and supination			
	Mean difference [°]	Std. Error [°]	95% Confidence Interval [°]	P-value	Mean difference [°]	Std. Error [°]	95% Confidence Interval [°]	P-value	Mean difference [°]	Std. Error [°]	95% Confidence Interval [°]	P-value	Mean difference [°]	Std. Error [°]	95% Confidence Interval [°]	P-value
Lunate	-0,1	0,5	-1,1 : 0,9	0,836	0,0	0,5	-1,2 : 1,1	,984	0,7	0,2	0,4 : 1,1	**<0,001**	0,2	0,2	-0,4 : 0,7	0,55
Scaphoid	-0,3	0,7	-1,8 : 1,1	0,629	0,5	0,7	-1,2 : 2,0	0,560	1,8	0,4	0,9 : 2,6	**<0,001**	1,2	0,3	0,6 : 1,8	**0,000**
Triquetrum	0,2	0,4	-0,6 : 1,1	0,598	0,6	0,5	-0,4 : 1,6	0,231	0,5	0,3	0,2 : 0,9	**0,007**	0,1	0,3	-0,4 : 0,7	0,630
Capitate	0,4	0,2	0,1 : 0,8	**0,023**	1,5	0,6	0,2 : 2,8	**0,025**	NA	NA	NA	NA	1,0	0,4	0,2 : 1,9	**0,011**
Hamate	0,6	0,3	-0,1 : 1,2	0,087	2,6	0,6	1,3 : 3,9	**<0,001**	-0,2	0,1	-0,5 : 0,0	0,061	1,3	0,4	0,5 : 2,1	**0,004**
Trapezoid	0,6	0,2	0,1 : 1,1	**0,011**	1,4	0,6	0,1 : 2,7	**0,038**	0,2	0,1	-0,0 : 0,4	0,091	1,3	0,4	0,5 : 2,1	**0,004**
Trapezium	1,1	0,3	0,5 : 1,6	**0,002**	1,6	0,7	0,2 : 3,1	**0,030**	0,3	0,3	-0,2 : 0,9	0,200	1,2	0,4	0,3 : 2,1	**0,010**

Table 2: The mean rotation differences between the tendon loaded and unloaded acquired kinematics during radioulnar deviation. Analyses are provided for the total rotation differences and separate flexion (+)-extension (-), radio (+) and ulnar (-) and pro(-) and supination(+) rotation components.

and pro- supination rotation components showed significant differences between loaded and unloaded condition. At each angle of global wrist motion the bones in the distal row were more flexed during the loaded experiments in contrast to the unloaded condition. On the other hand the radioulnar rotation component showed that during the loaded experiments scaphoid, lunate and triquetrum were more radially deviated at each angle of global wrist motion in contrast to the unloaded series. Dissimilar to the unloaded experiments, the scaphoid and the bones of the distal row showed more supination when tendon loading was applied.

The total amount of carpal translations along the helical axes was not different between the loaded and unloaded wrists. The mean difference for all carpal bones pooled was -0.02 mm (95% CI: -0.09:0.04, P=0.516.

The motion direction effect on the kinematics of the bones was not statistically significant for radioulnar deviation. For all carpal bones, the mean rotation difference between opposite direction motions of all carpal bones during the loaded measurements was only 0.0 degrees (95% CI: -0.1: 0.2. p=0.968). Also during unloaded measurements the difference was not statistically significant (0.0 degrees (95% CI: -0.2: 0.1, p=0.659)).

Discussion

The goal of this study was to investigate if the application of a load onto the tendons that cross the wrist joint alters the kinematics of the carpal bones in the wrist. The carpal bone kinematics of the 7 cadaver wrists in this study were qualitatively in agreement with previously published data by Moojen et al.[20] and Wolfe et al.[21], in the sense that during the flexion and extension bones of proximal row follow the motion direction of the capitate. During radio-ulnar deviation the bones of the proximal row moved together showing some out of plain

motion with extension in ulnar deviation and flexion in radial deviation.

Applying a load onto the flexor and extensor tendons of the wrist had a small but statistically significant effect on the kinematics of some carpal bones. Changes in orientation of the proximal row occurred in the same plane as the global wrist motion. During loaded flexion-extension, the proximal row's flexion-extension component of the rotation was more affected, while during the radio-ulnar deviation the proximal row showed significant rotational differences in the radio-ulnar component of the rotation.

Regarding the bones of the distal row, the amount of ulnar deviation during wrist flexion as well as flexion of the bones during ulnar deviation of the wrist both increased after applying axial loading. In accordance with our findings, applying a load seems to increase the tendency of the carpal bones to move along the more favorable the so-called "Dart Throwing Motion" (DTM) path. The DTM plane can be defined as a plane in which an anatomically oblique motion occurs, i.e. from extension and radial deviation to flexion and ulnar deviation[22–25]. The anatomically oblique plane of the physiologic DTM is unique to each wrist and depends on factors such as joint surface geometry and ligament constraints.

Carpal bones have a tendency to rotate into specific directions under load, depending on the direction of wrist motion, articular surface geometry, and mechanical properties of the capsule and ligaments[2,3]. The result of this study was that not the magnitude of the attitude vector was affected, but the direction of the attitude vector, as reflected by the effect on the rotation components. The compressive forces combined with the congruent articular surfaces may cause the motion to follow more closely the anatomic contours of the articular surfaces. According to Kobayashi et al.[2] and Gupta[3], at neutral wrist posture, the loaded scaphoid tends to rotate into flexion and pronation because of its oblique orientation relative to the long axis of the forearm. Although this might be the

case in experiments at a neutral wrist posture, this phenomenon was not observed in the present study where carpal motions were studied during motion. Accordingly, the observed kinematical differences revealed various rotational shifts throughout the entire course of the motion trajectories depending on the direction of wrist motion. From the dynamic data deduced differences at zero degree wrist motion similar kinematical changes were observed as throughout the rest of the motion trajectories. This dissimilarity with respect to previously conducted experiments may be explained by the absence of dynamic-static friction effects and the presence of visco-elastic properties when studying carpal kinematics during wrist motion. Nevertheless, due to different experimental conditions, a comparison between our findings and those of previous investigators remains difficult.

As in the case of carpal instabilities and scapholunar ligament dissociations, kinematical changes sometimes occur between pairs of carpal bones within the same row. In such cases, segmental analysis of carpal motions would be more interesting for understanding some clinically important conditions. Therefore, in future experiments, when kinematical changes are expected to be present between pairs of carpal bones, it would be valuable to study relative motions between pairs of carpal bones. In our study however, the main focus was on carpal kinematics relative to a fixed radius in which the changes mainly occurred between different carpal rows i.e. bones of the proximal and distal row.

Applying tendon loading has been conducted randomly in previous *in-vitro* experiments. Our purpose was to give answers to some basic questions regarding experimental conditions and the magnitude of kinematical effects when tendon loading is applied on unaffected cadaver wrists. For unaffected wrists, small but significant differences occur after tendon loading is applied. In cases of simulating pathological conditions of the wrist however, the conclusions of this experiment may not be applicable since we did not study these conditions. This requires additional

experiments on the effects of axial loading on joint kinematics in simulated pathological conditions such as wrist instabilities and ligamentous dissociations.

At last, it can be argued that applying a constant load is not the most realistic approach to simulate tendon forces in *in-vitro* experiments. During a natural wrist motion, flexor and extensor muscle groups are not activated simultaneously all the time. Therefore, for future experiments, it would be more favourable to develop tendon loading protocols for various passively imposed motions of the wrist based on *in-vivo* muscle activation patterns. The conclusion of this study is that in cadaver experiments the application of a constant load during passive motion of the wrist has a small but statistically significant influence on the carpal kinematics during flexion-extension and radio-ulnar deviation. Therefore, tendon loading is advised if studying *in-vitro* kinematics of normal wrists.

References

1. Crisco, J. J., McGovern, R. D. & Wolfe, S. W. Noninvasive technique for measuring in vivo three-dimensional carpal bone kinematics. J. Orthop. Res. 17, 96–100 (1999).

2. Kobayashi, M. et al. Axial loading induces rotation of the proximal carpal row bones around unique screw-displacement axes. J. Biomech. 30, 1165–1167 (1997).

3. Gupta, A. Change of carpal alignment under anaesthesia: Role of physiological axial loading on carpus. Clin. Biomech. 17, 660–665 (2002).

4. Carelsen, B. et al. 4D rotational x-ray imaging of wrist joint dynamic motion. Med. Phys. 32, 2771–6 (2005).

5. Tay, S. C. et al. Four-dimensional computed tomographic imaging in the wrist: Proof of feasibility in a cadaveric model. Skeletal Radiol. 36, 1163–1169 (2007).

6. De Lange, A., Kauer, J. M. & Huiskes, R. Kinematic behavior of the human wrist joint: a roentgen-stereophotogrammetric analysis. J. Orthop. Res. 3, 56–64 (1985).

7. Kaufmann, R. et al. Kinematics of the midcarpal and radiocarpal joints in radioulnar deviation: an in vitro study. J. Hand Surg. Am. 30, 937–42 (2005).

8. Savelberg, H. H., Kooloos, J. G., De Lange, A., Huiskes, R. & Kauer, J. M. Human carpal ligament recruitment and three-dimensional carpal motion. J. Orthop. Res. 9, 693–704 (1991).

9. Werner, F. W. et al. Wrist joint motion simulator. J. Orthop. Res. 14, 639–646 (1996).

10. Patterson, R. M., Williams, L., Andersen, C. R., Koh, S. & Viegas, S. F. Carpal Kinematics During Simulated Active and Passive Motion of the Wrist. J. Hand Surg. Am. 32, 1013–1019 (2007).

11. Carelsen, B. et al. Detection of in vivo dynamic 3-D motion patterns in the wrist joint. IEEE Trans. Biomed. Eng. 56, 1236–44 (2009).

12. Foumani, M. et al. In-vivo three-dimensional carpal bone kinematics during flexion-extension and radio-ulnar deviation of the wrist: Dynamic motion versus step-wise static wrist positions. J. Biomech. 42, 2664–2671 (2009).

13. Kobayashi, M. et al. Normal kinematics of carpal bones: A three-dimensional analysis of carpal bone motion relative to the radius. J. Biomech. 30, 787–793 (1997).

14. Woltring, H. J. & Huiskes, R. 3-D attitude representation of human joints: A standardization proposal. J. Biomech. 27, 1399–1414 (1994).

15. Neu, C. P., Crisco, J. J. & Wolfe, S. W. In vivo kinematic behavior of the radio-capitate joint during wrist flexion-extension and radio-ulnar deviation. J. Biomech. 34, 1429–1438 (2001).

16. Short, W. H., Werner, F. W., Fortino, M. D., Palmer, A. K. & Mann, K. A. A dynamic biomechanical study of scapholunate ligament sectioning. J. Hand Surg. Am. 20, 986–999 (1995).

17. Short, W. H., Werner, F. W., Fortino, M. D. & Mann, K. A. Analysis of the kinematics of the scaphoid and lunate in the intact wrist joint. Hand Clin. 13, 93–108 (1997).

18. Short, W. H., Werner, F. W., Green, J. K., Weiner, M. M. & Masaoka, S. The effect of sectioning the dorsal radiocarpal ligament and insertion of a pressure sensor into the radiocarpal joint on scaphoid and lunate kinematics. J. Hand Surg. Am. 27, 68–76 (2002).

19. Berdia, S., Short, W. H., Werner, F. W., Green, J. K. & Panjabi, M. The hysteresis effect in carpal kinematics. J. Hand Surg. Am. 31, 594–600 (2006).

20. Moojen, T. M. et al. In vivo analysis of carpal kinematics and comparative review of the literature. J. Hand Surg. Am. 28, 81–7 (2003).

21. Wolfe, S. W., Neu, C. & Crisco, J. J. In vivo scaphoid, lunate, and capitate kinematics in flexion and in extension. J. Hand Surg. Am. 25, 860–869 (2000).

22. Wolfe, S. W., Crisco, J. J., Orr, C. M. & Marzke, M. W. The Dart-Throwing Motion of the Wrist: Is It Unique to Humans? J. Hand Surg. Am. 31, 1429–1437 (2006).

23. Crisco, J. J. et al. In vivo radiocarpal kinematics and the dart thrower's motion. J. Bone Joint Surg. Am. 87, 2729–40 (2005).

24. Werner, F. W., Green, J. K., Short, W. H. & Masaoka, S. Scaphoid and lunate motion during a wrist dart throw motion. J. Hand Surg. Am. 29, 418–422 (2004).

25. Moritomo, H. et al. Capitate-based kinematics of the midcarpal joint during wrist radioulnar deviation: An in vivo three-dimensional motion analysis. J. Hand Surg. Am. 29, 668–675 (2004).

2

Seven Deadly Sins

**Wealth without work
Pleasure without
conscience
Science without
humanity
Knowledge without
character
Politics without
principle
Commerce without
morality
Worship without
sacrifice."**

Mahatma Gandhi

chapter 3

In-vivo three-dimensional carpal bone kinematics during flexion-extension and radio-ulnar deviation of the wrist: Dynamic motion versus stepwise static wrist positions

3

Abstract

An *in-vivo* approach to the measurement of three-dimensional motion patterns of carpal bones in the wrist may have future diagnostic applications, particularly for ligament injuries of the wrist. Static methods to measure carpal kinematics *in-vivo* only provide an approximation of the true kinematics of the carpal bones. This study is aimed at finding the difference between dynamically and statically acquired carpal kinematics.

For eight healthy subjects, static and a dynamic measurement of the carpal kinematics was performed for a flexion-extension and a radio-ulnar deviation movement. Dynamic scans were acquired by using a 4 dimensional x-ray imaging system during an imposed cyclic motion. To assess static kinematics of the wrists, three-dimensional rotational X-ray scans were acquired during stepwise flexion-extension and radio-ulnar deviation. The helical axis rotations and the rotation components. i.e. flexion-extension, radio-ulnar deviation and pro-supination were the primary parameters. Linear mixed model statistical analysis was used to determine the significance of the difference between the dynamically and statically acquired rotations of the carpal bones.

Small and in most cases negligible differences were observed between the dynamic motion and the step-wise static motion of the carpal bones. The conclusion is that in the case of individuals without any pathology of the wrist, carpal kinematics can be studied either dynamically or statically. Further research is required to investigate the dynamic in-vivo carpal kinematics in patients with dynamic wrist problems.

Introduction

An *in-vivo* approach to measurements of carpal kinematics may have future diagnostic applications, particularly following ligament injuries. Since complex changes in three-dimensional (3D) orientation and the position of carpal bones can occur during dynamic movement, various authors have pleaded for techniques which can image and analyze dynamic 3D information of a moving joint in-vivo[1,2].

To acquire *in-vivo* carpal kinematics, static CT- and MR-based methods were introduced to image and detect 3D carpal movements during a stepwise motion of the wrist[1,3–8]. Although *in-vivo* carpal kinematics can be measured by use of static methods, the resulting kinematics may only provide an approximation of the true *in-vivo* kinematics of the carpal bones. It has been suggested that the kinematics of the wrist that are acquired in a step-wise fashion may differ from those during a continuous dynamic motion[2,6]. Tendon contractions and time-dependent soft tissue properties may alter the kinematical outcomes during motion. Recently, Carelsen[9,10] introduced a method which allows acquiring dynamic *in-vivo* carpal kinematics by using the four-dimensional rotational x-ray imaging system (4D-RX). The aim of this study is to evaluate the differences between the dynamically and statically acquired carpal kinematics. The approach is to use the 4D-RX method both dynamically and statically and reconstruct the rotations and translations of the carpal bones in the wrist in healthy volunteers.

Materials and methods
Participants
The right wrists of eight healthy subjects (4 female/4 male, average age 23.5 years, range 22-26 years) were investigated in this study. The subjects had no history of wrist injury. This study was approved

by the Medical Ethical Committee of our hospital and informed consent was obtained from each subject.

Wrist motion

Wrists were scanned during flexion-extension motion and radio-ulnar deviation of the wrist. For dynamic scans, participants were scanned during an imposed motion of the wrist using the 4D-RX system. The 4D-RX method is combined with the so called handshaker. The handshaker consists of a detachable drive unit and a framework in which the drive unit is placed to impose flexion-extension and radio-ulnar deviation on the hand. The motor of the drive unit is attached to two parallel arms in a spatial linkage arrangement with carbon fiber rods to create a rotational axis (figure 1).

To impose a cyclic motion to the joint, the forearm was placed in a handshaker with the shoulder abducted 45 degrees and the elbow flexed 90 degrees. To allow the hand to follow the movements of the handshaker, the participants were asked to grasp the hand piece. To prevent a locked wrist, the forearms were placed in an axially slidable table allowing a free motion.

Both static and dynamic scans were subsequently obtained without releasing the arm between the experiments. While acquiring the static images, the handshaker was used to facilitate a fluent wrist motion between each position and to minimize the difference in arm and hand position and orientation between the experiments. A series of static scans were obtained during stepwise flexion-extension motion, from 40 degree extension to 40 degree flexion and back, in 10 degree increments. For radio-ulnar deviation, 3D images were acquired during a stepwise motion from 15 degrees radial deviation to 30 degrees ulnar deviation and back. For the ulnar part of the imposed trajectory motion steps of 10 degrees were selected. For the radial part motion steps of 7.5 degrees were selected.
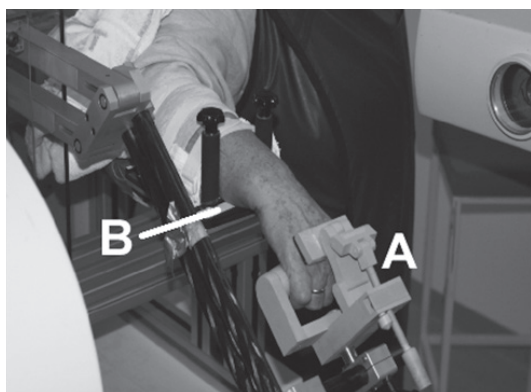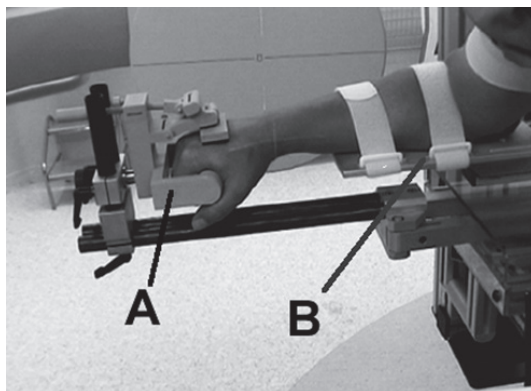
Figure 1: Handshaker: the wrist is brought into motion with the specially developed handshaker-device while rotational X-ray images are acquired. To allow the hand to follow the movements of the handshaker, the participants were asked to grasp the hand piece **(A)**. To prevent a locked wrist, the forearm was placed in an axially slidable table **(B)** allowing it to move freely. Left: view of the handshaker configuration during the radio-ulnar deviation. Right: forearm is placed in the handshaker for an imposed flexion-extension motion.

Image acquisition

For reconstruction of the bone geometry, CT images of the wrist were acquired while the hand was in a neutral position (MX8000 CT scanner, Philips Healthcare, the Netherlands). Subsequently, dynamic images were acquired by the previously described 4-Dimensional Rotational X ray (4D-RX) imaging method by using a modified rotational 3D-RX system (BV Pulsera, Philips Healthcare, The Netherlands).

For acquiring 4D-RX scans, 975 projection images were made during a cyclic motion of the wrist from which a set of 20 volume reconstructions were obtained. Each volume reconstruction belongs to a certain position of the hand during dynamic motion.

For the static images, static scans were acquired at different poses by using the same rotational 3D-RX system whereby volume reconstructions were obtained for each position. With a maximum effective dose of 0.1 mSv for a CT scan, 0.001 mSv for a single static 3D-RX scan and 0.026 mSv for a dynamic scan, the experimental setup was associated with a minor radiation exposure dose[11].

Segmentation of carpal bones and radius

The segmentation of the carpal bones and the radius from the CT image was performed by a region growing algorithm. Starting from a seed point, an average gray value was calculated within a small sphere (radius 1.5 voxel). Whenever this averaged gray value was higher than a predefined gray level of the bones, this voxel was classified as the bone tissue and assigned to the bone region in the process of growing. Seed points were placed manually starting with the most clearly visible bones. The segmented bones were used as inhibition area for the remaining bones during the segmentation process. The segmen-tation result comprises the high intensity bone voxels at the rim of the bone but does not always comprise the complete inner bone structure. Therefore, a binary closing operation is used in order to close the outline of the bones.

Estimation of translations and rotations of individual bones

To estimate the 3 translations and 3 rotations of the individual bones relative to those in the neutral position, we registered the segmented boundary voxels of each carpal bone to the corresponding bones in the volumes of the dynamic scan (4D-RX). The translations and rotations of the carpal bones in the static image series were estimated in a similar fashion. For this purpose we used a stack of double contours as bone boundary characterization: one outside the bone boundary (low gray value) and one on a short distance within the bone on the hard rim (high gray value). The method to register the segmented bone contour with their dynamic counterparts searches for the translations and rotations that maximize the cross correlation between the gray values of the double contours and those in the 4D RX volume.

The movement of the carpal bones between two successive time frames of the dynamic scan will be small. The result of a certain frame is used as an initialization of the next frame to achieve a fully automated registration procedure after initialization of the first registration.

The motion parameters as obtained from a segmented CT image and a 4D-RX image has a repeatability of 0.22±0.08 mm for translations and 0.5±0.1 degrees for rotations[10].

Describing kinematics

The motion parameters of the individual carpal bones were expressed relative to an anatomically based radial coordinate system (Figure 2) similar to that of *Kobayashi et al.*[12]. The longitudinal axis of the radius (Z-axis) was defined as the center line of a cylinder fitted through the segmented radius. The direction of the X-axis was defined by a line perpendicular to the Z-axis and passing through the tip of the radial styloid. The Y-axis was determined as the line perpendicular to the X- and the Z-axes. The point where the longitudinal axis of the radius intersects with

the cortical bone surface was defined as the origin of the global coordinate system. The coordinate axes of the carpal bones were defined as being parallel to the radial coordinate system for the neutral position of the wrist.

Carpal displacements are reported to be primarily rotations. The translations of carpal bones defined as translations along the helical axes were reported to be very small[5,13,14]. Therefore, only rotation parameters were evaluated in this study. For the rotation parameters, the attitude vector was used[15]. The finite helical axis is determined for the motion between the neutral position as the reference and each position during motion. The attitude vector is then defined as the multiplication of the rotation about the helical axis and the normal vector of the helical axis. The components of the attitude vector relative to the global coordinate system describe the component rotations.

The global wrist motion was defined as the rotation of the capitate with respect to the radius[16]. This is justified by findings of other authors since negligible differences were reported between the capitate and third metacarpal motion[13]. Flexion (+) and extension (-) were defined as rotations around the X-axis, radial (+) and ulnar (-) deviation as rotations around the Y-axis and pronation (-) and supination (+) as rotations around the Z-axis. For the flexion-extension motion, the radio-capitate X-component of the attitude vector was defined as the global wrist motion. For radio-ulnar deviation the radio-capitate Y-rotation component was defined as the global motion of the wrist. The scan acquired of the wrist in a neutral position during the static scan series was used for defining the neutral position of the wrist for both the dynamic and static scans. Neutral wrist position was defined clinically with the third metacarpal in line with the longitudinal axis of the radius.

For comparison with the literature, the average rotations of scaphoid, lunate and capitate of all subjects are reported with standard deviations at every 5 degrees of global wrist motion, for both the dynamically and statically acquired data.
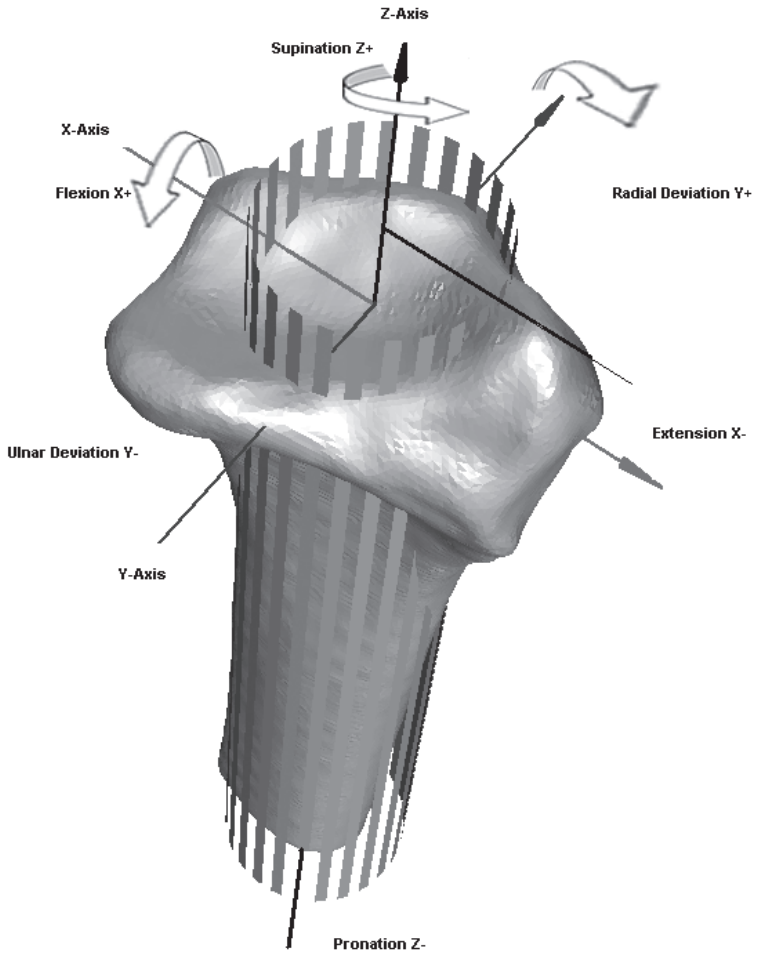
Figure 2: Palmar view of the anatomically based radial coordinate system. The direction of the carpal rotation is indicated by flexion, extension, pronation, supination, and radial and ulnar deviation.

Motion Direction Effect

Carpal bones are reported to show a motion direction effect or hysteresis, in the sense that the amount of carpal rotation at a particular wrist position is different depending on the direction the wrist is moved to get to that position[17–20]. The motion direction effect was calculated for both dynamically and statically acquired rotations, by computing differences between the two opposite motion trajectories.

Statistical Analysis

Each 4D-RX scan provides kinematic data for 20 different positions within one complete motion cycle. For the statically acquired scans, a total of 11 scans were acquired during radio-ulnar deviation, and 17 stepwise scans were acquired during flexion-extension. Both dynamically and statically acquired values were linearly interpolated to obtain data at every 5 degrees of global wrist motion.

To investigate the differences between the dynamically and statically acquired kinematics for each carpal bone, the actual helical rotations and the flexion-extension (X), radio-ulnar deviation (Y) and pro-supination (Z) rotation components of the attitude vector at every 5 degrees of global wrist motion, were defined as the primary outcome variables.

The linear mixed model statistical analysis was used to determine the significance of the difference between the dynamic and static measurements, assuming a first order autocorrelation between serial measurements which was observed during the analysis of the data.

Linear mixed models were also used to analyze the motion direction effect for the dynamically and statically measured rotations for each carpal bone. The differences of the actual helical rotations, and the rotation components between the 2 curves that represent opposite directions of wrist motion were defined as the primary outcome values. P-values of less than 0.05 were considered significant.

	Mean difference [°]	Std. Error [°]	95% Confidence Interval [°]	P-value
Lunate				
• Total rotation around the helical axis	0.45	0.42	-0.41: 1.31	0.294
• Flexion-extension (X)	-0.16	0.42	-1.02 : 0.69	0.697
• Radio-ulnar deviation (Y)	-0.07	0.21	-0.50 : 0.37	0.753
• Pro-supination (Z)	-0.01	0.30	-0.63 : 0.60	0.964
Scaphoid				
• Total rotation around the helical axis	-0.12	0.38	-0.90: 0.66	0.759
• Flexion-extension (X)	-0.22	0.37	-0.97 : 0.52	0.543
• Radio-ulnar deviation (Y)	0.44	0.23	-0.05 : 0.92	0.075
• Pro-supination (Z)	-0.03	0.27	-0.61 : 0.64	0.957
Capitate				
• Total rotation around the helical axis	0.37	0.22	-0.08: 0,83	0.099
• Flexion-extension (X)	NA	NA	NA	NA
• Radio-ulnar deviation (Y)	-0.02	0.41	-0.85 : 0.80	0.949
• Pro-supination (Z)	-0.08	0.27	-0.63 : 0.47	0.767
All carpal bones together				
• Total rotation around the helical axis	0.82	0.34	0.14 : 1.47	**0.018**
• Flexion-extension (X)	-0.35	0.11	-0.57 : -0.14	**<0.001**
• Radio-ulnar deviation (Y)	-.046	0.13	-0.30 : 0.21	0.722
• Pro-supination (Z)	-0.18	0.10	-0.38 : 0.01	0.058

Table 1: Lunate, scaphoid and capitate rotation difference between the dynamically and statically acquired kinematics during the flexion-extension. Analyses are provided for the differences of the actual helical rotations and the flexion-extension (X), radio-ulnar deviation (Y) and pro-supination (Z) rotation components.

Results

Dynamic motion versus statically acquired carpal positions

During flexion and extension there was a small but statistically significant difference between the dynamically and quasi-dynamically acquired rotations for all carpal bones grouped together (0.82 degrees (95% CI: 0.14:1.47, P=0.018)) (Table 1). The mean difference of helical rotation between the dynamic and statically acquired rotation parameters for lunate (0.45 degrees (95% CI: -0.41:1.32, P=0.294)), scaphoid (-0.12 degrees (95% CI: -0.90:0.66, P=0.759)) and capitate (0.37 degrees (95% CI: -0.08:0.83, P=0.759)) were statistically not significant (table 1). We found no statistically significant difference between the dynamically and statically acquired flexion-extension-, radioulnar- and pro- supination rotation components of the lunate, scaphoid and capitate during the flexion-extension.

Regarding the kinematics during radio-ulnar deviation of the wrist, we found that the mean difference of helical rotation between the dynamic and statically acquired rotation parameters all carpal bones together (-0.19 degrees (95% CI: -0.52:0.14, P=0.252)) were statistically not significant (table 2). The mean differences of helical rotation between the dynamic and statically acquired rotation parameters for lunate (0.47 degrees (95% CI: -0.37:1.31, P=0.254)), scaphoid (0.03 degrees (95% CI: -0.82:0.88, P=0.939)), capitate (-0.64 degrees (95% CI: -1.48:0.20, P=0.123)) were statistically not significant. We found no statistically significant difference between the dynamically and statically acquired flexion-extension-, radioulnar- and pro- supination rotation components of the lunate, scaphoid and capitate during the radioulnar deviation.

Carpal kinematics: flexion-extension

During flexion and extension, the scaphoid and lunate follow the motion of capitate (Figure 3). During wrist flexion, the scaphoid flexes and pronates slightly, while during wrist extension, the

	Mean difference [°]	Std. Error [°]	95% Confidence Interval [°]	P-value
Lunate				
• Total rotation around the helical axis	0.47	0.40	-0.37 : 1.31	0.254
• Flexion-extension (X)	0.16	0.46	-0.79 : 1.11	0.726
• Radio-ulnar deviation (Y)	-0.54	0.35	-1.38 : 0.31	0.185
• Pro-supination (Z)	0.27	0.25	-0.24 : 0.78	0.286
Scaphoid				
• Total rotation around the helical axis	0.03	0.40	-0.82 : 0.88	0.939
• Flexion-extension (X)	0.37	0.50	-0.67 : 1.40	0.472
• Radio-ulnar deviation (Y)	0.28	0.15	-0.04 : 0.60	0.082
• Pro-supination (Z)	-0.03	0.16	-0.36 : 0.31	0.857
Capitate				
• Total rotation around the helical axis	-0.64	0.39	-1.48 : 0.20	0.123
• Flexion-extension (X)	0.78	0.61	-0.47 : 2.03	0.210
• Radio-ulnar deviation (Y)	NA	NA	NA	NA
• Pro-supination (Z)	0.65	0.32	-0.01: 1.32	0.053
All carpal bones together				
• Total rotation around the helical axis	-0.19	0.17	-0.52 : 0.14	**0.252**
• Flexion-extension (X)	0.12	0.21	-0.29: 0.54	**0.556**
• Radio-ulnar deviation (Y)	0.06	0.08	-0.11: 0.22	0.500
• Pro-supination (Z)	0.15	0.11	-0.07: 0.37	0.184

Table 2: Lunate, scaphoid and capitate rotation difference between the dynamically and statically acquired kinematics during the radio-ulnar deviation. Analyses are provided for the differences of the actual helical rotations and the flexion-extension (X), radio-ulnar deviation (Y) and pro-supination (Z) rotation components.

Figure 3: Lunate, scaphoid and capitate average flexion-extension, radioulnar and pro- supination components of the rotation during the overlapping range of flexion-extension for all 8 participants. Standard deviations of the mean are provided for begin and end values and at every 5 degrees of global wrist motion. Dynamic measurements are plotted as red lines, while the blue lines represent the static measurements. Capitate rotations are plotted in black dotted lines as lines of identity.
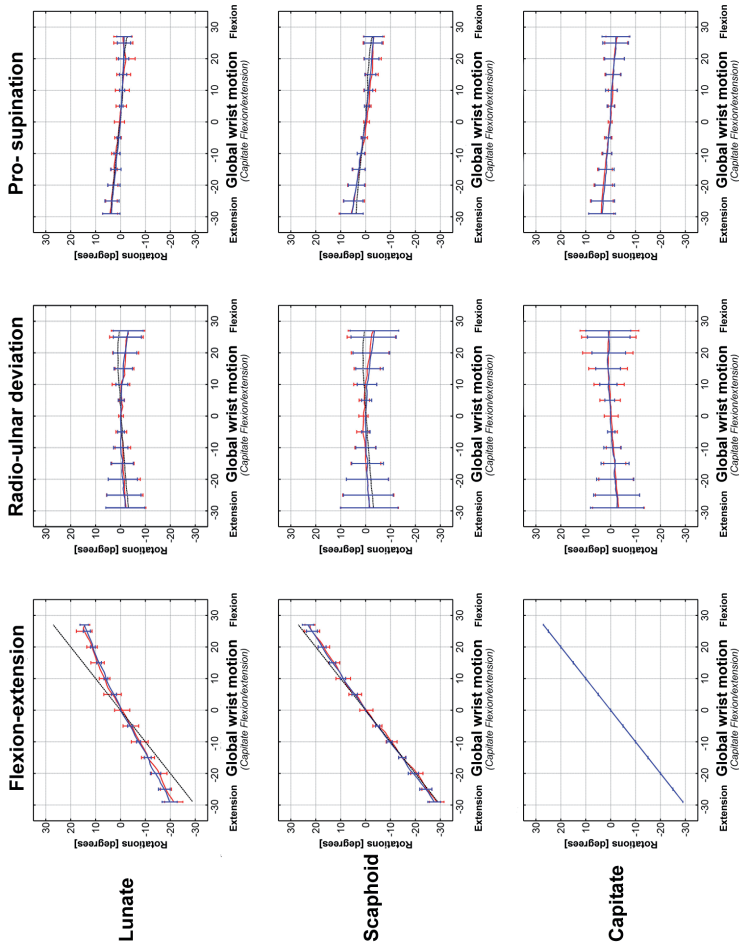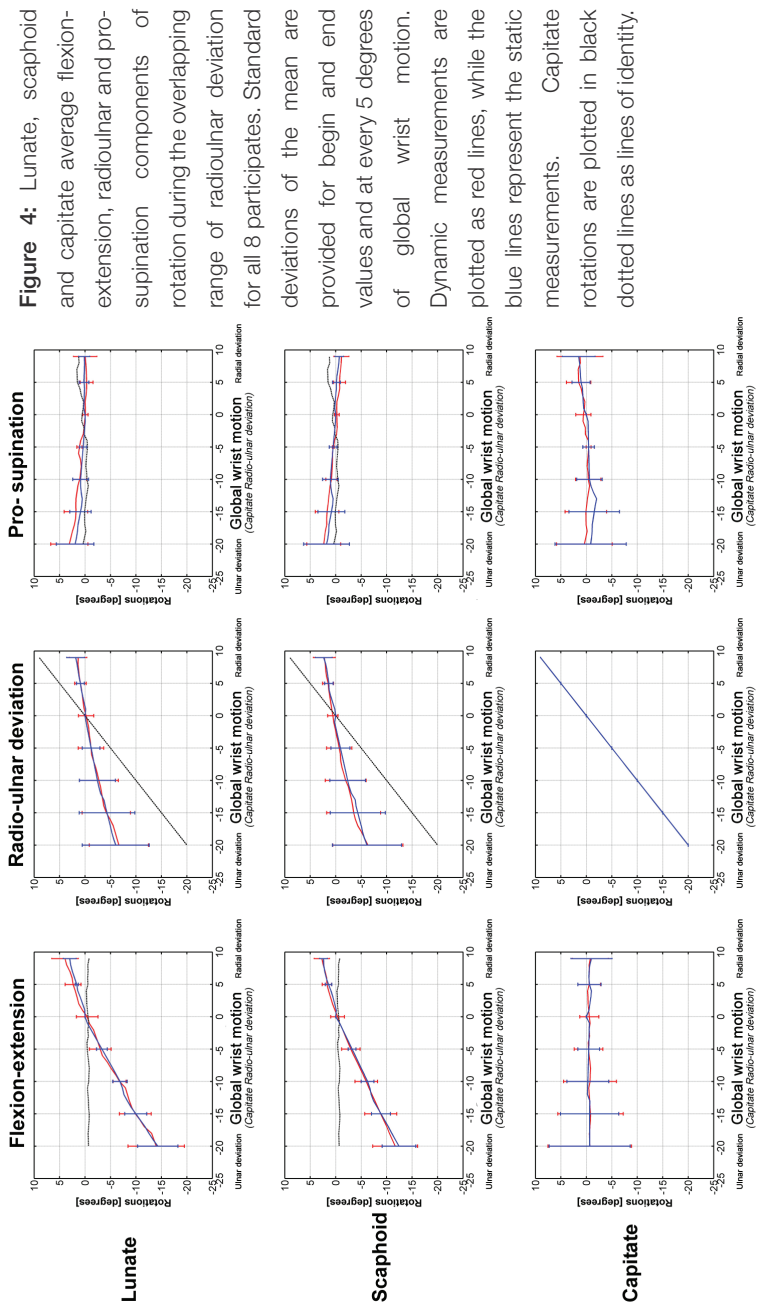
Figure 4: Lunate, scaphoid and capitate average flexion-extension, radioulnar and pro-supination components of rotation during the overlapping range of radioulnar deviation for all 8 participates. Standard deviations of the mean are provided for begin and end values and at every 5 degrees of global wrist motion. Dynamic measurements are plotted as red lines, while the blue lines represent the static measurements. Capitate rotations are plotted in black dotted lines as lines of identity.

scaphoid extends and supinates. The radio-ulnar deviation of the lunate, scaphoid and capitates was variable between the subjects. The lunate basically shows the same movements as the scaphoid but to a lesser degree. While the scaphoid follows the capitate rotations more closely the lunate lags behind allowing intercarpal motion between the scaphoid (scaphocapitate slope=0.93) and lunate (lunocapitate slope = 0.67).

Carpal kinematics: radio-ulnar deviation

Both for the dynamic and static radio-ulnar deviation the rotations of the proximal and the distal rows showed dissimilar rotation patterns (Figure 4). Radio- ulnar deviation was dominated by midcarpal motion since the carpal bones of the distal row followed the global wrist motion during the radio-ulnar deviation. In the case of the proximal row the scaphoid and lunate main rotations were primarily flexion and extension. The scaphoid and lunate rotate into flexion and radial deviation during radial deviation while during the ulnar deviation the scaphoid and lunate extend and rotate ulnary. The intercarpal motion between scaphoid and lunate both during radial and ulnar deviation is very small; scapholunate slope difference was less then 0.01.

Motion Direction Effect

During flexion-extension, dynamically acquired rotation para-meters of all carpal bones together showed very small motion direction effects which were only significant for the flexion-extension component of the attitude vector (-0.53 degrees (95% CI: -0.79:-0.27. P<0.001). No statistically significant differences were observed between opposite directions of wrist motion during static measurements. The rotation parameters of lunate, scaphoid and capitate show statistically no difference between opposite directions of wrist motion.

During the radio-ulnar deviation dynamically acquired radio-ulnar rotation parameters of all carpal bones together showed very small

motion direction effects to be found at the flexion-extension (0.43 degrees, 95% CI: 0.12:-0.74, P=0.007) and pro-supination-rotation (0.17 degrees, 95% CI: -0.56:-0.09, P=0.007) components. During the quasi-dynamically acquired measurements small significant differences were seen in the flexion-extension rotation component (0.59 degrees, 95% CI: 0.32:0.85, P<0.001). The acquired rotation parameters of lunate, scaphoid and capitate show statistically no significant difference between opposite directions of wrist motion.

Discussion

The goal of the study was to investigate the differences in carpal kinematics between dynamically and statically acquired wrist flexion-extension and radio-ulnar deviation. Eight subjects underwent dynamic 4D-RX and static 3D-RX scans in the same experimental setup without releasing the wrists throughout the experiments. Very small but mostly not-significant differences were observed between the dynamic scans and wrists scanned during a static motion.

The kinematics of the selected carpal bones were in agreement with previously published data. The kinematics for flexion extension and radio-ulnar deviation were within the same range as reported by Moojen et al.[2] and Wolfe et al[6], who also provided a review of other data from literature. Although scaphoid and lunate follow the capitate during the flexion and extension the lunate rotations lag behind showing some intercarpal motion between scaphoid and lunate.

During radio-ulnar deviation the scaphoid and lunate moved together showing extension in ulnar deviation and flexion in radial deviation with negligible intercarpal motions between the two bones. These findings are also in agreement with previous reports that show that during radio-ulnar deviation the motion between scaphoid and lunate is coupled[18,21].

	Lunate				Scaphoid				Capitate				All carpal bones together			
	Mean difference [°]	Std. Error [°]	95% Confidence Interval [°]	P-value	Mean difference [°]	Std. Error [°]	95% Confidence Interval [°]	P-value	Mean difference [°]	Std. Error [°]	95% Confidence Interval [°]	P-value	Mean difference [°]	Std. Error [°]	95% Confidence Interval [°]	P-value
Dynamic Flexion extension																
Flexion-extension (X)	-0.58	0.43	-1.54 : 0.38	0.210	0.10	0.44	-0.87 : 1.20	0.727	NA	NA	NA	NA	-0.53	0.13	-0.79 : -0.27	**<0.001**
Radioulnar deviation (Y)	-0.30	0.39	-1.17 : 0.59	0.480	0.02	0.32	-0.69 : 0.73	0.947	0.08	0.27	-0.34 : 0.26	0.846	0.01	0.11	-0.22 : 0.23	0.966
Pro-supination (Z)	-0.15	0.34	-0.90 : 0.61	0.672	0.14	0.14	-0.31 : 0.59	0.510	0.34	0.35	-0.48 : 1.15	0.365	0.17	0.11	-0.05 : 0.39	0.125
Total helical rotation difference	0.17	0.49	-0.91 : 1.26	0.732	0.16	0.60	-1.14 : 1.47	0.788	0.02	0.14	-0.29 : 0.33	0.901	0.16	0.15	-0.15 : 0.46	0.313
Static Flexion extension																
Flexion-extension (X)	0.26	0.24	-0.26 : 0.78	0.302	0.08	0.23	-0.43 : 0.59	0.723	NA	NA	NA	NA	0.11	0.06	-0.02 : 0.23	0.096
Radioulnar deviation (Y)	0.17	0.14	-0.14 : 0.48	0.250	0.09	0.14	-0.21 : 0.40	0.514	0.26	0.29	-0.39 : 0.90	0.398	0.16	0.09	-0.02 : 0.34	0.084
Pro-supination (Z)	-0.04	0.11	-0.28 : 0.20	0.715	-0.07	0.13	-0.36 : 0.21	0.576	-0.06	0.19	-0.47 : 0.36	0.776	-0.05	0.06	-0.18 : 0.08	0.432
Total helical rotation difference	0.06	0.28	-0.53 : 0.67	0.808	-0.03	0.24	-0.54 : 0.48	0.906	-0.14	0.07	-0.30 : 0.01	0.059	-0.03	0.07	-0.17 : 0.11	0.665
Dynamic Radio-ulnar deviation																
Flexion-extension (X)	-0,58	0.37	-1.42 : 0.26	0.150	0.50	0.49	-0.68 : 1.67	0.350	0.09	0.16	-0.22 : 0.37	0.506	0.43	0.15	0.12 : 0.74	**0.007**
Ulnar-radial deviation (Y)	-0.34	0.26	-0.95 : 0.26	0.228	-0.53	0.31	-1.25 : 0.20	0.130	NA	NA	NA	NA	-0.08	0.17	-0.36 : 0.19	0.539
Pro-supination (Z)	-0.24	0.31	-0.96 : 0.48	0.464	0.20	0.18	-0.20 : 0.60	0.275	-0.44	0.33	-1.22 : 0.33	0.221	-0.33	0.12	-0.56 : -0.09	**0.007**
Total helical rotation difference	0.63	0.35	-0.17 : 1.41	0.107	0.20	0.33	-0.59 : 0.99	0.565	0.13	0.22	-0.38 : 0.64	0.565	0.15	0.17	-0.19 : 0.49	0.379

Table 3: Continued

	Lunate				Scaphoid				Capitate				All carpal bones together			
	Mean difference [°]	Std. Error [°]	95% Confidence Interval [°]	P-value	Mean difference [°]	Std. Error [°]	95% Confidence Interval [°]	P-value	Mean difference [°]	Std. Error [°]	95% Confidence Interval [°]	P-value	Mean difference [°]	Std. Error [°]	95% Confidence Interval [°]	P-value
Static Radio-ulnar deviation																
Flexion-extension (X)	0.31	0.29	-0.33 : 0.96	0.302	0.51	0.37	-0.31 : 1.33	0.196	0.73	0.40	-0.16 : 1.62	0.098	0.59	0.13	0.32 : 0.85	**<0.001**
Radioulnar deviation (Y)	0.08	0.12	-0.19 : 0.35	0.509	-0.07	0.16	-0.43 : 0.28	0.663	NA	NA	NA	NA	-0.07	0.05	-0.17 : 0.02	0.130
Pro-supination (Z)	0.01	0.13	-0.27 : 0.30	0.916	0.02	0.16	-0.33 : 0.37	0.896	0.09	0.27	-0.51 : 0.70	0.740	0.01	0.09	-0.16 : 0.18	0.872
Total helical rotation difference	-0.42	0.29	-1.06 : 0.22	0.179	-0.58	0.31	-1.28 : 0.12	0.097	-0.17	0.23	-0.67 : 0.33	0.476	-0.28	0.10	-0.49 : -0.07	**0.009**

Table 3: The amount of carpal rotation at a particular wrist position is different depending on the direction the wrist is moved to get to that position. The mean difference of the lunate, scaphoid and capitate X-, Y- and Z- rotation components between the two directions is provided. The motion direction difference between the two directions is given for the dynamically and statically acquired datasets during flexion, extension and radio-ulnar deviation.

The variability of the of radio-ulnar deviation of the carpal bones with flexion between individuals was also previously reported[1,2,22]. Although some authors blamed this finding to positioning errors of the wrists during the experiments, a more reasonable explanation would be that actual rotations do not occur precisely around the anatomically defined axes of the radial coordinate system as was suggested by Kaufmann et al.[22]. While defining a radius based coordinate system, only the bony geometry of the radius as acquired from CT images was taken into account. Because of variable location of bony landmarks, such as the position of the radial styloid some error may be introduced as regard to the orientation of the coordinate axes. Other explanation is that cartilage geometry is not taken into account for defining the coordinate axes. Not the bone geometry but the articulating cartilage geometry determines the joint kinematics. It can be argued that inter-individual variability may be reduced by selecting a coordinate system based on cartilage geometry.

A clear motion direction effect or hysteresis, as previously reported by other authors was not found[17–20]. In contrast to the *in-vitro* methods to study carpal kinematics by Berdia et al.[20] we found that *in-vivo* carpal kinematics show very small and in most cases negligible motion direction effects. Opposite to Berdia et al.[20] who used a rectangular integration method to calculate the area between the two curves, we chose a statistical method to estimate the average difference between the two trajectory curves. This makes it possible to correct the results for variable ranges of global wrist motion between different subjects. Future studies will provide more information regarding the existence of motion direction effects in patients with wrist instabilities.

This study confirms that the previous experiments with static stepwise-acquired carpal kinematics during flexion-extension and radio-ulnar deviation approximate the true dynamic motion in healthy wrists. The conclusion of this study is that in the case of individuals without any pathology of the wrist, carpal kinematics

can be studied either dynamically or statically. However, as in the case of scapholunate or lunotriquetral ligament dissociations abrupt dynamic changes such as clicks and clunks cannot be detected with static measurement methods. Therefore, further research is required to investigate the dynamic *in-vivo* carpal kinematics in patients with dynamic wrist problems

3

Reference List

1. Crisco, J. J., McGovern, R. D. & Wolfe, S. W. Noninvasive technique for measuring in vivo three-dimensional carpal bone kinematics. J. Orthop. Res. 17, 96–100 (1999).

2. Moojen, T. M. et al. In vivo analysis of carpal kinematics and comparative review of the literature. J. Hand Surg. Am. 28, 81–87 (2003).

3. Feipel, V. & Rooze, M. Three-dimensional motion patterns of the carpal bones: an in vivo study using three-dimensional computed tomography and clinical applications. Surg. Radiol. Anat. 21, 125–31 (1999).

4. Snel, J. G. et al. Quantitative in vivo analysis of the kinematics of carpal bones from three-dimensional CT images using a deformable surface model and a three-dimensional matching technique. Med. Phys. 27, 2037–47 (2000).

5. Wolfe, S. W., Neu, C. & Crisco, J. J. In vivo scaphoid, lunate, and capitate kinematics in flexion and in extension. J. Hand Surg. Am. 25, 860–9 (2000).

6. Wolfe, S. W., Neu, C. & Crisco, J. J. In vivo scaphoid, lunate, and capitate kinematics in flexion and in extension. J. Hand Surg. Am. 25, 860–869 (2000).

7. Sun, J. S. et al. In vivo kinematic study of normal wrist motion: an ultrafast computed tomographic study. Clin. Biomech. (Bristol, Avon) 15, 212–6 (2000).

8. Moritomo, H. et al. Capitate-based kinematics of the midcarpal joint during wrist radioulnar deviation: an in vivo three-dimensional motion analysis. J. Hand Surg. Am. 29, 668–75 (2004).

9. Carelsen, B. et al. 4D rotational x-ray imaging of wrist joint dynamic motion. Med. Phys. 32, 2771–6 (2005).

10. Carelsen, B. et al. Detection of in vivo dynamic 3-D motion patterns in the wrist joint. IEEE Trans. Biomed. Eng. 56, 1236–44 (2009).

11. ICRP. The 2007 recommendations of the International Commission on Radiological Protection. Ann. ICRP 37, 1–332 (2007).

12. Kobayashi, M. et al. Normal kinematics of carpal bones: A three-dimensional analysis of carpal bone motion relative to the radius. J. Biomech. 30, 787–793 (1997).

13. Neu, C. P., Crisco, J. J. & Wolfe, S. W. In vivo kinematic behavior of the radio-capitate joint during wrist flexion-extension and radio-ulnar deviation. J. Biomech. 34, 1429–1438 (2001).

14. Kaufmann, R. et al. Kinematics of the midcarpal and radiocarpal joints in radioulnar deviation: an in vitro study. J. Hand Surg. Am. 30, 937–42 (2005).

15. Woltring, H. J. & Huiskes, R. 3-D attitude representation of human joints: A standardization proposal. J. Biomech. 27, 1399–1414 (1994).

16. De Lange, A., Kauer, J. M. & Huiskes, R. Kinematic behavior of the human wrist joint: a roentgen-stereophotogrammetric analysis. J. Orthop. Res. 3, 56–64 (1985).

17. Short, W. H., Werner, F. W., Fortino, M. D., Palmer, A. K. & Mann, K. A. A dynamic biomechanical study of scapholunate ligament sectioning. J. Hand Surg. Am. 20, 986–999 (1995).

18. Short, W. H., Werner, F. W., Fortino, M. D. & Mann, K. A. Analysis of the kinematics of the scaphoid and lunate in the intact wrist joint. Hand Clin. 13, 93–108 (1997).

19. Short, W. H., Werner, F. W., Green, J. K., Weiner, M. M. & Masaoka, S. The effect of sectioning the dorsal radiocarpal ligament and insertion of a pressure sensor into the radiocarpal joint on scaphoid and lunate kinematics. J. Hand Surg. Am. 27, 68–76 (2002).

20. Berdia, S., Short, W. H., Werner, F. W., Green, J. K. & Panjabi, M. The hysteresis effect in carpal kinematics. J. Hand Surg. Am. 31, 594–600 (2006).

21. Ruby, L. K., Cooney, W. P., An, K. N., Linscheid, R. L. & Chao, E. Y. Relative motion of selected carpal bones: a kinematic analysis of the normal wrist. J. Hand Surg. Am. 13, 1–10 (1988).

22. Kaufmann, R. A. et al. Kinematics of the Midcarpal and Radiocarpal Joint in Flexion and Extension: An In Vitro Study. J. Hand Surg. Am. 31, 1142–1148 (2006).

3

The saddest aspect of life right now is that science gathers knowledge faster than society gathers wisdom.

Isaac Asimov

chapter 4

In-vivo dynamic and static three-dimensional joint space distance maps for assessment of cartilage thickness in the radiocarpal joints

4

Abstract

Background: The assessment of the joint space thickness is an important clinical parameter for diagnosing osteoarthritis. The accuracy of joint space thickness evaluation from radiographs is limited due to anatomical complexity of the wrist. We propose using distance maps estimated from 3-dimensional and 4-dimensional images reflecting joint space thickness distribution over the relevant part of the articular surface.

Methods: In this paper we investigate the difference between joint space thicknesses acquired from dynamic distance maps to static distance maps. A dynamic distance map gives for every point on a subchondral bone surface the shortest distance to the opposing subchondral bone surface during wrist motion. We hypothesize that the joint space thickness calculated from dynamic distance maps provide a better reflection of the functional joint space thickness. The diagnostic potential of the dynamic joint space thickness measurement is illustrated by comparing data from distance maps of osteoarthritic wrists with normal wrists.

Findings: In 10 healthy wrists which are examined, dynamic joint space thickness is smaller than static acquired joint space thickness suggesting that dynamic distance maps provide a better estimate of the measured joint space thickness than joint space thickness based on a static joint space thickness. In 3 examined osteoarthritic wrists the joint space thickness is smaller than in healthy individuals. Moreover, the difference between dynamic and static joint space thickness is smaller in pathological joint parts.

Interpretation: The method presented in this paper demonstrates the feasibility of *in-vivo* dynamic distance maps to detect joint space thickness in the radiocarpal joint of healthy individuals.

Introduction

It is of clinical importance to diagnose cartilage injuries in the wrist at an early stage before more severe osteoarthritis has occurred that cannot be treated without residual problems in joint function[1]. A non-invasive image-based measurement method for assessing cartilage thickness is the preferred method to more invasive techniques such as wrist arthroscopy.

Cartilage degradation is reflected on radiographs as a reduction of the distance between the adjacent subchondral bone surfaces, called "joint space narrowing". Plain radiographs may be misleading as the two-dimensional (2D) projection can only show joint space thickness for a small part of the articular surfaces. Moreover, the diagnosis of cartilage degeneration is hampered by the anatomical complexity of the wrist in combination with overlapping of the anatomic structures on the radiographic images. Plain radiographs have therefore a limited value for the evaluation of degenerative joint disease in the wrist[2]. Consequently, a three-dimensional (3D) distribution of joint space thickness is required for a full evaluation of cartilage damage in the wrist.

A 3D imaging method that allows analysis of joint space thickness of the wrist is computed tomography (CT). For measuring joint space thickness, CT scans are often acquired with the wrist in a neutral position. A general drawback is that joint space thickness measured in one position may not be representative for the overall joint space for all possible wrist positions over the entire articulation during motion. The joint space thickness can therefore be overestimated in regions where cartilage adjacent surfaces are not in contact.

A second disadvantage of CT scans is that standard axial, sagittal and coronal reconstructions of image slices from CT scans are not precisely perpendicular to a joint gap which makes the clinically measured joint space thickness less accurate. Finally, the joint space thickness is often measured manually by clinicians and is therefore subject to observer errors.

In contrast to CT, where cartilage layers are not visible in the acquired images, magnetic resonance imaging (MRI) is a reliable clinical method to detect cartilage layers in larger joints and to diagnose cartilaginous injuries with high degrees of sensitivity and specificity[3,4]. However, contrary to the knee joint, which has thick cartilage layers, the measurement of submillimeter cartilage layers of the wrist still remains a challenging task. Due to resolution issues, Haims[1] and Mutimer[5] suggested that MRI was not sensitive or accurate enough for diagnosing cartilage defects or cartilage thinning in the wrist, where the cartilage is thinner than 1 mm. If MRI is combined with the use of invasive contrast material, Haims[1] found that this did not improve the sensitivity, specificity or the accuracy when diagnosing cartilage degradation of the wrist. Recent improvements in MRI techniques are however more promising. The delayed gadolinium-enhanced MR imaging and sodium 23 (^{23}Na) MRI have promising advantages over conventional MR imaging methods for investigation of cartilage quality in larger joints[6,7]. However, their usage in the carpal joint is not investigated and their diagnostic benefits in submillimeter range cartilage levels must still be proven.

The purpose of this study is to adapt a newly developed CT-based imaging method for measuring *in-vivo* three-dimensional kinematics of the carpal bones during motion[8,9]. The essence of the method is to calculate the joint space thickness using dynamic distance maps during different wrist motions instead of calculating the joint space thickness from a static CT scan[10].

A dynamic distance map gives for every point on a subchondral bone surface the shortest distance to the opposing subchondral bone surface within a set of different joint poses. The method enables a non-user- dependent *in-vivo* quantification of the joint space thickness during motion. We hypothesize that the measure of joint space thickness during wrist motion is smaller than the joint space thickness measured in one single 3D CT scan acquired in a neutral position, giving less overestimation of the joint space thickness.

The starting point for our distance map generation is the method described by Marai[10] who used static CT scans to calculate the joint space thickness (JST) in the wrist joint by using a pre-defined threshold distance to select areas on the cortical surface where bones articulate near each other. In contrast to Marai 10 who used a single distance threshold to define the joint contact areas a second criterion was introduced to define the articulation areas based on the parallelism of the opposing subchondral bone surfaces. We extend the method introduced by Marai[10] by using dynamic distance maps of the radiocarpal joint that are obtained from wrist joint motion patterns *in-vivo*, acquired by a 4-dimensional X-ray imaging system (4D-RX)[8,9]. These dynamic distance maps are compared to 3D static distance maps acquired from a single CT scan. Subsequently, the diagnostic potential of the distance maps are illustrated by comparing distance maps from wrists with osteoarthritis of the radiocarpal joint with those from normal joints. In our experiments, distance maps were calculated for the radiocarpal joints since it is the most affected articulation of the wrist joint in osteoarthritic wrists[11].

Materials and methods
Participants
The right wrists of 10 healthy subjects (5 female and 5 male, average age 37.6 years, range 27–48 years old) and affected wrists of 3 individuals (42 year old male, 53 year old male, 76 year old male) with clinically proven radiocarpal osteoarthritis (OA) due to a scapho-lunate ligament disruption were scanned for this study. The healthy subjects had no history of wrist injury. This study was approved by the Medical Ethical Committee of our hospital and informed consent was obtained from each subject.

Image acquisition and wrist motion

For reconstruction of the bone geometry, CT images of the wrist were acquired while the hand was in a neutral position. The images were acquired on an Mx8000 Quad CT scanner (Philips Medical Systems; Best; The Netherlands). The acquisition parameters were: collimation 20.5 mm, tube voltage 120 kV, effective dose 150 mAs, rotation time 0.75 s, pitch 0.875; the scans were made in 'ultra high resolution' mode (i.e. small focal spot size). Reconstructions were made with convolution kernel E, a field of view of 150 mm, a slice increment of 0.3 mm and a matrix of 512 × 512 pixels. The voxel size was 0.3 × 0.3 × 0.3 mm. Subsequently, dynamic images were acquired by the previously described 4-dimensional rotational X-ray (4D-RX) imaging method by using a modified rotational 3D-RX system (BV Pulsera, Philips Healthcare, The Netherlands)[8,9]. For acquiring 4D-RX scans, 975 projection images were made during a cyclic motion of the wrist from which a set of 20 volume reconstructions were obtained. Each volume reconstruction belongs to a certain pose of the hand during dynamic motion.

The cyclic motion was achieved by using a mechanical device, called handshaker, that consists of a detachable drive unit and a framework in which the drive unit is placed to impose flexion–extension, radio-ulnar deviation and dart throwing motion on the hand[8,9]. The forearm was placed in the handshaker with the elbow flexed 90°. To allow the hand to follow the movements of the handshaker, the participants were asked to grasp the hand piece. To prevent a locked wrist, the forearms were placed in an axial sliding table allowing a free motion of the wrist in the desired direction.

Scans were acquired during a comfortably achieved extension to maximum flexion and back. For radio-ulnar deviation, images were acquired during a dynamic motion from radial deviation to ulnar deviation and back. For the dart throwing motion the hand was moved from radial extension to ulnar flexion.

Estimation of translations and rotations of individual bones from acquired datasets

The segmentation of the carpal bones, radius and ulna from the CT images was performed by a region growing algorithm[8]. To estimate the 3 translations and 3 rotations of each individual bone relative to those in the neutral position, the segmented boundary voxels of each carpal bone were registered to the corresponding bones in each of 20 volume datasets for each dynamic scan (4D-RX)[8,9]. Custom made software packages were developed in C/C++ and Matlab. The kinematic data as well as the relative positions of the surface points for all bones were calculated for flexion–extension, radioulnar deviation and the dart-throwing motion.

α

Opposing bone surface

Final area of interest

First area of interest

Bone surface of interest
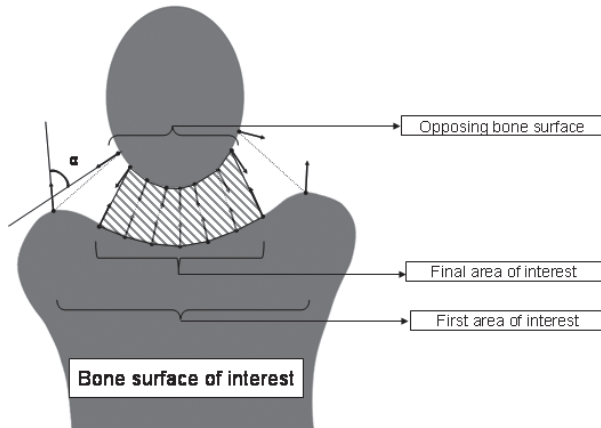
Figure 1: For each point on the bone surface of interest the closest distance to the opposite target bone surface is found (dotted lines) for a given position and orientation of the opposing bones. The first area of interest is the collection of bone surface points with a distance of less than 4 mm to the opposing bones surface. A point on the bone surface is included in the final area of interest when the angle between its normal vector and the normal vector of the closest point of opposing bone surfaces deviates less than angle α (0 to 30°) from 180° as demonstrated by the hatched area in the picture.

Calculation of static and dynamic distance maps

For each point on a bone of interest, the smallest distance to the opposite bone is determined[12,13]. The set of points with a distance smaller than 4 mm defines the first estimate of the area of interest on the bone surface. A parallelism criterion was applied similar to van de Giessen et al.[12,13]. As a result, a point on the bone surface is included in the final area of interest if the angle between its normal vector (i.e. a vector perpendicular to the bone surface for the surface point under consideration) and the normal vector of the closest point of the opposing bone surface deviates less than angle α (0 to 30°) from 180° (Fig. 1). The collection of points on the final area of interest, with associated distances to the opposite bone surface is referred to as a distance map. The static distance map (SDM) is a distance map generated from a single CT-scan in the neutral position.

A dynamic distance map (DDM) is generated from the collection of 60 distance maps of all poses of the hand from the 4D-RX acquisitions during flexion–extension, radioulnar deviation and the dart throwing motion. The final area of interest of a dynamic distance map is the union of areas of interest of all 60 poses. Within this final area of interest the minimal distance was determined for each point as the minimum distance for all 60 motion phases. The distance maps then represent the collection of minimal distances to the opposing bone within the final area of interest.

Data analysis

Both for the dynamic- (DDM) and static distance maps (SDM), the mean radioscaphoid joint space thickness (JST) was calculated by taking the average of the separately calculated radius-to-scaphoid and scaphoid-to-radius average distances of all included points. The same method was applied to calculate the average radiolunate joint space thickness.

The average JST of a distance map was defined as the primary out- come variable. Since the magnitude of the parallelism criterion influences the final outcome, each analysis was performed for different angles of α between 5 and 30°, in 5 degree increments. In addition, the average size of the final area of interest of all individuals was also estimated. The static final areas of interest were compared to the dynamic final area of interest for different values of α.

To compare the dynamic- (D-JST) and static joint space thickness (S-JST) for the healthy individuals the JST based on the SDM was compared to the JST from the DDM for different values of α. To summarize the presented data, only the outcomes for an α value of 15° were presented. A Student's t-test was used to determine the statistical significance of the difference of the JST between two methods for the healthy individuals. Wilcoxon/ Mann–Whitney statistical test or two- sample t-test was used for both dynamic and static distance maps to compare the joint space between healthy individuals and patients with osteoarthritis.

Reproducibility analysis

For determining the reliability of the JST calculation method a repeated measurement reproducibility test was applied by computing the root mean squared error (RMSE) of 20 JST's calculated from one single 4D-RX run in one individual with a non-moving wrist.

Results

Reproducibility

The root mean squared errors in the estimation of radio-scaphoid and radiolunate JST's from a 3D CT image were less than 0.01 mm for all values of the α.

The effect of the parallelism criterion on the average area size of the selected points in healthy and affected wrists

For the ten healthy individuals, the final area of interest was considerably different between the static distance map (SDM) and the dynamic distance map (DDM) (Fig. 2). The total surface area of the DDM was larger than the surface area of the SDM. The average radioscaphoid area of the SDM for the parallelism criterion α equal to 15° was 89 mm^2 (std: 26 mm^2) while the average radioscaphoid area of the DDM was 151 mm^2 (std: 23 mm^2 (P<0.01)).
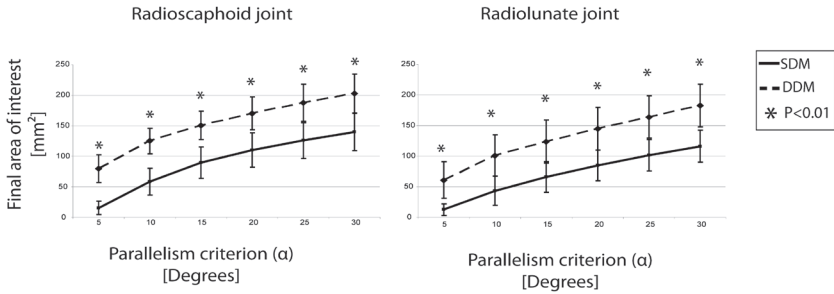
The average radiolunate final area of interest of the SDM for an α of 15° was 66 mm^2 (std: 25 mm^2) while the final area of interest of the DDM was 124 mm^2 (std: 35 mm^2, (P<0.01)). Although the final area of interest increases with increasing α, the difference between dynamic and static final area of interest remains similar for both joints.

For the affected wrists, the final area of interest was different between the SDM and DDM in the radioscaphoid and radiolunate joint. Similar to healthy individuals, the total surface area of the DDM was larger than the surface area of the SDM.

Average joint space thickness in dynamic and in static distance maps: healthy individuals

For the healthy wrists, there was a difference between the statically determined joint space thickness (S-JST) and the dynamically determined joint space thickness (D-JST) of the radioscaphoid and radiolunate joints (Fig. 3). The D-JST was smaller than the S-JST for all values of α. The radioscaphoid D-JST in healthy individuals

Final area of interest

Figure 2: The mean and standard deviation of the final area of interest used for the calculation of JST measured in 10 healthy individuals using different parallelism criterions. DDM: dynamic distance map; SDM: static distance map.

Joint Space Thickness
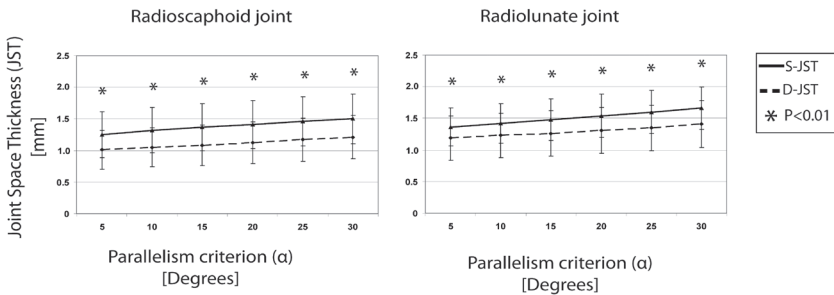
Figure 3: The average radioscaphoid and radiolunate joint space thickness measured in 10 healthy individuals using different parallelism criterions α. S-JST: joint space thickness from static CT images; D-JST: joint space thickness measured from dynamic images.

for α equal to 15° was 0.91 mm (std: 0.32 mm) while the S-JST was 1.37 mm (std: 0.37 mm. P<0.01). The corresponding radiolunate D- JST (1.17 mm (std: 0.36 mm)) was significantly different from S-JST (1.48 mm (std: 0.33 mm)). For both joints, the value of α did only marginally influence the difference between the two methods.

Average joint space thickness in dynamic and in static distance maps: affected wrists

Similar to our findings in the healthy wrists, in affected wrists the D-JST was smaller than the S-JST. However, there was only a small difference between the D-JST and the S-JST for the radioscaphoid joint. The difference of the radiolunate D-JST and S-JST in affected wrists was however more distinct (Fig. 4).

Average joint space thickness in dynamic and in static distance maps: healthy individuals vs. affected wrists

The JST was smaller in all pathological wrists (n = 3) compared to the average value in healthy wrists (Fig. 5). This is most prominently seen in the radioscaphoid joint and less in the radiolunate joint. This difference was observed for the JST from the DDM and for the SDM. The average radioscaphoid D-JST of pathological wrists was 0.44 mm (std: 0.22), which was significantly smaller in respect to D-JST of healthy individuals (0.91 mm, std: 0.32, P<0.05). The S-JST of the radioscaphoid joint space in pathological wrists was 0.49 mm (std: 0.20), which was significantly smaller, then the S-JST in healthy individuals (1.37 mm, std: 0.37 mm, P<0.01). In contrast to the findings in the radioscaphoid D-JST, the average radiolunate D-JST and S-JST were not significantly different between healthy individuals and pathological wrists.

Joint Space Thickness
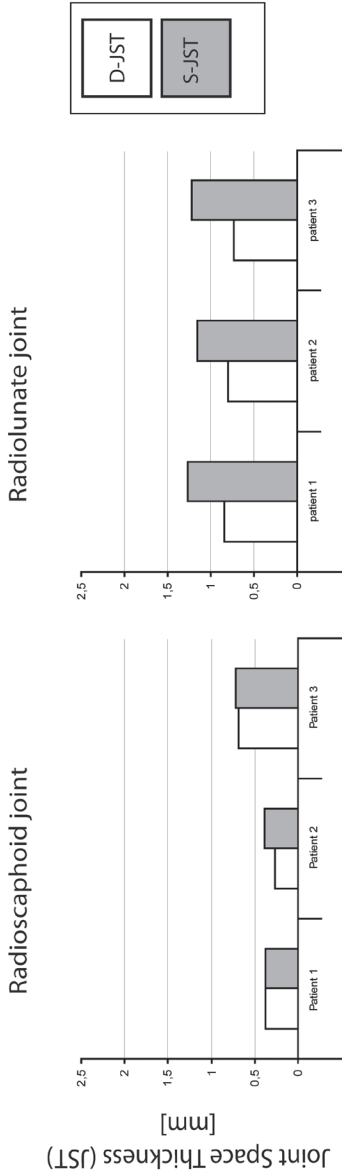
Figure 4: The individual radioscaphoid and radiolunate joint space thickness measured in 3 affected wrists using the parallelism criterion of 15°. D-JST: joint space thickness from dynamic images; S-JST: the joint space thickness measured from the static CT images.
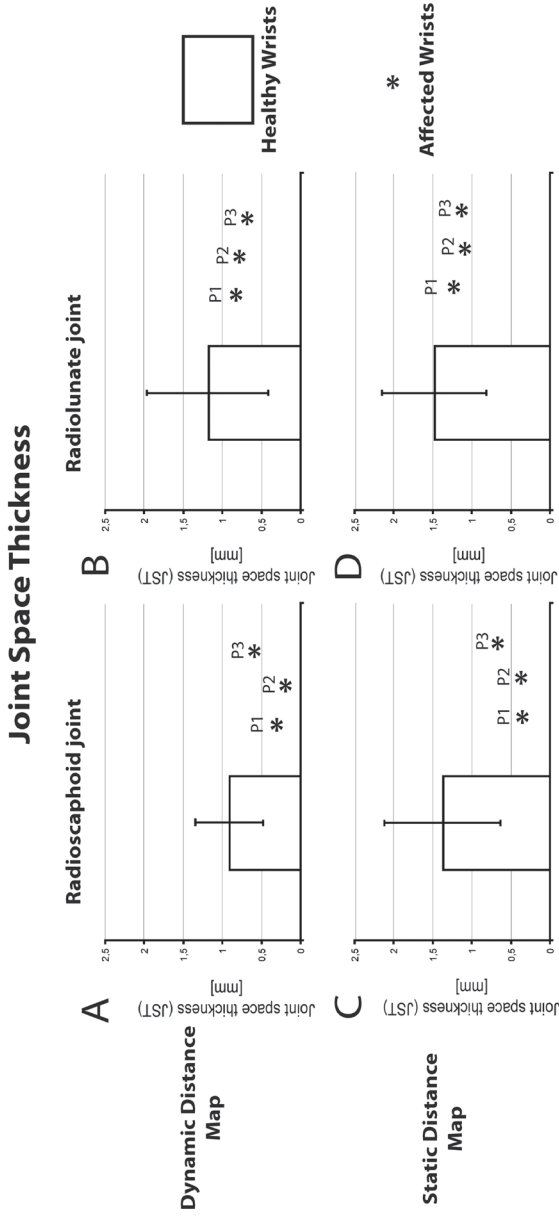
Figure 5: Radius-scaphoid and radius-lunate joint space thickness compared between 10 healthy and 3 affected wrists for both dynamic and static minimal distance maps. Outcomes are given for the parallelism criterion of 15 degrees. Errorbars represent the 95% confidence intervals.
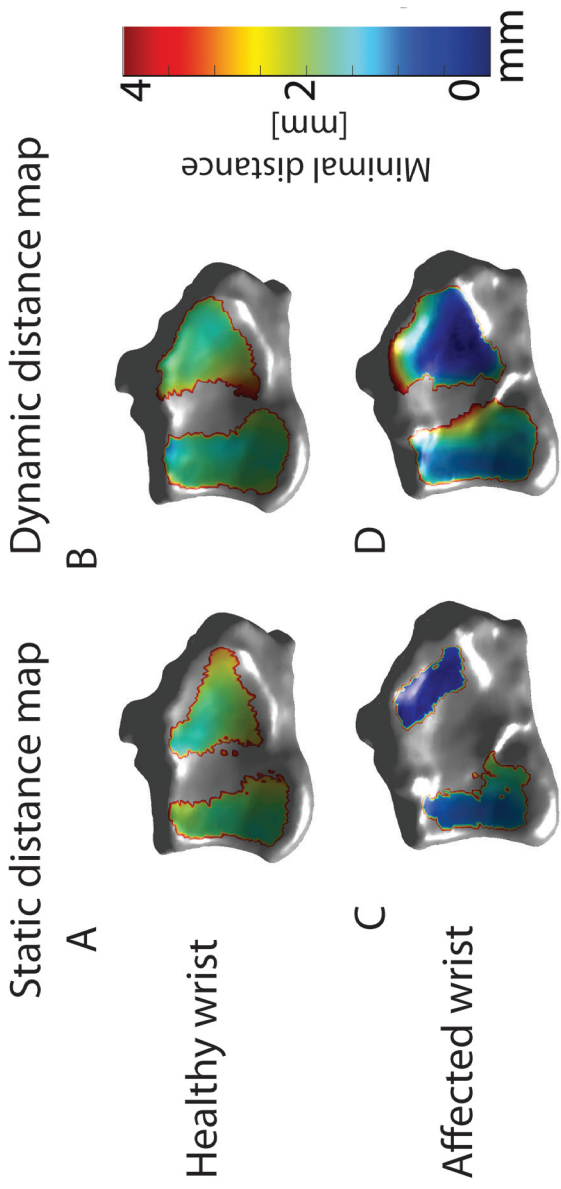
Figure 6: Joint space thickness of 2 typical examples, a healthy wrist (A,B) and from an affected wrist (C,D, patient 2), acquired from a single CT scan (A,C) and from dynamic images (B,D). For the parallelism criterion α, the value of 15° was chosen.

Discussion

The assessment of the JST is essential for diagnosing cartilage degeneration in arthritis of the wrist joint. The goal of the study was to evaluate the differences between calculated JST of radiocarpal bones acquired during wrist motion and JST acquired from one single CT scan in a neutral pose in healthy individuals. The repeated measurements to determine the reproducibility of the JST method show small deviations, which render the method sufficiently precise for further clinical research purposes. In healthy wrists, DDM provide a smaller value of JST compared to SDM. During motion, a larger area of the articulation surface is comprised within the DDM.

In the osteoarthritic wrists, radioscaphoid joint degeneration was reflected by a reduced JST while the radio-lunate joint was more preserved. This is in agreement with the clinical findings of Watson and Ballet[11] based on their clinical observations. Moreover, in contrast to the healthy wrists, in affected wrists the S-JST and the D-JST were not considerably different in the radioscaphoid joints. As a possible explanation we hypothesize that affected joints have a higher level of conformity due to an increased friction over a longer period. As a result, a more rigid situation is established which thwarts the free motion between the joint parts.

It was found that in healthy wrists an increase of α affects the magnitude of the area of interest, as more points on the distance maps are included. However, in healthy wrists, the extent of the area of interest does not affect the average JST considerably. The difference between the D-JST and S-JST also remains constant if more points are included by an increase of α. Therefore it can be confirmed that the value of α is not critical if comparing the JST between healthy individuals.

This study reveals that in individuals without any pathology of the wrist the JST calculated from dynamic distance maps are smaller than the statically acquired distance maps. This implicates that that the joint space thickness is overestimated if one static CT

scan is acquired and therefore the dynamic distance maps provide a better reflection of the functional joint space thickness.

It is important to realize that the calculation of the average JST as one single numerical parameter is a method to simplify and summarize the information from an extended amount of available data, which is useful for scientific purposes and statistical calculations. However, since the calculated JST reflects the average amount of cartilage thickness across the entire articular surface it is understandable that more localized cartilage damages cannot be evaluated by using this parameter. Therefore, a visual approach to present the data (e.g. Fig. 6) is a more informative way to understand the outcomes and place them in relation to their anatomical localization. This visual approach to link the minimal distance maps to their 3-dimensional anatomical counterparts is a powerful instrument that has potential clinical benefits that covers both diagnostic and therapeutic purposes. The role of the DDM for detection of smaller localized cartilage wear is an issue that deserves more attention in subsequent clinical experiments.

The 4D-RX method to acquire *in-vivo* kinematical information is used to calculate the JST that is a labor-intensive method. It can be anticipated that advances in CT technology with faster temporal resolution and wider detector coverage will facilitate dynamic joint studies in larger patient groups. Due to the small number of patients with osteoarthritis in this study no general conclusions could be derived from our findings in this group of patients since it was not within the scope of this experiment to perform a diagnostic accuracy study. Further research is required to investigate the benefits of dynamic assessment of the joint space thickness in early stages of arthritis and in more patients.

4

References

1. Haims, A. H. et al. MRI in the diagnosis of cartilage injury in the wrist. AJR. Am. J. Roentgenol. 182, 1267–70 (2004).

2. Peh, W. C., Patterson, R. M., Viegas, S. F., Hokanson, J. A. & Gilula, L. A. Radiographic-anatomic correlation at different wrist articulations. J. Hand Surg. Am. 24, 777–80 (1999).

3. Bredella, M. A. et al. Accuracy of T2-weighted fast spin-echo MR imaging with fat saturation in detecting cartilage defects in the knee: comparison with arthroscopy in 130 patients. AJR. Am. J. Roentgenol. 172, 1073–80 (1999).

4. Potter, H. G., Linklater, J. M., Allen, A. A., Hannafin, J. A. & Haas, S. B. Magnetic resonance imaging of articular cartilage in the knee. An evaluation with use of fast-spin-echo imaging. J. Bone Joint Surg. Am. 80, 1276–1284 (1998).

5. Mutimer, J., Green, J. & Field, J. Comparison of MRI and wrist arthroscopy for assessment of wrist cartilage. J. Hand Surg. Eur. Vol. 33, 380–2 (2008).

6. Shapiro, E. M., Borthakur, A., Gougoutas, A. & Reddy, R. 23NA MRI accurately measures fixed charge density in articular cartilage. Magn. Reson. Med. 47, 284–291 (2002).

7. Welsch, G. H. et al. In vivo biochemical 7.0 Tesla magnetic resonance: preliminary results of dGEMRIC, zonal T2, and T2* mapping of articular cartilage. Invest. Radiol. 43, 619–626 (2008).

8. Carelsen, B. et al. Detection of in vivo dynamic 3-D motion patterns in the wrist joint. IEEE Trans. Biomed. Eng. 56, 1236–44 (2009).

9. Foumani, M. et al. In-vivo three-dimensional carpal bone kinematics during flexion-extension and radio-ulnar deviation of the wrist: Dynamic motion versus step-wise static wrist positions. J. Biomech. 42, 2664–2671 (2009).

10. Marai, G. E., Crisco, J. J. & Laidlaw, D. H. A kinematics-based method for generating cartilage maps and deformations in the multi-articulating wrist joint from CT images. in Annual International Conference of the IEEE Engineering in Medicine and Biology - Proceedings 2079–2082 (2006). doi:10.1109/IEMBS.2006.259742

11. Watson, H. K. & Ballet, F. L. The SLAC wrist: scapholunate advanced collapse pattern of degenerative arthritis. J. Hand Surg. Am. 9, 358–65 (1984).

12. Van De Giessen, M. et al. Constrained registration of the wrist joint. IEEE Trans. Med. Imaging 28, 1861–1869 (2009).

13. Van de Giessen, M. et al. A statistical description of the articulating ulna surface for prosthesis design. in Proceedings - 2009 IEEE International Symposium on Biomedical Imaging: From Nano to Macro, ISBI 2009 678–681 (2009). doi:10.1109/ISBI.2009.5193138

4

If we knew what it was we were doing, it would not be called research, would it?

Albert Einstein

chapter 5

Dynamic *in vivo* evaluation of radiocarpal contact after a 4-corner arthrodesis

Abstract

Purpose: To understand the mechanisms that preserve joint integrity after 4-corner arthrodesis (FCA).

Methods: We investigated the long-term changes of the radiolunate articulation after an FCA for different motions of the wrist in a cross-sectional study that included wrists of 10 healthy participants and both operated and nonoperated wrists of 8 individuals who had undergone FCA on 1 side. The average postoperative follow-up period of the FCA group was 5.7 years. The radiolunate articulation was assessed from dynamic 3-dimensional distance maps during wrist motion. Contact surface area, centroid position of the articular area, and distance between radiolunate articular surfaces were measured and compared between healthy subjects and operated and nonoperated wrists of FCA patients.

Results: The total radiolunate articulation area was larger in patients with FCA. The average radiolunate joint space thickness was preserved in the operated FCA wrists. The centroid of the articulation area was shifted radially and dorsally in FCA wrists.

Conclusions: Changes of the motion pattern of the lunate during radioulnar deviation and flexion-extension of the wrist after FCA can explain the shift of the centroid radially and dorsally.

Type of study/level of evidence: Diagnostic IV.

Introduction

The four-corner arthrodesis (FCA) is used to treat various pathological conditions of the wrist and involves arthrodesis of the lunate, capitate, hamate and triquetrum combined with scaphoid excision[1], and it preserves a limited but functional range of motion[2].

The carpal height and the physiological radiolunate articulation are preserved whereas the midcarpal joint is eliminated, which results in kinematic changes[1]. Despite these changes, clinical studies reveal a long-term pain relief and cartilage preservation reflected by sufficient joint space thickness (JST) on conventional radiographs[3].

Our questions were how the radiolunate articulation changes after a FCA procedure and to understand why, despite changes in biomechanics of the joint, only minor radiological and functional long-term abnormalities are observed[3]. The purpose our study was to study the long-term changes of the radiolunate articulation after a FCA for different motions of the wrist.

Material and methods

In a cross-sectional experimental study, wrists of 10 healthy participants and both operated and nonoperated wrists of 8 individuals who had undergone unilateral FCA were included. The radiolunate articulation was assessed from dynamic 3-dimensional distance maps during wrist joint motion[4]. A dynamic distance map gave, for every point on a subchondral bone surface, the shortest distance to the opposing subchondral bone surface during wrist motion. These distance maps were estimated from 3- dimensional image data of 60 different joint positions of the wrist as acquired by a 4-dimensional x-ray imaging system[5,6]. The subchondral bone surface area of the radiolunate articulation, position of the

articulation area, and joint space distance of the radiolunate joint were measured. These parameters were acquired in wrists of healthy subjects and operated and nonoperated wrists of FCA patients for comparison.

Participants

The wrists of 10 healthy subjects (5 women and 5 men; average age, 38 y; range, 27-48 y) and both wrists of 8 individuals (5 men and 3 women; average age, 56 y; range, 45-66 y) who had undergone FCA were included for this study. Healthy subjects were included if they had no history of congenital wrist abnormalities or wrist injury. FCA patients were included if they had a unilateral FCA and a normal, nonoperated contralateral wrist. Eight patients treated with unilateral FCA (4 left, 4 right wrists) between 1999 and 2007 volunteered for this study. The average postoperative follow-up of the FCA group was 5.7 years (range, 24 mo to 9.8 y; median, 5.3 y). Informed consent was obtained from each participant. The local medical ethical committee approved this study.

4-Dimensional imaging of the wrist

A 4-dimensional rotational x-ray imaging method was used to acquire *in-vivo* position data of the wrist for dynamic motion assessment[5,6]. The 4- dimensional rotational x-ray combines a statically obtained reconstruction of the bone geometry reconstructed from computed tomography images with dynamic scans using a 3-dimensional rotational x-ray system (BV Pulsera, Philips Healthcare, The Netherlands). For acquiring the joint positions during dynamic wrist motion, 975 projection images were made during an imposed cyclic motion with the x-ray source rotating around the wrist. From the 975 projection images, sets of 20 volume reconstructions were obtained. During an imposed wrist motion, the wrist was moved back and forth in 1.6 seconds. During this motion cycle, 20 incremental volume reconstructions were acquired every 0.08 second. Each reconstruction belonged to

Group	Range of motion (mean and standard deviations)
Healthy participants	Flexion-extension motion: Flexion: 49.2(8.3) Extension: 42.4 (7.3) Radio-ulnar deviation: Radial deviation: 26.7 (6.1) Ulnar deviation: 31.2 (7.2) Dart-throwing motion: Radial extension: Radial deviation: 15.5(5.1) Extension: 32.9(4.8) Ulnar flexion: 31.7 (4.3) Ulnar deviation: 23.9(5.9) Flexion: 32.6(6.8)
FCA patients unaffected wrists	Flexion-extension motion: Flexion: 46.0 (4.6) Extension: 38.0 (6.8) Radio-ulnar deviation: Radial deviation: 23.3 (4.6) Ulnar deviation: 26.8 (3.6) Dart-throwing motion: Radial extension: Radial deviation: 14.7(4.8) Extension: 29.0(3.8) Ulnar flexion: Ulnar deviation: 20.4(6.3) Flexion: 30.6(6.5)
FCA operated wrist	Flexion-extension motion: Flexion: 31.5 (10.2) Extension: 22.9 (6.9) Radio-ulnar deviation: Radial deviation: 17.4 (3.0) Ulnar deviation: 21.4 (6.9) Dart-throwing motion: Radial extension: Radial deviation: 12.5(5.6) Extension: 18.3(6.4) Ulnar flexion: Ulnar deviation: 17.3(4.8) Flexion: 27.0(5.1)

Table 1: Average imposed range of motion in healthy individuals; non-operated wrists and operated wrists in patients who underwent a four-corner arthrodesis (FCA).

a certain position of the wrist during dynamic motion. Wrist motion was achieved by using the handshaker device that comprises a motor unit to drive the handshaker and a framework to hold the forearm and hand. Using the handshaker device to obtain 4-dimensional rotational x-ray images has a repeatability of 0.22± 0.08 mm for translations and 0.5° ± 0.1° for rotations[6].

The handshaker can be adjusted such that it can impose a wrist motion in different directions. All subjects were requested to grasp the hand piece of the handshaker to permit the hand to follow the imposed motion of the handshaker. To put motion onto the wrist without motion restraints and to prevent a fully constrained motion to the wrist, the forearm was placed in a sliding table allowing it to move freely in the axial direction. During the experiments, the forearm was positioned with the shoulder abducted 45° and the elbow flexed 90° (Video 1, available on the Journal's Web site at www.jhandsurg.org). Four-dimensional rotational x-ray scans were made during an imposed cyclic motion of the wrist during flexion-extension motion (FEM), radioulnar deviation (RUD), and dart-throwing motion (DTM) of the wrist, thus achieving a total of 60 wrist positions. The measurements were performed for a comfortably achieved maximum range of motion (Table 1).

Estimation of kinematic parameters

For estimation of kinematic parameters, the segmented boundary voxels acquired from the static computed tomography scan at a neutral position were registered to the corresponding bone reconstructions in each wrist position acquired from the dynamic scan (4-dimensional rotational x-ray)[5–7]. Each dynamic scan contained 20 individual dynamic volume data sets from which the kinematics parameters of the carpal bones at each position of wrist motion were estimated.

Dynamic distance maps: definition of the articulation surface and calculation of the JST

For defining the actual articulation surface and calculation of the JST, dynamic distance maps were generated by a previously described joint space distance calculation method[4]. The dynamic distance map was generated from the collection of distance maps of all positions of the hand from the 4-dimensional rotational x-ray acquisitions during FEM, RUD, and DTM. First, for each point on a bone of interest, the smallest distance to the opposite bone was determined for each position during the wrist motion. For each position, the set of points with a distance smaller than 4 mm defined the first estimate of the area of interest on the bone surface. A point on the bone surface was included in the final area of interest if the angle between its normal vector (ie, a vector perpendicular to the bone surface for the surface point under consideration) and the normal vector of the closest point of the opposing bone surface deviated less than 15° from a straight line. The collection of points on the area of interest for each position, with associated distances to the opposite bone surface, was referred to as a distance map. The final area of interest of a dynamic distance map contained the union of areas of interest of all poses for each of the motions. This final area of interest was defined as the articulation surface.

Within the final area of interest, the minimal distance was determined for each point as the minimum distance of that point to the opposite bone surface for all joint positions. The distance maps then represented the minimal distances of all points within the final area of interest. Because only the smallest measured distance during all positions was regarded as the final JST, a 4-mm threshold had only limited consequence for the final calculations of the wrist joint thickness[4]. From the dynamic distance maps, the mean JST was calculated by taking the average of the separately calculated radius-to-lunate or radius-to-FCA and lunate-to-radius or FCA-to-radius average distances of all included points. Dynamic distance maps were generated for REM, RUD, and DTM.

Describing the position of the articular surface relative to an anatomically based radial coordinate system

The positions of points on the articular surface were expressed relative to an anatomically based radial coordinate system (Fig. 1) similar to that of Kobayashi et al[8]. The longitudinal axis of the radius was defined as the z-axis. The x-axis was defined as a line perpendicular to the z axis intersecting the most distal point of the radial styloid. The y-axis was calculated as the line perpendicular to the x-and the z-axes. The origin of the radial coordinate system was defined as the intersection between the radius longitudinal axis and the distal cortical bone surface. Radioulnar and dorsovolar shifts were defined to be along the x-axis and the y-axis, respectively. To analyze the position of articulation areas, geometrical centers of gravity (ie, centroids of geometrical surface areas) were calculated for the radiolunate and radio-FCA articulation areas derived from the dynamic distance maps. The geometrical centroid of each articular surface was projected on the x-y plane of the radial coordinate system.

Centroid projections on an anatomically coordinate system are dependent on morphological properties of the radius. Therefore, an experiment was conducted to investigate the consistency of the radial coordinate system between the operated and the nonoperated FCA wrists. First, an anatomically based coordinate system was computed on both wrists similar to that of Kobayashi et al.[8]. Subsequently, the operated radius was volumetrically registered to the radius on the healthy side. The translation and rotation parameters acquired from this matching were also performed on the anatomically based radial coordinate system of the operated side. Finally, for each participant, the positions of the coordinate system between the 2 wrists were compared.
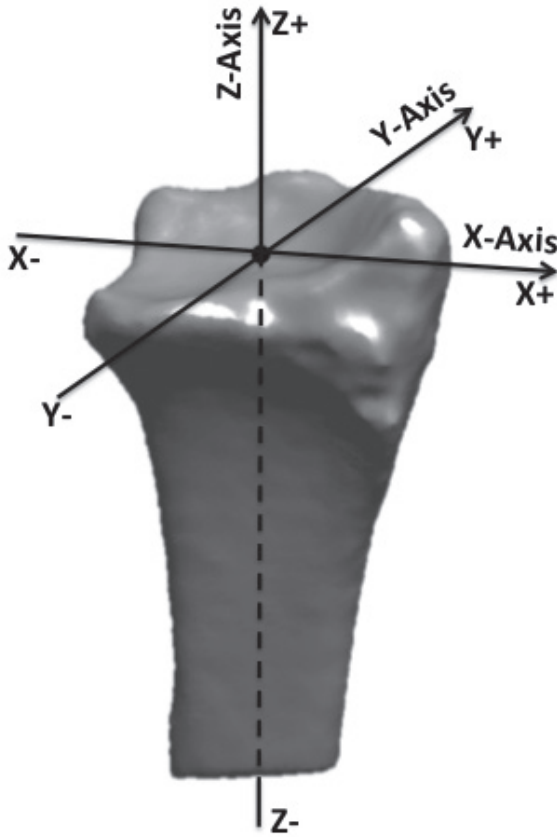
Figure 1: Palmar view of the anatomically based radial coordinate system. Radioulnar, dorso-volar and system. Radioulnar, dorso-volar and respectively.

proximal-distal translations are defined to be along the X-axis, Y-axis and Z-axis respectively.

Data analysis

The articulation surface area, position of the centroid on the radial coordinate system, and the JST were the main outcome parameters. All data were analyzed for FEM, RUD, DTM, and the combination of all 3 motions. The combination of all 3 motions for calculation of both articulation area and the JST was performed mathematically by pooling the information from all 60 positions acquired from FEM, RUD, and DTM data sets. Comparisons were made between operated side of FCA patients, the nonoperated side of FCA patients, and the healthy individuals by using 1-way analysis of variance and Tukey post hoc test at P less than 0.05 is significant.

Results

Radiolunate articulation area

The average articulation area of the radiolunate articulation during FEM, RUD, DTM, and the combination of all 3 motions was larger in FCA wrists than in nonoperated wrists of FCA subjects and also larger if compared with the wrists of healthy subjects (Figs. 2, 3). This difference was statistically significant in all 3 measured motion patterns of the wrist.

Joint space thickness

Evaluation of data from combination of all 3 motions revealed that there was no statistically significant difference of the JST between the operated (0.9 mm; SD, 0.7 mm) and nonoperated wrists (0.9 mm; SD, 0.2 mm) of FCA subjects and between the wrists of the nonoperated wrists of the FCA subjects and the healthy subjects (1.2 mm; SD, 0.4 mm) (Fig. 4). However, the SD of the JST measured in the radiolunate joint in FCA wrists was larger than the nonoperated side and wrists of healthy individuals.
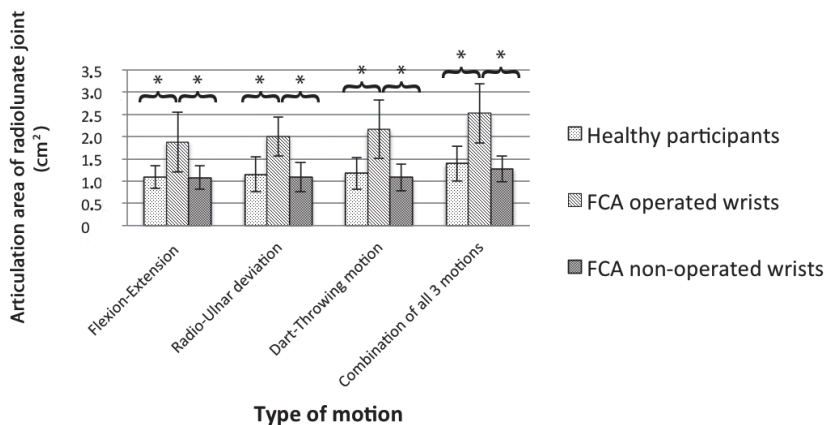
Figure 2: The average articulation area of the radiolunate joint during flexion-extension, radioulnar deviation and dart-throwing motion in the wrists of 10 healthy individuals and in healthy and operated wrists of patients who have undergone an unilateral four-corner arthrodesis. Error-bars represent the standard deviation of the mean. Asterisks represent a statistically significant difference between the groups (P<0,05).

Consistency of the anatomically based radial coordinate system

The centroid projections of radiolunate articulation on anatomically defined coordinate systems were not dependent on bilateral morphological differences between radii. There was no statistically significant difference in position of the defined radial coordinate system's origin between operated and nonoperated wrists in FCA patients after a volume registration. The average difference of the origin's x coordinates was 0.3 mm (SD, 0.9 mm; *P* 0.45), and the difference in the y coordinates was 0.2 mm (SD 0.5 mm; *P* 0.40).

Location of the radiolunate articulation

In operated wrists, the articular centroid of the articulation area was located more radially (-6.4 mm; SD, 1.0 mm) than nonoperated

Healthy individual

FCA patient: operated wrist

FCA patient: non-operated wrist
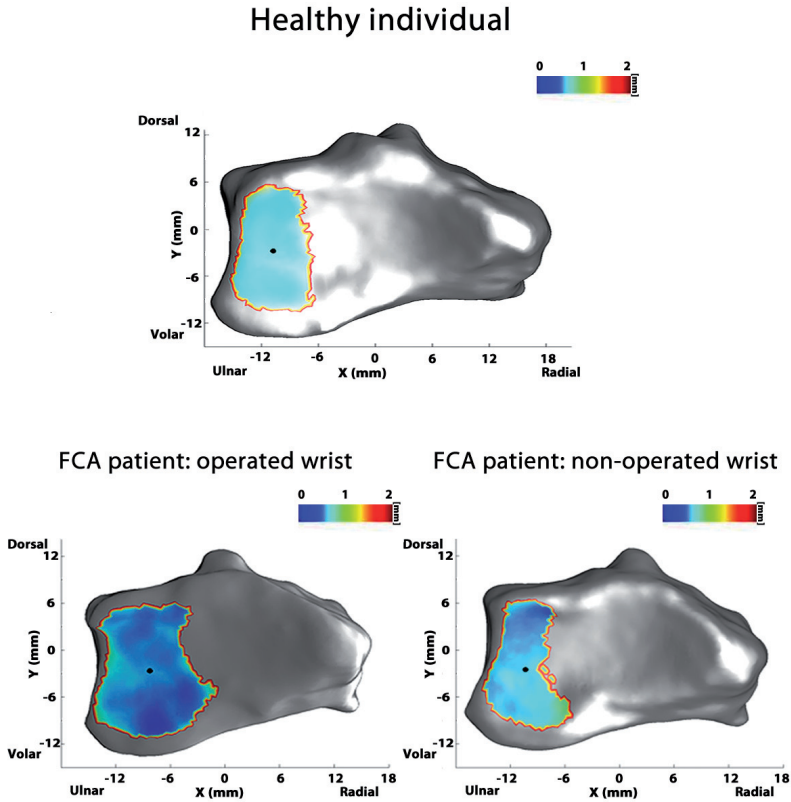
Figure 3: Dynamic distance maps of an healthy individual (above) and operated (left) and non-operated (right) wrist of a typical patient with four-corner arthrodesis. Data are derived from the union of all areas of interest combining all wrist positions during flexion-extension, radioulnar deviation and dart-throwing motion. The dots represent the centroid of the articulation area.
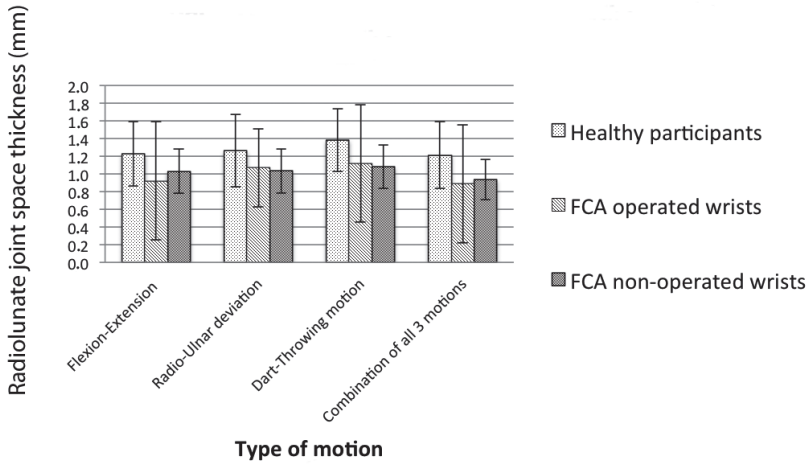
Figure 4: The average joint space thickness measured in the radiolunate joint during flexion-extension, radioulnar deviation and dart-throwing motion in 10 healthy individuals and in healthy and operated wrists of patients who have undergone an unilateral four-corner arthrodesis. Error-bars represent the standard deviation of the mean. No statistically significant differences were found between the groups.

wrists in the FCA group (-8.6 mm; SD, 1.3 mm) and the healthy individuals (-8.9 mm; SD, 1.6 mm) ($P < 0.01$) (Figs. 3, 5).

In operated wrists, the centroid was also located more dorsally (-1.5 mm; SD, 1.4 mm) than in nonoperated wrists (-3.3 mm; SD, 0.6 mm) in the FCA group ($P < 0.01$). There was no statistically significant difference in the dorsal position of the centroids between the healthy individuals (-2.5 mm; SD, 0.8) and both the operated and the nonoperated wrists in FCA patients.

Discussion

The aim of this study was to investigate the radiolunate contact articulation after FCA. The articulation area, the position of the centroid in the radial coordinate system, and the JST in the operated and nonoperated FCA patients and in healthy participants were evaluated and compared.

The main finding was that the JST was preserved after FCA. This confirms the conclusions from the studies of Cohen and Kozin[3] who found no evidence of radiographic joint space narrowing at the radiolunate articulation after FCA after a follow-up of 28 months. Although our follow-up period was twice as long as that of Cohen and Kozin[3] it seems that, on average, in FCA wrists the JST remains preserved. However, the results also show a larger standard deviation in the JST in patients, reflecting minor joint space narrowing in individual cases.

Another finding was that the surface area of total articulation of the radiolunate joint was larger after an FCA than that of the normal articulation (Fig. 3). The smaller contact area in healthy wrists can be explained by the fact that only 40% of the forces are transferred through the radiolunate articulation, and the remaining 60% are transferred through the radioscaphoid joint[9]. This changes radically after an FCA where most of the load is
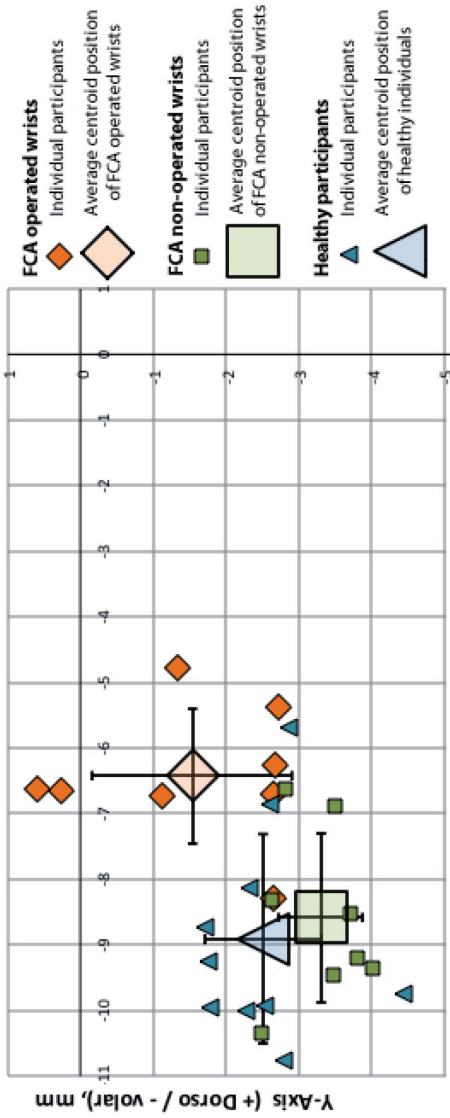
Figure 5: The centroid position of the radiolunate articulation in wrists of healthy individuals (blue marks) and in operated (orange marks) and non-operated wrists (green marks) of patients who have undergone a four-corner arthrodesis projected on the X-Y plane. The centroid is based on the articulation areas obtained from a combination of all three-motion patterns of the wrist. For individual participants, centroid positions of the radiolunate articulations are plotted by using small marks. Average centroid position of each group is plotted by large marks. Error-bars represent the standard deviations of the mean, both in the X and Y positions.

transferred through the radiolunate joint. In cadaver wrists, the force in the radiolunate articulation almost doubled after an FCA[10]. Also, the motion pattern of the lunate changed after FCA, leading to an increased area of the radius that was in contact with the lunate during the motion cycle. This is a second mechanism explaining the larger surface area of articulation. Nevertheless, despite an increased axial loading on the radiolunate articulation, the radiolunate joint space thickness remained preserved over the long term as seen in our results. Therefore, an increased articulation area decreased the average contact stress, which can be the explanation of joint preservation after FCA.

We observed that the centroid of the radiolunate articulation moved dorsoradially after FCA. This change can be explained by the fact that, after an arthrodesis of the lunate to the distal carpal row, lunate motion is now fully linked to the motion of the distal carpal row. In healthy wrists, the main lunate motion is flexion and extension, both during RUD and FEM of the wrist[8,11–18]. For the distal carpal row, both RUD and FEM are seen during RUD and FEM of the wrist[8,11–18].

However, in a previous study, we found that, after FCA owing to fixation of the proximal row to the distal row, the out-of-plane flexion motion is changed to a nonphysiological in-plane deviation motion in the FCA wrist. As a result, the carpus becomes a single pivotal joint in which the lunate is forced into a larger radioulnar motion during RUD of the wrist. Owing to the absence of the scaphoid after FCA, radial shift of the lunate is now less limited, which explains the radial shift of the centroid of the articulation[19].

A limitation of this study was the younger age of the healthy participants compared with the patients in the FCA group. Owing to ethical issues and radiation safety issues, the results from the healthy patient group were extracted from the raw data of our historical control group that were available from previously conducted experiments[4].

However, there was no statistically significant difference between the healthy group and the nonoperated wrists of FCA patients concerning the JST, articular area, and centroid localization. In the FCA-operated wrist, the SD of the average JST was larger than the SD measured in the nonoperated wrists. This means that a large variation in JDT existed in the operated FCA wrists, which can be explained by preoperative condition of the affected wrists. This extended to postoperative continuation of degenerative changes in some FCA patients. However, because of the small number of participants, additional analyses lacked statistical power to make any conclusions concerning a correlation between the postoperative period and the measured JST and area. Owing to our relatively short follow-up period, our data present midterm outcomes after FCA. Therefore, we emphasize the need for prospective studies in which pre- and postoperative dynamic distance maps are acquired to study biomechanical and degenerative changes before and after FCA with longer follow-up.

5

References

1. Watson, H. K. & Ballet, F. L. The SLAC wrist: scapholunate advanced collapse pattern of degenerative arthritis. J. Hand Surg. Am. 9, 358–65 (1984).
2. Mulford, J. S., Ceulemans, L. J., Nam, D. & Axelrod, T. S. Proximal row carpectomy vs four corner fusion for scapholunate (Slac) or scaphoid nonunion advanced collapse (Snac) wrists: a systematic review of outcomes. J. Hand Surg. Eur. Vol. 34, 256–263 (2009).
3. Cohen, M. S. & Kozin, S. H. Degenerative arthritis of the wrist: Proximal row carpectomy versus scaphoid excision and four-corner arthrodesis. J. Hand Surg. Am. 26, 94–104 (2001).
4. Foumani, M. et al. In-vivo dynamic and static three-dimensional joint space distance maps for assessment of cartilage thickness in the radiocarpal joint. Clin. Biomech. 28, 151–156 (2013).
5. Foumani, M. et al. In-vivo three-dimensional carpal bone kinematics during flexion-extension and radio-ulnar deviation of the wrist: Dynamic motion versus step-wise static wrist positions. J. Biomech. 42, 2664–2671 (2009).
6. Carelsen, B. et al. Detection of in vivo dynamic 3-D motion patterns in the wrist joint. IEEE Trans. Biomed. Eng. 56, 1236–44 (2009).
7. Carelsen, B. et al. 4D rotational x-ray imaging of wrist joint dynamic motion. Med. Phys. 32, 2771–6 (2005).
8. Kobayashi, M. et al. Normal kinematics of carpal bones: A three-dimensional analysis of carpal bone motion relative to the radius. J. Biomech. 30, 787–793 (1997).
9. Tang, P., Wei, D. H., Ueba, H., Gardner, T. R. & Rosenwasser, M. P. Scaphoid excision and 4-bone arthrodesis versus proximal row carpectomy: A comparison of contact biomechanics. J. Hand Surg. Am. 37, 1861–1867 (2012).
10. Skie, M., Grothaus, M., Ciocanel, D. & Goel, V. Scaphoid excision with four-corner fusion: A biomechanical study. Hand 2, 194–198 (2007).

11. Ruby, L. K., Cooney, W. P., An, K. N., Linscheid, R. L. & Chao, E. Y. Relative motion of selected carpal bones: a kinematic analysis of the normal wrist. J. Hand Surg. Am. 13, 1–10 (1988).

12. Savelberg, H. H., Kooloos, J. G., De Lange, A., Huiskes, R. & Kauer, J. M. Human carpal ligament recruitment and three-dimensional carpal motion. J. Orthop. Res. 9, 693–704 (1991).

13. Short, W. H., Werner, F. W., Fortino, M. D. & Mann, K. A. Analysis of the kinematics of the scaphoid and lunate in the intact wrist joint. Hand Clin. 13, 93–108 (1997).

14. Wolfe, S. W., Neu, C. & Crisco, J. J. In vivo scaphoid, lunate, and capitate kinematics in flexion and in extension. J. Hand Surg. Am. 25, 860–869 (2000).

15. Neu, C. P., Crisco, J. J. & Wolfe, S. W. In vivo kinematic behavior of the radio-capitate joint during wrist flexion-extension and radio-ulnar deviation. J. Biomech. 34, 1429–1438 (2001).

16. Moojen, T. M. et al. In vivo analysis of carpal kinematics and comparative review of the literature. J. Hand Surg. Am. 28, 81–7 (2003).

17. Moritomo, H. et al. Capitate-based kinematics of the midcarpal joint during wrist radioulnar deviation: An in vivo three-dimensional motion analysis. J. Hand Surg. Am. 29, 668–675 (2004).

18. Kaufmann, R. et al. Kinematics of the midcarpal and radiocarpal joints in radioulnar deviation: an in vitro study. J. Hand Surg. Am. 30, 937–42 (2005).

19. Dvinskikh, N. A., Blankevoort, L., Strackee, S. D., Grimbergen, C. A. & Streekstra, G. J. The effect of lunate position on range of motion after a four-corner arthrodesis: A biomechanical simulation study. J. Biomech. 44, 1387–1392 (2011).

5

Great Minds Discuss Ideas; Average Minds Discuss Events; Small Minds Discuss People

5

Eleanor Roosevelt

chapter 6

General discussion

Early diagnosis of carpal instabilities and cartilage degeneration is a prerequisite for a fast and adequate treatment that may prevent further irreversible damage of the carpus. Unfortunately, current diagnostic imaging modalities have shown to have limited value in early detection of ligament injuries and cartilage damage[1–4]. As a result, cartilage and ligament injuries often leads to damage of the cartilage layers that cannot be treated without residual problems in joint function. In these cases, the problem has progressed to such extent that the chances for success after surgical reconstruction are strongly reduced. Unfortunately this is a frequently observed situation for many patients seen in the clinic[5].

To solve this diagnostic problem analysis of 3D wrist joint motion patterns as a tool to detect carpal pathologies was proposed in this thesis. This seems feasible since carpal instabilities can cause a pathological motion of carpal bones that can occur during a dynamic motion of the wrist[6]. Therefore, an approach based on acquisition of *in-vivo* carpal kinematics in combination with geometry of carpal structures may have future diagnostic applications.

To acquire *in-vivo* carpal kinematics, CT- and MR-based methods have been introduced to image and detect 3D carpal movements during a step-wise motion of the wrist[7–13]. However, the resulting kinematics may only provide an approximation of the true continuous kinematics of the carpal bones during a dynamic activity. In the case of ligament dissociations, abrupt dynamic changes such as clicks and clunks cannot be detected with static measurement methods. Therefore, a method to investigate the dynamic carpal kinematics in patients with dynamic wrist problems is highly desirable. Carelsen et al.[14,15] introduced such a method to acquire the dynamic *in-vivo* carpal kinematics by using the four-dimensional rotational X-ray imaging system (4D-RX). With 4D-RX it is possible to make quantitative measurements of carpal

kinematics during wrist motion. This creates an opportunity to study *in-vivo* wrist joint biomechanics both in healthy and affected wrists.

In the first part of this thesis the value of the 4D-RX method as a dynamic tool for acquiring carpal kinematics was studied. The 4D-RX method was applied to study the role of tendon loading on the measured carpal kinematics. Applying a load onto the flexor and extensor tendons of the wrist had a small but statistically significant effect on the kinematics of carpal bones. The result of this study was that not the magnitude of the rotations were affected, but the rotations occurred in different directions, as reflected by the effect on the rotation components. Changes in orientation of the proximal row occurred in the same plane as the global wrist motion.

It seems that carpal bones have a tendency to rotate in specific directions under load, depending on the direction of wrist motion, articular surface geometry, and mechanical properties of the capsule and ligaments[16–18]. Tendon loading and subsequent compressive forces combined with the congruent articular surfaces may cause the motion to follow more closely the anatomic contours of the articular surfaces. In accordance with the findings, in experiments presented in this thesis it was found that the application of a load seems to increase the tendency of the carpal bones to move along a path that is more close to the path of the so-called "Dart Throwing Motion" (DTM) path. The DTM plane can be defined as a plane in which an anatomically oblique motion occurs, i.e. from extension and radial deviation to flexion and ulnar deviation[12,19–21]. The anatomically oblique plane of the physiologic DTM is unique to each wrist and depends on factors such as joint surface geometry and ligament constraints[19]. For the clinical practice this means that this knowledge could be applied for improvement of existing treatments. A better understanding of the carpal kinematics during the DTM may benefit the development of more durable prosthetic devices and implants that more closely mimic normal carpal motion.

The 4D-RX method was compared to previously applied methods to measure carpal kinematics. It was found that in healthy individuals the carpal kinematics measured during dynamic motion closely resembles the step wise acquired kinematics as estimated previously by other investigators. Small and mostly insignificant differences were observed between wrists scanned dynamically and wrists scanned during a sequence of static poses. It was found that the *in-vivo* measured carpal kinematics for flexion extension and radio-ulnar deviation were within the same range as reported by Moojen et al.[13] and Wolfe et al.[10] who measured the kinematics of the wrist joint by using quasi-dynamic step-wise methods. Although the scaphoid and lunate follow the capitate during flexion and extension, the lunate rotations lag behind showing some intercarpal motion between scaphoid and lunate. During radio-ulnar deviation the scaphoid and lunate moved together showing extension in ulnar deviation and flexion in radial deviation with small intercarpal motions between the two bones. These findings are also in agreement with previous reports that show that during radio-ulnar deviation the motion between scaphoid and lunate is coupled[22,23].

Remarkable progress has been achieved by recent developments in dynamic evaluation of *in-vivo* joint kinematics since the introduction of the 4D-RX method. Recently, 4-dimensional computed tomography (4D-CT) was introduced for obtaining of dynamic 3D images of a moving wrist joint[24–27]. It yields a series of time-resolved 3D images that permits studying individual carpal kinematics in a non-invasive way. Since the method uses the already available computed tomography scanner the expectation is that it may fit better in the clinical workflow than the more experimental setup of the 4D-RX method. However, the method is still under development and the first data of its reliability are expected soon. Other non-invasive methods for dynamic wrist imaging are MRI and ultrasound. With a lower spatial resolution compared to

CT, the MRI has better contrast characteristics for imaging soft tissues such as muscles and tendons 3. MRI provides the ability to evaluate the complex anatomy of bone and soft tissues of the wrist without the use of ionizing radiation. Recent developments of MRI protocols for evaluating the wrist during continuous active motion show promising results[28–30].

Rebmann and Sheehan et al.[28,29] applied Cine-phase contrast magnetic resonance imaging to measure the velocity profiles of the patella, femur, and tibia in 18 unimpaired knees during leg extensions. This method allows acquisition of 2D time-resolved images. Bone displacements were acquired in one plain and then calculated through integration of the measured velocity field and then converted into three-dimensional orientation angles. Recently, a similar method was applied for studying carpal kinematics. The investigators managed to make dynamic images of a moving joint in one single plane and manually measured some metrics commonly evaluated for dynamic wrist instability. Specifically, the precision of Cine-phase in measuring knee joint kinematics ranged from 0.22 degrees -1.16 degrees. However, this precision could not be achieved for the calculation of carpal joint kinematics due to the small size of carpal bones. Therefore an automated quantitative assessment of the carpal kinematics as in the 4D-RX and 4D-CT method is currently not possible when using dynamic MRI protocols[28–30].

Ultrasound provides a real time but noisy and non-quantitative measures of carpal motion[31]. For diagnosing of ligamentous injuries ultrasound methods have a low sensitivity when compared to arthroscopy[32].

At the present time, it can be stated that a CT based method as presented in this thesis is a method of choice for dynamic evaluation and quantification of carpal kinematics. It is both able to acquire high-resolution images for segmentation of bony geometry and the speed for acquiring carpal kinematics during wrist motion. It can be anticipated that with advances in CT technology with

6

higher temporal resolution and wider detector coverage, it would be possible to obtain dynamic images of moving joints easier than the technique presented in this thesis.

In the second part of this thesis the feasibility and clinical usefulness of the 4D-RX method for evaluation of outcome of therapy was investigated. In experiments presented in this thesis the diagnostic potential of dynamically acquired joint space thickness was illustrated by comparing data from distance maps of osteoarthritic wrists with normal wrists. A dynamic distance map provides a 3D map of the contact area between adjacent bones with the corresponding joint space thickness for each surface point.

Joint space thickness measurement is routinely used as a major parameter in the diagnosis and monitoring of progression of osteoarthritis from statically acquired radiological images[33]. It is defined as the measured distance between two bones of a joint measured on images from a X-ray based modality. The joint space thickness is therefore an indirect approximation of the thickness of the existing cartilage layers. As the intra articular space of the joint also contains other elements such as the articular synovial fluid this approximation is of course not always true. As an example, in the case of increased articular synovial fluid levels the measured joint space thickness might be increased. In this case the value of the cartilage thickness might be overestimated. In this thesis it was found that dynamically acquired distance maps provide less overestimation of the measured joint space thickness compared to statically acquired distance maps. Since the dynamic distance maps comprise a larger area of contact due to wrist motion they also ensue a better reflection of the actual cartilage thickness over a larger area.

In patients with already existing osteoarthritis, the quantification of cartilage thickness in different areas of the radiocarpal joint is an important prognostic factor for choosing the best operative

therapy. Since the wrist consists of different subordinate joints, the localization of the cartilage degeneration is essential for choosing between different types of surgery. As an example, problems caused by osteoarthritis limited to the midcarpal joint might be treated by using a Four-corner arthrodesis while radiocarpal cartilage degeneration is better managed by applying a radius-scaphoid-lunar arthrodesis. Currently, an operative arthroscopy is often necessary for the assessment of the cartilage quality and the localization of cartilage degeneration prior to the final operative treatment. Further development of the dynamically acquired distance maps would enable localization of spots on the articular surface with a reduced joint space thickness non-invasively. The usage of a non-invasive method for acquisition of dynamic distance maps may make an operative arthroscopy unnecessary, which might be of great benefit for both the patient and the healthcare system by reducing the risks associated with an operative treatment and associated costs.

A number of approaches for calculating articular joint space thickness have been presented in the literature. The most common methods include manual segmentation and reconstruction of MRI[30] or CT data[34,35]. The automated method presented in this thesis extends the approach of Marai et al.[35]. The cortical surface of interest was defined to be less than a prescribed threshold distance of 2 mm from a neighboring bone. However, from our experiments it was observed that the usage of an arbitrary distance threshold alone would give an overestimation of the JST in pathological wrists since in these cases the area of interest will keep growing until the arbitrarily chosen threshold value is reached based on the joint space thickness in healthy wrists. Therefore, in contrast to Marai et al., a distance threshold in combination with a parallelism criterion that defines an articulation surface based on the joint conformity characteristics was used in this thesis.

Assessment of dynamic distance maps can be used as a tool to describe and study articular changes after wrist surgery. A potential usage of studying dynamic distance maps is for evaluation of outcome of therapy. *In-vivo* carpal motion analyses make it possible to study the alterations of joint kinematics after an operation and understand the long-term effects of an intervention or placement of an implant on the wrist joint. This helps the surgeon to understand the reasons why some interventions or implants succeed while other fail. Already an increasing number of *in-vivo* studies concerning therapy evaluation based on biomechanical study of articular kinematics are reported in the literature. With a majority of these studies concerning the larger joints, various methods are applied to acquire pre-, per- and post operative *in-vivo* joint kinematics by use of Dynamic CT[24–27], dynamic MRI[30] and orthogonal uniplane and biplane fluoroscopic imaging[36] modalities. Using these methods some existing surgical procedures were evaluated and adjusted based on the knowledge gained by *in-vivo* measurements[36].

In this thesis, the four-corner arthrodesis (FCA) of the wrist was analyzed as an example to study the changes in the radiocarpal articulation. The FCA has been advocated for the treatment of various pathological conditions of the wrist. It involves the arthrodesis of joints between the lunate, capitate, hamate, and triquetrum combined with excision of the scaphoid[37].

In experiments presented in this thesis it was found that the radiolunate joint space thickness is preserved after a four-corner arthrodesis when the joint space thickness was compared to the uninjured contralateral wrist. Another finding was that the surface area of total articulation of the radiolunate joint is larger after a FCA than that of the normal articulation. The radiolunate articulation and the motion pattern of the lunate changes after FCA, leading to an increased area of the radius that is in contact with the lunate during the motion cycle. An possible explanation for joint preservation after FCA could be found in the fact that

due to an increased articulation area the average contact stress on each point is decreased which is also supported by statically examined cadaveric experiments by Tang et al.[38].

A limitation of the experimental procedure presented in this thesis has to do with the fact that for the acquisition of dynamic wrist scans a cyclic motion of the wrist is required. Since for every 4D-RX scan 50 motion cycles are needed it is imaginable that this method is less suitable for usage in a clinical situation as this could be painful in some individuals with complaints and pathological conditions of the wrist. It is expected that with the introduction of Dynamic CT protocols, dynamic scans could be acquired without the need of a repetitive cyclic motion[24–27]. This will lower the total acquisition time and provide more comfort for the patients

The number of participants was limited in different studies presented in this thesis. To be able to diagnose dynamic pathologies of the wrist by use of kinematical information it is necessary to gather more data on normal carpal kinematics in a large number of healthy participants. More variables such as age, gender, race, hand dominancy, soft tissue characteristics etc. might influence the measured kinematics of the wrist and therefore future work on this topic must study the effect of each of these variables. Development of patient specific biomechanical models containing all these variables combined with patient specific information would be a valuable clinical tool for diagnosis and surgical planning where the effects of different operative procedures on the wrist biomechanics could be better predicted. In line with this, future development of prosthetic implant devices could be enhanced by use of dynamic evaluation of the joint function. With current advances in rapid prototyping techniques, the possibility to develop custom made implant devices fitted to personal joint characteristics fall within the range of possibilities.

6

In conclusion, assessment of dynamic distance maps and the *in-vivo* acquired carpal kinematics have valuable diagnostic characteristics that may further improve the clinical processes.

References:

1. Pliefke, J. et al. Diagnostic accuracy of plain radiographs and cineradiography in diagnosing traumatic scapholunate dissociation. Skeletal Radiol. 37, 139–45 (2008).

2. Peh, W. C., Patterson, R. M., Viegas, S. F., Hokanson, J. A. & Gilula, L. A. Radiographic-anatomic correlation at different wrist articulations. J. Hand Surg. Am. 24, 777–80 (1999).

3. Haims, A. H. et al. MRI in the diagnosis of cartilage injury in the wrist. AJR. Am. J. Roentgenol. 182, 1267–70 (2004).

4. Mutimer, J., Green, J. & Field, J. Comparison of MRI and wrist arthroscopy for assessment of wrist cartilage. J. Hand Surg. Eur. Vol. 33, 380–2 (2008).

5. Jones, W. A. Beware the sprained wrist. The incidence and diagnosis of scapholunate instability. J. Bone Joint Surg. Br. 70, 293–7 (1988).

6. Nielsen, P. T. & Hedeboe, J. Posttraumatic scapholunate dissociation detected by wrist cineradiography. J. Hand Surg. Am. 9A, 135–8 (1984).

7. Crisco, J. J., McGovern, R. D. & Wolfe, S. W. Noninvasive technique for measuring in vivo three-dimensional carpal bone kinematics. J. Orthop. Res. 17, 96–100 (1999).

8. Feipel, V. & Rooze, M. Three-dimensional motion patterns of the carpal bones: an in vivo study using three-dimensional computed tomography and clinical applications. Surg. Radiol. Anat. 21, 125–31 (1999).

9. Snel, J. G. et al. Quantitative in vivo analysis of the kinematics of carpal bones from three-dimensional CT images using a deformable surface model and a three-dimensional matching technique. Med. Phys. 27, 2037–47 (2000).

10. Wolfe, S. W., Neu, C. & Crisco, J. J. In vivo scaphoid, lunate, and capitate kinematics in flexion and in extension. J. Hand Surg. Am. 25, 860–869 (2000).

11. Sun, J. S. et al. In vivo kinematic study of normal wrist motion: an ultrafast computed tomographic study. Clin. Biomech. (Bristol, Avon) 15, 212–6 (2000).

12. Moritomo, H. et al. Capitate-based kinematics of the midcarpal joint during wrist radioulnar deviation: An in vivo three-dimensional motion analysis. J. Hand Surg. Am. 29, 668–675 (2004).

13. Moojen, T. M. et al. In vivo analysis of carpal kinematics and comparative review of the literature. J. Hand Surg. Am. 28, 81–7 (2003).

14. Carelsen, B. et al. 4D rotational x-ray imaging of wrist joint dynamic motion. Med. Phys. 32, 2771–6 (2005).

15. Carelsen, B. et al. Detection of in vivo dynamic 3-D motion patterns in the wrist joint. IEEE Trans. Biomed. Eng. 56, 1236–44 (2009).

16. Kobayashi, M. et al. Axial loading induces rotation of the proximal carpal row bones around unique screw-displacement axes. J. Biomech. 30, 1165–1167 (1997).

17. Kobayashi, M. et al. Normal kinematics of carpal bones: A three-dimensional analysis of carpal bone motion relative to the radius. J. Biomech. 30, 787–793 (1997).

18. Gupta, A. Change of carpal alignment under anaesthesia: Role of physiological axial loading on carpus. Clin. Biomech. 17, 660–665 (2002).

19. Wolfe, S. W., Crisco, J. J., Orr, C. M. & Marzke, M. W. The Dart-Throwing Motion of the Wrist: Is It Unique to Humans? J. Hand Surg. Am. 31, 1429–1437 (2006).

20. Crisco, J. J. et al. In vivo radiocarpal kinematics and the dart thrower's motion. J. Bone Joint Surg. Am. 87, 2729–40 (2005).

21. Werner, F. W., Green, J. K., Short, W. H. & Masaoka, S. Scaphoid and lunate motion during a wrist dart throw motion. J. Hand Surg. Am. 29, 418–422 (2004).

22. Ruby, L. K., Cooney, W. P., An, K. N., Linscheid, R. L. & Chao, E. Y. Relative motion of selected carpal bones: a kinematic analysis of the normal wrist. J. Hand Surg. Am. 13, 1–10 (1988).

23. Short, W. H., Werner, F. W., Fortino, M. D. & Mann, K. A. Analysis of the kinematics of the scaphoid and lunate in the intact wrist joint. Hand Clin. 13, 93–108 (1997).

6

24. Shores, J. T., Demehri, S. & Chhabra, A. Kinematic '4 Dimensional 'CT Imaging in the Assessment of Wrist Biomechanics Before and After Surgical Repair. Eplasty 62–72 (2013).

25. Choi, Y. S. et al. Four-dimensional real-time cine images of wrist joint kinematics using dual source CT with minimal time increment scanning. Yonsei Med. J. 54, 1026–1032 (2013).

26. Leng, S. et al. Dynamic CT technique for assessment of wrist joint instabilities. Medical Physics 38, S50 (2011).

27. Tay, S. C. et al. Four-dimensional computed tomographic imaging in the wrist: Proof of feasibility in a cadaveric model. Skeletal Radiol. 36, 1163–1169 (2007).

28. Rebmann, A. J. & Sheehan, F. T. Precise 3D skeletal kinematics using fast phase contrast magnetic resonance imaging. J. Magn. Reson. Imaging 17, 206–213 (2003).

29. Sheehan, F. T., Zajac, F. E. & Drace, J. E. In vivo tracking of the human patella using cine phase contrast magnetic resonance imaging. Journal of biomechanical engineering 121, (1999).

30. Boutin, R. D. et al. Real-time magnetic resonance imaging (MRI) during active wrist motion--initial observations. PLoS One 8, e84004 (2013).

31. Boutry, N. et al. Ultrasonographic evaluation of normal extrinsic and intrinsic carpal ligaments: Preliminary experience. Skeletal Radiol. 34, 513–521 (2005).

32. Dao, K. D., Solomon, D. J., Shin, A. Y. & Puckett, M. L. The efficacy of ultrasound in the evaluation of dynamic scapholunate ligamentous instability. The Journal of bone and joint surgery. American volume 86-A, (2004).

33. Altman, R. D. et al. Radiographic assessment of progression in osteoarthritis. Arthritis Rheum. 30, 1214–1225 (1987).

34. Van de Giessen, M. et al. A statistical description of the articulating ulna surface for prosthesis design. in Proceedings - 2009 IEEE International Symposium on Biomedical Imaging: From Nano to Macro, ISBI 2009 678–681 (2009). doi:10.1109/ISBI.2009.5193138

35.   Marai, G. E., Crisco, J. J. & Laidlaw, D. H. A kinematics-based method for generating cartilage maps and deformations in the multi-articulating wrist joint from CT images. in Annual International Conference of the IEEE Engineering in Medicine and Biology - Proceedings 2079–2082 (2006). doi:10.1109/IEMBS.2006.259742

36.   Li, G. et al. Three-dimensional tibiofemoral articular contact kinematics of a cruciate-retaining total knee arthroplasty. J. Bone Joint Surg. Am. 88, 395–402 (2006).

37.   Watson, H. K. & Ballet, F. L. The SLAC wrist: scapholunate advanced collapse pattern of degenerative arthritis. J. Hand Surg. Am. 9, 358–65 (1984).

38.   Tang, P., Wei, D. H., Ueba, H., Gardner, T. R. & Rosenwasser, M. P. Scaphoid excision and 4-bone arthrodesis versus proximal row carpectomy: A comparison of contact biomechanics. J. Hand Surg. Am. 37, 1861–1867 (2012).

6

Great minds are to make others great. Their superiority is to be used, not to break the multitude to intellectual vassalage, not to establish over them a spiritual tyranny, but to rouse them from lethargy, and to aid them to judge for themselves.

William Ellery Channing

chapter 7

Summary

7

Introduction

Wrist complaints are responsible for the longest absence period from work of employees, with substantial financial consequences due to workers' compensation, medical expenses, and productivity losses with an annually cost of approximately €600 million in the Netherlands. Therefore, it is of great importance to recognize and properly diagnose problems in the wrist at an early stage to prevent irreversible degenerative pathologies of the wrist.

Currently, quantification of wrist instabilities is not possible by commonly available clinical diagnostic modalities. Ligament injuries frequently go undiagnosed and untreated, often being passed off as a simple sprain. If left untreated, such injuries often leads to damage of the cartilage layers that cannot be treated without residual problems in joint function. In these cases, the problem has progressed to such extent that the chances for success after surgical reconstruction are strongly reduced. Unfortunately this is a frequently observed situation for many patients seen in the clinic.

To solve this diagnostic problem the use of quantitative analysis of wrist joint motion patterns was proposed in this thesis. The hypothesis was that an approach to acquire *in-vivo* carpal kinematics in combination with the geometry of the carpal bones may have future diagnostic applications. For this purpose the Four-dimensional rotational X-ray imaging method (4D-RX) was used to make quantitative measurements of *in-vivo* joint kinematics during wrist motion. In this method a rotational x-ray system is used to image a cyclic moving joint during a period of time. This results in multiple sets of projection images, which are reconstructed to a series of time resolved 3D images i.e. 4D-rotational X-ray. The resulting data then are processed whereby 3 dimensional motion of carpal bones could be quantified and studied.

Axial loading is often applied during experiments to simulate the natural stabilizing joint compression in the wrist joint caused by muscle tension. However, the effect of axial loading on the measurement of carpal kinematics is unclear. The question is whether applying axial loading has an effect on the kinematics of the wrists in passive motion experiments, whereby the movement of the hand is externally controlled and not by muscle coordination.

It has been suggested that the kinematics of the wrist that are acquired statically in a step-wise fashion may differ from those during a continuous dynamic motion. Therefore, the next question answered in this thesis was whether the step-wised acquired carpal kinematics differs from dynamically acquired carpal kinematics.

In the case of osteoarthritis of the wrist, cartilage degradation is reflected on radiographs as a reduction of the distance between the adjacent subchondral bone surfaces, the so called Joint Space Thickness (JST). Although the JST can be measured from static radiographs or 3D CT scans of the wrist, the hypothesis is that analysis of the joint space thickness during wrist motion enables a better reflection of the actual JST since it would allow analysis of a larger extent of the functional articulation surface. Concerning this issue, the question answered in this thesis was whether the calculated joint space thickness of radiocarpal bones acquired during wrist motion differs from JST acquired from one single CT scan in a neutral pose.

Assessment of dynamic carpal kinematics may be used as a tool to describe and study articular changes after wrist surgery. The four-corner arthrodesis (FCA) has been advocated for the treatment of various pathological conditions of the wrist, that involves the arthrodesis of joints between the lunate, capitate, hamate, and triquetrum combined with scaphoid excision. The question to be answered was how the radiolunate articulation changes after a FCA

procedure and to understand why, despite changes in kinematic and morphology of the joint, only minor radiological and functional long-term abnormalities are observed.

In the subsequent sections we present the approach chosen to answer each of the questions raised above and present the related results and main conclusions.

Chapter 2. The effect of tendon loading on *in-vitro* carpal kinematics of the wrist joint

A point of discussion is that experimental conditions for studying carpal kinematics have not been standardized or investigated properly. In this chapter, the effect of axial loading was investigated during a passive motion of the wrist in cadaver arm specimens. The question was whether applying axial loading has an effect on the kinematics of the wrists. A cyclic movement was imposed on 7 cadaveric forearms while the carpal kinematics were acquired by a 4-dimensional rotational X-ray imaging system. In a first experiment, the extensor- and flexor tendons were loaded with constant force springs of 50 N, respectively. The measurements were repeated without a load on the tendons. The effect of loading on the kinematics was tested statistically by using a linear mixed model.

During flexion and extension, the proximal carpal bones were more extended with tendon loading. The lunate was on the average 2.0 degrees (p=0.012) more extended. With tendon loading the distal carpal bones were more ulnary deviated at each angle of wrist motion. The capitate was on the average 2.4 degrees (p=0.004) more ulnary deviated. During radioulnar deviation, the proximal carpal bones were more radially deviated with the lunate 0.7 degrees more into radial deviation with tendon loading (p<0.001). Conversely, the bones of distal row were more flexed and supinated with the capitate 1.5 degrees more into flexion (p=0.025) and 1.0 degrees more into supination (p=0.011). It was observed that not the magnitudes of the rotations were affected,

but the rotations occurred in different directions, as reflected by the effect on the rotation components.

Tendon loading and subsequent compressive forces combined with the congruent articular surfaces may cause the motion to follow more closely the anatomic contours of the articular surfaces. It was found that the application of a load seems to increase the tendency of the carpal bones to move along a path that is more close to the path of the so-called "Dart Throwing Motion" (DTM) path.

The conclusion of this study is that in cadaver experiments the application of a constant load during passive motion of the wrist has a small but statistically significant influence on the carpal kinematics during flexion–extension and radioulnar deviation. Therefore, tendon loading is advised if studying *in-vitro* kinematics of normal wrists.

Chapter 3. *In-vivo* three-dimensional carpal bone kinematics during flexion-extension and radio-ulnar deviation of the wrist: Dynamic motion versus step-wise static wrist positions

Another experimental condition that could influence the carpal kinematics is the nature of the motion pattern applied to the hand. It has been suggested that the kinematics of the wrist that are acquired in a step-wise fashion may differ from those during a continuous dynamic motion. The underlying hypothesis is that muscle contractions and time-dependent soft tissue properties may alter the kinematic outcomes during motion.

The differences between the dynamically and statically acquired *in-vivo* carpal kinematics were compared in a group of healthy volunteers during flexion-extension and radio-ulnar deviation of the wrist. For eight healthy subjects, static and a dynamic measurements of the carpal kinematics were performed for a flexion-extension and a radio-ulnar deviation movement.

Dynamic scans were acquired by using the four-dimensional X-ray imaging system during an imposed cyclic motion. To assess static kinematics of the wrists, three-dimensional rotational X-ray scans were acquired during step-wise flexion-extension and radio-ulnar deviation. The helical axis rotations and the rotation components, i.e. flexion-extension, radio-ulnar deviation and pro-supination were the primary outcome parameters. Linear mixed model statistical analysis was used to determine the significance of the difference between the dynamically and statically acquired rotations of the carpal bones. Small and in most cases negligible statistically significant differences were observed between the dynamic motion and the step-wise static motion of the carpal bones. The conclusion is that in the case of individuals without any pathology of the wrist, carpal kinematics can be studied either dynamically or statically. Further research is required to investigate the effect of the nature of the motion pattern of the hand on carpal kinematics in patients with dynamic wrist problems.

Chapter 4. *In-vivo* dynamic and static three-dimensional joint space distance maps for assessment of cartilage thickness in the radiocarpal joint.

In the case of osteoarthritis of the wrist, cartilage degradation is reflected on radiographs as a reduction of the distance between the adjacent subchondral bone surfaces, the so called Joint Space Thickness (JST). Although the JST can be measured from static radiographs or 3D CT scans of the wrist, the hypothesis is that analysis of the joint space thickness during wrist motion enables to generate a better reflection of the actual joint space thickness. The main question answered in this study was whether the calculated joint space thickness of radiocarpal bones acquired during wrist motion differs from JST acquired from one single CT scan in a neutral pose.

The feasibility to quantify cartilage degeneration by using dynamically acquired distance maps was demonstrated. The

purpose was to combine both geometrical and kinematical information to acquire *in-vivo* joint space information of articulating surfaces during wrist motion. The essence of the method is to calculate the joint space thickness using dynamic distance maps. A dynamic distance map gives for every point on a subchondral bone surface the shortest distance to the opposing subchondral bone surface within a set of different joint poses. The diagnostic potential of the distance maps was illustrated by comparing distance maps from wrists with osteoarthritis of the radiocarpal joint with those from normal joints.

In 10 healthy wrists which were examined, dynamic joint space thickness was smaller than static joint space thickness suggesting that dynamic distance maps provide a better estimate of the actual joint space thickness than joint space thickness based on a static joint space thickness. In 3 examined osteoarthritic wrists the joint space thickness was smaller than in healthy individuals. Moreover, the difference between dynamic and static joint space thickness is smaller in pathological joint parts. In conclusion, the method presented demonstrates the feasibility of *in-vivo* dynamic distance maps to detect joint space thickness in the radiocarpal joint of healthy individuals and patients.

Chapter 5. Dynamic *in-vivo* evaluation of radiocarpal contact after a 4-corner arthrodesis.

The four-corner arthrodesis (FCA) has been advocated for the treatment of various pathological conditions of the wrist, that involves the arthrodesis of joints between the lunate, capitate, hamate, and triquetrum combined with scaphoid excision. The question was how the radiolunate articulation changes after a FCA procedure and to understand why, despite changes in kinematic and morphology of the joint, only minor radiological and functional long-term abnormalities are observed.

A method was presented to describe articular changes after wrist surgery by using *in-vivo* acquired kinematical data. The FCA

operated wrists was analyzed as a model to study the radiocarpal articulation changes after a surgical procedure. In a cross-sectional experimental study, the radiocarpal articulation of 10 healthy participants and both operated and non-operated wrists of 8 individuals who have undergone FCA on one side were assessed from dynamic three-dimensional distance maps acquired during wrist joint motion. The average postoperative follow-up period of the FCA group was 5.7 years. The radiolunate articulation was assessed from dynamic 3-dimensional distance maps during wrist motion. Contact surface area, centroid position of the articular area, and distance between radiolunate articular surfaces were measured and compared between healthy subjects and operated and non-operated wrists of FCA patients.

It was found that the radiolunate joint space thickness is preserved after a four-corner arthrodesis when the joint space thickness was compared to the uninjured contralateral wrist. The total radiolunate articulation area was larger in patients with FCA due to the absence of scaphoid bone, which allows more radial deviation of the FCA bone block. Changes of the motion pattern of the lunate during radioulnar deviation and flexion-extension of the wrist after FCA can explain the shift of the centroid radially and dorsally.

Chapter 6. General discussion

Early diagnosis of carpal instabilities and cartilage degeneration is a prerequisite for a fast and adequate treatment that may prevent further irreversible damage of the carpus. Current 3D diagnostic imaging modalities have shown to have limited value in detection of ligament injuries and cartilage damage. Currently, an operative arthroscopy is often necessary for the assessment of the ligamentous integrity, cartilage quality and the localization of cartilage degeneration prior to the final operative treatment. To solve this diagnostic problem analysis of 3 dimensional wrist joint motion patterns as a tool to detect carpal pathologies was proposed in this thesis.

Joint space thickness measurement is routinely used as a major parameter in the diagnosis and monitoring of progression of osteoarthritis from statically acquired radiological images. The feasibility to quantify cartilage degeneration by using dynamically acquired distance maps was demonstrated in this thesis. By combining both geometrical and kinematical information to acquire *in-vivo* joint space information of articulating surfaces during wrist motion it was found that dynamic distance maps provide less overestimation of the measured joint space thickness compared to traditional static methods. As dynamic distance maps are acquired during wrist motion, a greater area of articular contact can be analyzed compared to static radiological modalities. The expectation is that dynamic distance maps containing information on large areas of articular contact provide a superior decision-making tool to better identify and treat local cartilage defects without the need of an arthroscopy.

In this thesis it was also demonstrated that the usage of dynamic distance maps could be used as a tool to describe and study articular changes after wrist surgery. A potential usage of studying dynamic distance maps is for evaluation of outcome of therapy. This would be a rational and more objective addition to the current applied methods for evaluation of outcome of therapy where assessors have to rely on questionnaires, surveys and more subjective methods to evaluate the long-term outcomes of a surgical procedure.

In line with this, future development of prosthetic implant devices could be enhanced by use of dynamic evaluation of the joint function. With current advances in rapid prototyping techniques, the possibility to develop custom made implant devices fitted to personal joint characteristics fall within the range of possibilities.

In conclusion, assessment of dynamic distance maps and the *in-vivo* acquired carpal kinematics is a valuable tool that may further improve the decision-making in the clinical process of diagnosis and treatment. For the clinical situation the usage of a non-invasive method for acquisition of dynamic distance maps could make an operative arthroscopy unnecessary more often. This might be of great benefit for both the patient and the healthcare system by reducing the risks associated with an operative treatment and associated costs.

7

As great minds have the faculty of saying a great deal in a few words, so lesser minds have a talent of talking much, and saying nothing.

Francois de La Rochefoucauld

Nederlandse samenvatting

8

Introductie

Polsklachten zijn de voornaamste oorzaak van langdurig werkverzuim bij werknemers, met aanzienlijke financiële gevolgen, zoals werknemerscompensatie, medische kosten en productiviteitsverlies. De jaarlijkse kosten in Nederland bedragen ongeveer € 600 miljoen euro. Het is van belang om al in een vroeg stadium polsklachten te herkennen en te voorzien van een correcte diagnose, om zo onomkeerbare degeneratieve polsaandoeningen te voorkomen.

Het is op dit moment niet mogelijk om met de beschikbare klinische diagnostische methoden de mate van carpale instabiliteit vast te stellen. Bandletsels worden veelal niet gediagnosticeerd en behandeld, omdat ze vaak worden afgedaan als een verstuiking. Onbehandeld leidt dit soort kwetsuren vaak tot schade aan de kraakbeenlagen, die niet verholpen kan worden zonder blijvende klachten aan de gewrichtsfunctie. In deze gevallen is de aandoening zodanig gevorderd dat de succeskans van een chirurgische reconstructie sterk is verminderd. Dit is een veelvoorkomende situatie bij patiënten in de kliniek.

Om dit probleem op te lossen, stelt dit proefschrift een kwantitatieve analyse van bewegingspatronen van het polsgewricht voor. De hypothese is dat in-vivo kinematica van de carpalia in combinatie met geometrie van de handwortelstructuren in de toekomst verbetering van de diagnostische mogelijkheden biedt. De *four-dimensional X-ray imaging-methode* (4D-RX) is gebruikt om kwantitatieve metingen te verkrijgen van in-vivo gewrichtskinematica tijdens bewegingen van de pols. Bij deze methode wordt gebruikgemaakt van een roterende röntgenbron die een cyclisch bewegend gewricht gedurende enige tijd vanuit meerdere richtingen vastlegt. Dit resulteert in meerdere sets van projecties, die worden gereconstrueerd tot een serie van

tijdgeresolveerde driedimensionale beelden. De verkregen data worden verwerkt, waarna de driedimensionale bewegingen van carpalia kunnen worden gekwantificeerd en bestudeerd.

Onderzoeksvragen
Axiale belasting wordt tijdens experimenten veelal toegepast om de natuurlijke stabiliserende gewrichtscompressie in het polsgewricht te simuleren die wordt veroorzaakt door spierspanning. Het effect van axiale belasting op carpale kinematica blijft tijdens de metingen echter onduidelijk. De vraag is of het toepassen van axiale belasting bij passieve bewegingsexperimenten effect heeft op de polskinematica, waarbij de bewegingen worden opgelegd en niet door spiercontracties tot stand komen.

Polskinematica die stapsgewijs op een statische wijze wordt verkregen, kan afwijken van de kinematica bij een continue dynamische beweging. Daarom is de te beantwoorden vraag in dit proefschrift of de stapsgewijs verkregen kinematica van de carpalia verschilt van dynamisch verkregen carpale kinematica.

Bij artrose in de pols laten röntgenfoto's de afbraak van kraakbeen zien als een reductie in de afstand tussen de aangrenzende onderliggende botoppervlakken, de zogeheten gewrichtsspleetdikte of *joint space thickness*. Hoewel de gewrichtsspleetdikte op statische röntgenfoto's of 3D-CT-scans van de pols kan worden gemeten, is de hypothese dat een analyse van de gewrichtsspleetdikte tijdens polsbewegingen een beter beeld van de daadwerkelijke gewrichtsspleetdikte oplevert.

De vraag die wordt beantwoord in dit proefschrift is of de berekende gewrichtsspleetdikte van de radiocarpale botjes verkregen tijdens polsbewegingen verschilt van de gewrichtsspleetdikte verkregen via een eenmalige CT-scan in een neutrale houding.

Een beoordeling van dynamische kinematica van de carpalia kan als hulpmiddel worden gebruikt om veranderingen van het gewricht na een polsoperatie te omschrijven en te bestuderen. Een zogenaamde *four-corner arthrodesis*-operatie (FCA) wordt als behandeling voor verschillende pathologische polsaandoeningen vaak aanbevolen. Hierbij worden gewrichten tussen het lunatum, capitatum, triquetrum en hamatum vastgezet en de scaphoïdeum wordt verwijderd. De vraag is hoe de radiolunaire articulaire beweging na een FCA-behandeling verandert en waarom er ondanks de veranderingen in de kinematica en morfologie van het gewricht op de lange termijn alleen geringe radiologische en functionele afwijkingen worden gezien.

De belangrijkste doelstellingen van dit proefschrift zijn:
- het introduceren van een nieuwe methode voor het dynamisch beoordelen en kwantificeren van radiocarpale kinematica;
- het bestuderen van de contactvlakken in het polsgewricht in gezonde en geopereerde polsen en
- het dynamisch kwantificeren van de gewrichtsspleetdikte als maat voor de kraakbeenbedekking ten behoeve van diagnostische en prognostische doeleinden.

Een dynamische evaluatie van driedimensionale carpale kinematica met behulp van 4D-RX-techniek is de voornaamste methode in het onderzoek voor dit proefschrift.

Hoofdstuk 2. Het effect van peesbelasting op *in-vitro* carpale kinematica van het polsgewricht

Een discussiepunt in de literatuur is dat proefomstandigheden voor het bestuderen van carpale kinematica nauwelijks zijn onderzocht of gestandaardiseerd. Dit hoofdstuk onderzoekt het effect van axiale belasting tijdens een passieve polsbeweging bij kadaverpreparaten. De vraag is of het toepassen van axiale belasting bij passieve bewegingsexperimenten effect heeft op de polskinematica, waarbij de handbeweging extern wordt gecontroleerd en niet door spiercoördinatie. Het effect van axiale belasting is onderzocht door het meten van carpale kinematica met en zonder het uitoefenen van kracht op de strek- en buigpezen. Er is een cyclische beweging opgelegd bij zeven kadaverpolsen, terwijl de carpale kinematica is verkregen middels de 4D-RX methode. De strek- en buigpezen zijn beide belast met constante krachtveren van 50 N. De metingen zijn nog eens herhaald zonder de pezen te belasten.

Er is vastgesteld dat niet zozeer de grootte van de rotaties wordt beïnvloed door peesbelasting, maar wel de richting van de rotaties. Tijdens het buigen en strekken van de pols is de proximale rij, bestaande uit lunatum, scaphoïd en triquetrum, meer in extensie wanneer peesbelasting wordt opgelegd.

Bij radio-ulnaire deviatie is de proximale rij carpalia juist meer radiaal gedevieerd. Terwijl de distale rij meer in flexie en supinatie komt te staan bij toepassen van peesbelasting.

Het blijkt dat bij toepassen van peesbelasting de bewegingen van de carpalia meer langs het zogeheten dart *throwing motion*-pad plaatsvinden. De dart *throwing motion*-beweging wordt door veel onderzoekers aangemerkt als de meest fysiologische beweging van de pols. Het is een gecombineerde beweging waarbij de pols van radiair deviatie en extensie naar ulnair deviatie en flexie beweegt. Peesbelasting met als gevolg meer compressie op de gewrichtsdelen leidt ertoe dat de bewegingen meer langs de anatomische gewrichtsoppervlakken plaatsvinden, waar de meeste congruentie kan worden verwacht.

De conclusie van deze studie is dat bij experimenten op kadavers toepassen van een constante belasting tijdens een passieve polsbewegingen een kleine maar statistisch significante invloed op de gemeten carpale kinematica. Omwille hiervan wordt peesbelasting aanbevolen als er in-vitro normale polskinematica wordt bestudeerd.

Hoofdstuk 3. *In-vivo* driedimensionale kinematica van carpalia tijdens flexie-extensie en radio-ulnaire deviatie van de pols: Dynamische beweging versus stapsgewijze statische polsposities

Een andere experimentele factor die de carpale kinematica kan beïnvloeden, is de aard van het bewegingspatroon dat wordt toegepast op de hand. Polskinematica die stapsgewijs op een statische wijze wordt verkregen, kan afwijken van die bij een continue dynamische beweging. Spiercontracties en tijdsafhankelijke eigenschappen van weke delen kunnen de kinematische uitkomsten tijdens beweging beïnvloeden.

De verschillen tussen de dynamisch en statisch verkregen in-vivo carpale kinematica zijn vergeleken binnen een groep gezonde vrijwilligers tijdens flexie-extensie en radio-ulnaire deviatie van de pols. Dynamische scans zijn verkregen met behulp van de 4D-RX-methode tijdens een opgelegde cyclische beweging van de pols. Statische metingen zijn gedaan tijdens een stapsgewijze flexie-extensie en radio-ulnaire deviatie van de pols. De primaire uitkomstparameters zijn de afzonderlijke componenten van de helische rotatieassen. Linear mixed model-statistische analyses zijn toegepast om de significantie vast te stellen van het verschil tussen de dynamisch en statisch verkregen rotaties van de carpalia.

Kleine, en in de meeste gevallen verwaarloosbare verschillen zijn aangetoond tussen de dynamische beweging en de stapsgewijze statische beweging van de carpalia bij gezonde proefpersonen.

De conclusie is dat bij gezonde individuen de carpale kinematica zowel dynamisch als statisch kan worden bestudeerd.

8

Hoofdstuk 4. *In-vivo* dynamische en statische driedimensionale joint space distance maps voor het evalueren van kraakbeendikte in het radiocarpale gewricht

Bij artrose in de pols wordt het kraakbeenverlies op röntgenfoto's vaak afgeleid van een afname van de afstand tussen de aangrenzende onderliggende botoppervlakken, de zogeheten gewrichtsspleetdikte of *joint space thickness*. Hoewel de gewrichtsspleetdikte op statische röntgenfoto's of stilstaande CT-scans van de pols kan worden gemeten, is de hypothese dat een analyse van de gewrichtsspleetdikte tijdens pols-bewegingen een beter beeld van de daadwerkelijke gewrichts-spleet laat zien. De hoofdvraag in dit proefschrift is of de berekende gewrichtsspleetdikte van het radiocarpale gewricht verkregen tijdens bewegingen van de pols verschilt van de gewrichtsspleetdikte gemeten op een statische CT-scan in een neutrale houding.

Dynamisch kwantificeren van de gewrichtsspleetdikte kan worden bewerkstelligd door kinematische metingen en geometrie van de ossale structuren te combineren in zogenaamde dynamische *distance maps*. Een dynamische *distance map* geeft de kortste afstand aan van elk punt op het bot tot het tegenoverliggende bot, binnen een set van verschillende gewrichtsposities.

Bij onderzochte polsen van tien gezonde proefpersonen is de dynamisch gemeten gewrichtsspleetdikte significant kleiner gebleken dan de gemeten dikte in stilstaande scans. Daaruit blijkt dat de dynamische *distance maps* minder overschatting geven van de gemeten gewrichtsspleetdikte dan de statische *distance maps*. Tevens is het diagnostische potentieel van de dynamische *distance maps* aangetoond door het vergelijken van de distance maps van polsen met artrose met de gezonde polsen van de proefpersonen.

Samenvattend kan worden geconcludeerd dat het dynamisch meten van de gewrichtsspleetdikte met dynamische *distance maps* als een afgeleide maat voor het beoordelen van kraakbeenbedekking van het polsgewricht haalbaar is.

8

Hoofdstuk 5. Dynamische *in-vivo* evaluatie van contactvlakken in het radiocarpale gewricht na een four corner-artrodese.

Een four corner-artrodese (FCA) wordt vaak aanbevolen als behandeling voor verschillende pathologische polsaandoeningen. Bij een FCA worden gewrichten tussen het lunatum, capitatum, triquetrum en hamatum vastgezet en het scaphoïd-bot wordt verwijderd. De vraag is hoe de radiolunaire articulaire beweging na een FCAverandert en waarom er ondanks de veranderingen in de kinematica en morfologie van het gewricht op lange termijn alleen geringe radiologische en functionele afwijkingen worden gezien.

Dit onderzoek introduceert een methode om de articulaire veranderingen na een polsoperatie te beschrijven aan de hand van in-vivo verkregen kinematische data. De met FCA geopereerde polsen zijn geanalyseerd om de veranderingen in radiocarpale articulatie na een chirurgische ingreep te bestuderen.

In een cross-sectioneel onderzoek zijn de radiocarpale articulaties onderzocht van tien gezonde deelnemers en van zowel de geopereerde als niet-geopereerde polsen van acht individuen die aan één zijde FCA hebben ondergaan. Radiocarpale articulaties zijn in kaart gebracht met behulp van dynamische driedimensionale *distance maps* die tijdens bewegingen van het polsgewricht zijn verkregen. De grootte van contactoppervlakken, het zwaartepunt van de articulaire gebieden en de gewrichtsspleetdikte in de radiolunaire articulaties zijn vergeleken tussen gezonde deelnemers en geopereerde en niet-geopereerde polsen van FCA-patiënten.

Uit de experimenten in dit proefschrift blijkt dat de gewrichts-spleetdikte in radiolunaire gewrichtsruimte na een FCA-behandeling redelijk bespaard blijft. Het totale radiolunaire contactoppervlak in een geopereerde pols is groter vergeleken met een ongedeerde contralaterale pols. Een veranderend bewegingspatroon van het lunatum, veroorzaakt door de afwezigheid van het scaphoïd in combinatie met een gekoppelde beweging met de distale rij, kan verklaren waarom het zwaartepunt van de articulatievlak meer naar radiaal en dorsaal verschuift.

8

Hoofdstuk 6. Algemene discussie

Vroege diagnose van polsinstabiliteiten en kraakbeendegeneratie is een voorwaarde voor een snelle en adequate behandeling, die verdere, onomkeerbare schade van de pols kan verhinderen. De huidige diagnostische modaliteiten hebben een beperkte waarde in de detectie van bandletsels van de pols en daaropvolgende instabiliteit en kraakbeenschade. Momenteel is een operatieve artroscopie vaak noodzakelijk voor de beoordeling van de gewrichtsbanden, de kwaliteit van het kraakbeen en de lokalisatie van kraakbeendefecten voor een uiteindelijke operatieve behandeling.

Als oplossing voor dit diagnostisch probleem stelt dit proefschrift een analyse van driedimensionale bewegingspatronen van de polsbeenderen voor. De haalbaarheid van het gebruik van de gewrichtsspleetdikte als maat voor het kwantificeren van de kraakbeendegeneratie met behulp van dynamisch verkregen *distance maps* wordt aangetoond in dit proefschrift.

De gewrichtsspleetdikte verkregen uit radiologische beelden wordt routinematig toegepast als een belangrijke parameter in de diagnose en monitoring van de progressie van artrose. In onderzoeken beschreven in dit proefschrift wordt duidelijk dat het meten van de gewrichtsspleetdikte in een stilstaande scan van de pols een overschatting geeft ten opzichte van metingen die zijn verkregen in een dynamische situatie.

Ook kan door het dynamische karakter van de metingen een groter gebied van het articulaire contactoppervlak worden geanalyseerd in vergelijking met statische modaliteiten.

De verwachting is dat door het dynamisch en kwantitatief meten van de gewrichtsspleetdikte objectievere informatie over grotere delen van het articulerend contactoppervlak wordt verkregen. De lokale kraakbeendefecten kunnen hierdoor beter worden geïdentificeerd en behandeld.

In dit proefschrift wordt ook aangetoond dat dynamische distance maps kunnen worden toegepast als instrument voor het beschrijven en bestuderen van articulaire veranderingen na polschirurgie. Een potentiële toepassing hiervan is de evaluatie van het resultaat van een behandeling. Dit heeft meerwaarde en is daarom een aangename aanvulling op de bestaande methoden, waarbij onderzoekers moeten vertrouwen op subjectievere methoden om de resultaten van een chirurgische procedure op korte en lange termijn te evalueren.

De toekomstige ontwikkeling van operatietechnieken en prothetische implantaten kan worden versneld en verbeterd door het dynamisch en kwantitatief evalueren van de gewrichtsfunctie. Gelet op de snelle ontwikkelingen in simulatie- en *rapid prototyping*-technieken is het niet ondenkbaar dat patiëntspecifieke operaties met op maat gemaakte implantaten in de nabije toekomst vaker tot de mogelijkheden behoren.

Samenvattend kan worden geconcludeerd dat het beoordelen van de gewrichtsfunctie met behulp van dynamische *distance maps* de besluitvorming in het klinische proces van diagnose en behandeling kan verbeteren. In de klinische situatie maakt dit een operatieve artroscopie vaker overbodig. Dit heeft een meerwaarde voor zowel de patiënten als de gezondheidszorg, aangezien het leidt tot het reduceren (van de risico's) van operatieve ingrepen en de bijbehorende kosten voor de maatschappij.

Let your vision be world embracing

Bahai scriptures

Addendum

9

PhD Portofolio

Name: Mahyar Foumani, MD
Research school: AMC Graduate School for Medical
                       Sciences, University of Amsterdam

PhD Training
Courses
- Practical Bio-Statistics and SPSS
  (AMC Graduate school, 2008, 1.14 ECTS points)
- Epidemiology
  (AMC Graduate school, 2008, 1.0 ECTS points)
- Clinical data management
  (AMC Graduate school, 2008, 0.20 ECTS points)
- Radiation protection
  (Boerhave institute-LUMC Leiden, 2007, 1.71 ECTS points)
- Scientific Writing in English for Publication
  (AMC Graduate school, 2007, 1.5 ECTS points)
- Oral Presentation in English
  (AMC Graduate school, 2007, ECTS points 0.78)
- Project Management
  (AMC Graduate school, 2007, AMC 0.57 ECTS points)

Conference Presentations

- M. Foumani, S.D. Strackee, L. Blankevoort, G.J. Streekstra. Advanced imaging in carpal kinematics. Belgian Hand Group President's Congress: Saturday 22 March 2014 - Eupen, Belgium. 22 March 2014. (ECTS points 0.5)
- M. Foumani, S.D. Strackee, M. van de Giessen, R. Jonges, L. Blankevoort, G.J. Streekstra. In-vivo dynamic and static three-dimensional joint space distance maps in the radiocarpal Joint. 11th Triennial Congress of the International Federation of Societies for surgery of the Hand. 31 october-4November 2010, Seoul, Korea. (ECTS points 0.5)
- M. Foumani, L. Blankevoort, N. Dvinskikh, R. Jonges, G.J. Streekstra, S.D. Strackee. In vitro Carpal Kinematics of the Wrist Acquired by the New Developed Four Dimensional Rotational X-Ray Imaging System: the Effect of Tendon Load on Carpal Kinematics. 11th Triennial Congress of the International Federation of Societies for surgery of the Hand. 31 october-4 November 2010, Seoul, Korea. (ECTS points 0.5)
- M. Foumani, S.D. Strackee, R. Jonges, L. Blankevoort, A.H. Zwinderman, B. Carelsen, G.J. Streekstra. Dynamic versus Quasi-Dynamic In Vivo Carpal Bone Kinematics during Flexion-Extension and Radio-Ulnar Deviation of the Wrist. 11th Triennial Congress of the International Federation of Societies for surgery of the Hand. 31 october-4November 2010, Seoul, Korea. (ECTS points 0.5)
- M. Foumani, S.D. Strackee, R. Jonges, L. Blankevoort, A.H. Zwinderman, B. Carelsen, G.J. Streekstra. Dynamic versus Quasi-Dynamic In Vivo Carpal Bone Kinematics during Flexion-Extension and Radio-Ulnar Deviation of the Wrist. Brussels Hand/Upper limb international symposium. 29-30 January 2010. (ECTS points 0.5)

- M. Foumani, L. Blankevoort, N. Dvinskikh, R. Jonges, G.J. Streekstra, S.D. Strackee. In vitro Carpal Kinematics of the Wrist Acquired by the New Developed Four Dimensional Rotational X-Ray Imaging System: the Effect of Tendon Load on Carpal Kinematics. Brussels Hand/Upper limb international symposium. 29-30 January 2010. (ECTS points 0.5)
- M. Foumani, S.D. Strackee, R. Jonges, L. Blankevoort, A.H. Zwinderman, B. Carelsen, G.J. Streekstra. Dynamic vs. Quasi-dynamic in-vivo carpal bone kinematics during flexion-extension and radio-ulnar deviation of the wrist. ASSH 2009 san Fransisco. (ECTS points 0.5)   M. Foumani, S.D. Strackee, R. Jonges, L. Blankevoort, A.H. Zwinderman, B. Carelsen, G.J. Streekstra. Dynamic vs. quasi-dynamic in vivo carpal bone kinematics during flexion-extension and radio-ulnar deviation of the wrist. XXII Congress of the International Society of Biomechanics. Cape Town, South Africa. 5th to 9th July 2009. (ECTS points 0.5)
- M. Foumani, Stekelenburg C, Blankevoort L, Dvinskikh N, Jonges R, Streekstra GJ, Strackee SD. In vitro Carpal kinematics of the wrist acquired by the new developed 4 dimensional rotational x-ray imaging system: the effect of tendon load on carpal kinematics. Nederlandse verenging van handchirurgie, 20 juni 2009. (ECTS points 0.5)   M. Foumani, Strackee SD, Jonges R, Carelsen B, Blankevoort L, Streekstra GJ. Dynamic and quasi-dynamic acquired in vivo carpal kinematics XIVth International Congress of Federation of the European Societies for Surgery of the Hand - FESSH, Poznan, Poland, june 3rd-6thh 2009. (ECTS points 0.5)
- M. Foumani, M. van de Giessen, GJ. Streekstra, R. Jonges. SD. Strackee - Influence of scaphoid morphology on scapho-capitate kinematics. Nederlandse vereniging van Plastische, Reconstructieve en Hand chirurgie & Koninklijke Belgische Vereniging voor Plastische, Reconctructieve chirurgie, Benelux scientific meeting. 4th October 2008. 'S Hertogenbosch. (ECTS points 0.5)

List of publications

2015

- M. Foumani, S. D. Strackee, C. M. Stekelenburg, L. Blankevoort, and G. J. Streekstra, Dynamic in vivo evaluation of radiocarpal contact after a 4-corner arthrodesis. J. Hand Surg. Am., vol. 40, no. 4, pp. 759–66, Apr. 2015.
- P. W. ten Berg, M. Foumani, S. D. Strackee. Carpal Intraosseous Cyst Formation in Scaphoid Nonunion Wrists. J. Hand Surg. Eu., vol. 2015 accepted for publication. DOI: 10.1177/1753193415600147
- P. W. ten Berg, M. Foumani, S. D. Strackee. A Rare Case of Bilateral Luno-triquetral Coalition and Bilateral Scaphoid Nonunion. J J. Hand Surg. Am., vol. Epub. 2015 accepted for publication. DOI: 10.1016/j.jhsa.2015.07.003

2013

- M. Foumani, S. D. Strackee, M. Van De Giessen, R. Jonges, L. Blankevoort, and G. J. Streekstra. In-vivo dynamic and static three-dimensional joint space distance maps for assessment of cartilage thickness in the radiocarpal joint. Clin. Biomech., vol. 28, no. 2, pp. 151–156, 2013.

2012

- M. Van De Giessen, M. Foumani, F. M. Vos, S. D. Strackee, M. Maas, L. J. Van Vliet, C. A. Grimbergen, and G. J. Streekstra. A 4D statistical model of wrist bone motion patterns. IEEE Trans. Med. Imaging, vol. 31, no. 3, pp. 613–625, 2012.

2010

- M. Foumani, L. Blankevoort, C. Stekelenburg, S. D. Strackee, B. Carelsen, R. Jonges, and G. J. Streekstra. The effect of tendon loading on in-vitro carpal kinematics of the wrist joint. J. Biomech., vol. 43, no. 9, pp. 1799–1805, 2010.

- M. van de Giessen, M. Foumani, G. J. Streekstra, S. D. Strackee, M. Maas, L. J. van Vliet, K. A. Grimbergen, and F. M. Vos. Statistical descriptions of scaphoid and lunate bone shapes. J. Biomech., vol. 43, no. 8, pp. 1463–1469, 2010.
- N. A. Dvinskikh, L. Blankevoort, M. Foumani, J. A. E. Spaan, and G. J. Streekstra. Quantitative detection of cartilage surfaces and ligament geometry of the wrist using an imaging cryomicrotome system. J. Biomech., vol. 43, no. 5, pp. 1007–1010, 2010.

2009
- M. Foumani, S. D. Strackee, R. Jonges, L. Blankevoort, A. H. Zwinderman, B. Carelsen, and G. J. Streekstra. In-vivo three-dimensional carpal bone kinematics during flexion-extension and radio-ulnar deviation of the wrist: Dynamic motion versus step-wise static wrist positions. J. Biomech., vol. 42, no. 16, pp. 2664–2671, 2009.

2008
- S.D. Strackee, J. van Loon, M. Foumani, M. Maas, G.J. Streekstra, B. Carelsen. Intraoperative 3D rotational X-ray in wrist surgery: initial experiences. Medicamundi. Volume 52(3), pp. 30-35. 2008.
- N. A. Dvinskikh, L. Blankevoort, M. Foumani, S.D. Strackee, G.J. Streekstra. Function evaluation of the extrinsic wrist ligaments using a 3D biomechanical model. J. Biomech. p.S452-, 2008.

9

Curriculum vitae

Mahyar Foumani was born at 4th of July 1982, in Teheran, Iran, where he spent all his childhood. At the age of 11 he left Iran for the Netherlands. He attended high schools (VWO) at the Hellen Parkhurst College in Almere, and graduated in 2001. Hereafter, he started to study Medicine at the Vrije University of Amsterdam, where he graduated with a cum laude on June 2010. During his study he was a teacher in Anatomy and Embryology at the Vrije University of Amsterdam under supervision of prof. dr. P.V.J.M. Hoogland. During his internships he started his PhD. research in the field of hand surgery at the Academic Medical Center in Amsterdam.

In January 2011 he started his Plastic surgery residency for a period of 6 years at the Academic Medical Center in Amsterdam (supervision Prof. dr. C.M.A.M. van der Horst).

Acknowledgements / Dankwoord

'Occasionally in life there are those moments of unutterable fulfillment which cannot be completely explained by those symbols called words. Their meanings can only be articulated by the inaudible language of the heart'

Martin Luther King, Jr.

Dit proefschrift is mede tot stand gekomen dankzij steun van velen. Een aantal personen wil ik hieronder in het bijzonder noemen.

Prof.dr. C.M.A.M. van der Horst, geachte professor van der Horst, veel dank dat u mijn promotor wilt zijn en voor de steun waar ik altijd op heb kunnen rekenen gedurende de afgelopen jaren.

Prof.dr. Ir. C.A. Grimbergen, geachte professor Grimbergen, Hierbij wil ik u bedanken voor alle moeite en inspanning voor tot stand brengen van mijn proefschrift.

Co promotoren
Dr. ir. Geert Streekstra, beste Geert, bedankt voor het onvoorwaardelijke steun gedurende de afgelopen jaren. Met je ongelofelijke vastbeslotenheid en het vermogen om dit project tot een goed einde te laten komen kan ik niet anders dan bekennen dat het zonder jouw hulp niet was gelukt.

Dr. ir. Leendert, beste Leendert, uw kennis, enthousiasme en scherpte waren van onschatbare waarde waar ik altijd uit kon putten.

Dr. Simon D. Strackee, beste Simon, Ik denk dat woorden tekort zullen schieten als ik alles zou willen opnemen waar ik erg dankbaar voor ben. Ontzettend bedankt voor je wijze adviezen, tact en vooral je luisterende oor.

9

Overige leden van de promotiecommissie, prof. dr. H.E.J. Veeger, prof. dr. M.J.P.F. Ritt, prof. dr. F. Schuind, prof. dr. S.E.R. Hovius, prof. dr. M. Maas, prof. dr. C.N. van Dijk, hartelijk dank voor het plaats nemen in de promotiecommissie en voor het beoordelen van het manuscript.

Mijn paranimfen, Martijn van de Giessen en Tan Duy Nguyen.

Beste Martijn, heel veel dank voor je heldere uitleg over de technische aspecten van beeldverwerking. Onze vele gezamenlijke publicaties vormen een goede basis voor toekomstige samenwerking waar we hopelijk meer tijd in gaan steken de komende jaren.

Tan, heel veel dank voor je steun en luisterende oor. Je fijne karakter, doorzettingsvermogen en vastberadenheid zijn een voorbeeld voor velen. Het koffie apparaat is reeds uitgebreid besproken in het dankwoord van jouw proefschrift en het wekelijkse Kam Kee etentje natuurlijk niet te vergeten.

Het AMC. Remmet Jonges, Al ben je al een tijdje niet meer in het AMC en geniet je van je welverdiende pensioen, was dit proefschrift niet tot stand gekomen zonder jouw uitgebreid voorbereidende werk. Bart Carelsen, beste Bart, veel dank voor je steun en hulp. Tevens bedankt voor het achterlaten van de 3D-RX scanner inclusief een onderhoudscontract van de firma die gelukkig een aantal keren van pas kwam. Ivan Dobbe, beste Ivan, veel dank voor je steun en heldere tips. Beste Natallia Dvinskikh, veel dank voor de fijne samenwerking.

Vera van Vuure, beste Vera, ik denk dat weinig mensen beseffen hoeveel werk jij op de achtergrond verzet. Hiervoor dank!
Ook wil ik hierbij mijn overige mede auteurs bedanken: Carlijn Stekelenburg en prof. A.H Zwinderman. Veel dank!

Last but not least wil ik mijn familieleden bedanken. Mijn moeder die mij altijd onvoorwaardelijk heeft gesteund en mijn vader die een luisterend oor bood en mij altijd adviseerde hoe om te gaan met de dagelijkse beslommeringen van het leven. Mahrouz, Kirsten, Jasmyn en Reza ontzettend bedankt voor alle hulp en steun.

En tot slot, mijn vrouw Maaike en mijn lieve zoon David, eindelijk is het nu af en kunnen we nu nog meer tijd samen doorbrengen. Lieve Maaike bedankt voor je onvoorwaardelijke steun en geduld.

9